REACTIVITY MEASUREMENTS ON THE UNIVERSITY OF MARYLAND REACTOR BY CONVENTIONAL METHODS AND STATISTICAL PROCESSES AND COMPARISON WITH CALCULATIONAL METHODS

by

Agustin Diaz Zubieta

Dissertation submitted to the Faculty of the Graduate School
of the University of Maryland in partial fulfillment
of the requirements for the degree of
Doctor of Philosophy
1970

APPROVAL SHEET

Title of Thesis: Reactivity Measurements on the University of Maryland Reactor by Conventional Methods and Statistical Processes and Comparison with Calculational Methods

Name of Candidate: Agustin Diaz Zubieta
Doctor of Philosophy, 1970

Thesis and Abstract Approved: Dick Duffey
Dr. Dick Duffey
Professor of Nuclear Engineering

Date Approved: 9 Sept '69

ABSTRACT

Title of Thesis: Reactivity Measurements on the University of Maryland Reactor by Conventional Methods and Statistical Processes and Comparison with Calculational Methods

Agustin Diaz Zubieta, Doctor of Philosophy, 1970

Thesis Directed by: Dr. Dick Duffey, Professor of Nuclear Engineering

The accurate experimental determination of nuclear reactor core physics parameters is of great importance for its safe operation. In particular, the accurate determination and prediction of criticality during the initial fuel loading of a nuclear reactor are essential for a safe nuclear reactor startup. Also, the degree of subcriticality or shutdown margin of a nuclear core with its control rods inserted is an important parameter for the operation of a nuclear reactor throughout the core operating lifetime.

There are several methods utilized to determine both the criticality and the shutdown margins. All of these methods depend on measuring the response of neutron detectors and the calibration of the control rods. However, neutron detectors respond only to the neutron flux in the core in the vicinity of the nuclear detectors. During initial reactor core fuel loading, the reactivity of the core is determined from the multiplication of the neutrons of the startup source by the addition of nuclear fuel. Reactivity is determined from the multiplication factor by a constant which is related to the source-detector geometry in the core.

In this research a method was studied which allowed the determination of reactivity independent of the source-detector geometry. Reactivity measurements of the 10 kw University of Maryland pool training reactor (UMR) were made by conventional methods and by a statistical process, the variance-to-mean ratio method, and the results were compared with calculational methods.

The theoretical method selected to determine the UMR core reactivity was based on the multigroup, multiregion, diffusion theory. The accuracy of the theoretical model was determined for the just critical UMR core. Agreement to within 0.2% $\Delta K/K$ was obtained between the control rod measured and the calculated reactivity for the UMR full core, and smaller UMR supercritical cores.

The statistical technique of the variance-to-mean ratio of the number of counts for various counting gate openings, as a means to determine the degree of subcriticality, or shutdown margin, has been proven to be an effective method.

A BF_3, thermal neutron proportional detector, with a sensitivity of 12.1 counts/sec per $n/cm^2/sec$, was placed inside of an eleven feet long aluminum tubing. The end of the tubing containing the detector was inserted in the center Glory Hole of the UMR core. The current pulses from the proportional detector was amplified and fed to a TMC 1024-channel pulse analyzer. The pulses were counted for different Δt gate openings from 10^{-4} seconds to 10 seconds. For each Δt gate opening, 1023 samples were taken. The printed output from the TMC-1024 was collected, giving the number of counts received per Δt, as well as the

integral of all the counts received during a period of time, equal to $1023 \times \Delta t$ seconds.

From the integrated value for the number of counts the average count $\overline{c}$ for the gate opening Δt was obtained.

The printed output was transferred to IBM cards acceptable to a "Reactor Noise" code written for the IBM-7090. This code calculated the average value, $\overline{c}$, for each Δt (which gave a check on the validity of the data transferred to the IBM cards by comparing it with the value obtained during the measurement), the standard deviation σ, and the variance-to-mean ratio for all the data taken for each Δt seconds gate opening.

Plots of the values of the variance-to-mean ratio versus gate openings were obtained for several UMR full core with the rods banked at various degrees of insertion (shutdown margins), and also for various UMR subcritical cores.

Measurements of the shutdown margins by the variance-to-mean technique were in agreement with the values obtained from the rod calibration for negative reactivities of less than -1.00% $\Delta K/K$, and within ten percent for negative reactivities of approximately -2.0% $\Delta K/K$.

Measurements of the reactivity of small UMR cores indicated that for UMR core conditions of 0.5% $\Delta K/K$ subcritical, experiment and theory for $1-K_{eff}$ were found to be only 6 parts in 100 apart, and for 2.0% $\Delta K/K$ subcritical, experiment and theory were found to be only 8 parts in 100 apart.

The variance-to-mean technique was compared to the inverse multiplication method for determination of criticality during the UMR fuel loading, and was found to be a more accurate method, primarily, because of its independence of the source-detector geometry effects.

The system utilized for the statistical data processing is exact, however cumbersome, due to the amount of data to process and the amount of peripheral hardware utilized in the reduction of the data.

It appears from this study that greater overall counting efficiency for the same amount of statistical data would permit more accurate measurements at larger degrees of subcriticality, perhaps, in the region of -4.0% $\Delta K/K$ to -5.0% $\Delta K/K$. A system is proposed in this study to measure negative reactivity continuously, and directly, by means of a small computer capable of accepting the output of a multi-channel scaler. The computer would have a fixed internal logic capable of calculating reactivity from the variance-to-mean analysis of the neutron detector counts.

ACKNOWLEDGEMENTS

It is difficult to acknowledge fully the guidance and assistance given the author by members of the University of Maryland Nuclear Engineering staff. However, the author is especially grateful to Dr. Dick Duffey, his thesis advisor, for his patient encouragement, direction and suggestions; the reactor operating staff especially Mr. Fred Brittle, for his assistance in the many hours of reactor operation; and my wife, for her encouragement and assistance in the preparation of the manuscript.

An especial note of gratitude to Dr. Joseph A. Thie for introducing and guiding the author in the field of reactor noise.

The computer time used in this research was supported by National Aeronautics and Space Administration Grant NsG-398 to the Computer Center of the University of Maryland.

The author wishes to thank the General Electric Company for their assistance in the final typing and preparation of this dissertation.

TABLE OF CONTENTS

LIST OF TABLES

LIST OF FIGURES

SECTION I

INTRODUCTION

A. Introductory Remarks

The author has been very closely associated with the University of Maryland Reactor (UMR), reference 1, from its early design and construction stages as a member of the Allis-Chalmers Manufacturing Company, Nuclear Power Department, Physics Group, in 1960, through the reactor start-up and testing, and later as a graduate student of the Nuclear Engineering Department of the University of Maryland, from 1960 through 1966. The author held an Atomic Energy Commission (AEC) license to operate the UMR from 1962 to 1966.

In January 1962, the University of Maryland was granted permission by the Atomic Energy Commission to change the core configuration of their reactor. The primary objective of this core configuration change, was to arrive at a core which would be capable of incorporating a water filled hole, "Glory Hole," surrounded by fuel near the center of the core, and at the same time obtain a core excess reactivity between 0.5% $\Delta K/K$ and 1.0% $\Delta K/K$ available for experiments. The procedures and results for the UMR core configuration change are described in reference 2.

The author was first exposed to the theory of reactor noise analysis, i.e., statistical analysis of the fluctuations of the neutron

population about a mean value, during the initial start-up and testing of the Elk River Boiling Water Reactor, ERR, 58.2 Mwt., in 1962. Under the direction of Dr. J.A. Thie, an experiment was performed to analyze the ERR power fluctuations. The raw data was taken directly from the linear power recorder. The power fluctuations were digitized and computer processed to determine the standard deviation of the Elk River Reactor at constant power levels. This important experiment permitted us to attain a degree of safety in the initial power escalation, since from the data obtained at lower power levels, the stability at higher power levels could be predicted with a certain degree of accuracy.

From the experience gained on these tests, the author decided to apply similar techniques, as described in Section III of this dissertation, for subcritical and slightly supercritical UMR cores.

Another important reason for this research, as the author saw it at its beginning, was to find an alternate method to determine core reactivity, both for subcritical and supercritical assemblies, by other means, different from the conventional techniques utilized in reactor experimentation up to date, namely, the rod-bump, period, and reactivity measurement associated with the measured period. In subcritical cores and during initial core loadings, criticality is normally predicted by the 1/M method, where M is the number of times the source neutron population is multiplied by the subsequent addition of reactor fuel. By plotting the inverse of the multiplication factor, M, against the fuel

mass added at each step, prediction of the critical fuel loading can be had, by extrapolating to zero the data gathered from early fuel loadings. However, this method is highly affected by the neutron source-detector geometry, overestimating or underestimating the critical loading. Further, this method does not provide the core reactivity, nor the shutdown margin (degree of subcriticality of a fuel assembly with the control rods fully inserted).

The author has been very keenly interested in the accurate definition of the UMR core parameters, both from theoretical and experimental approaches. This dissertation describes the theory and experimental techniques used to calculate and measure the UMR core reactivity and UMR core physics parameters. Experimental results were obtained both by conventional techniques and by statistical analysis of the fluctuations of the neutron population, "reactor noise," under steady state core power conditions.

B. Organization of the Test

Section II presents background information regarding reactor noise, and reasons for the selection of the variance-to-mean ratio technique for the reactivity measurements of the University of Maryland Reactor.

Section III presents the theory and mathematical model selected, references 3, 4, 5, and 6, correlating the variance-to-mean ratio of the neutron population to reactivity for the UMR core.

Section IV describes the equipment used in the experiments.

Section V describes the calibration of the nuclear instrumentation used and Section VI outlines the experiment performed to test the model by means of a random neutron source.

Section VII describes the calculation of the physics parameters of the University of Maryland Reactor.

Section VIII describes the calibration of the UMR control rods, which is basic for the accurate determination of reactivity and shutdown margin.

Section IX describes the reactivity measurements of UMR full core and two slightly supercritical cores, and its comparison with calculated results for the same core configurations.

Section X describes the experiment and measurements by means of the statistical model presented in Section III for UMR fuel in sub-critical assemblies and for the UMR full core with the control rods at different degrees of insertion.

Section XI summarizes the results of the experiments and Section XII formulates conclusions based on the results.

SECTION II

REACTOR NOISE

A. General Description

The term "noise" is commonly used today in many areas of science and engineering. It is normally associated with a random behavior of events as distinguished from regular or determinable behavior. In the field of reactor theory, "noise" normally describes the random fluctuation of the neutron population about its average at a constant power level at steady state operation.

Since de Hoffman's initial utilization of noise theory in reactors in 1946, reference 3, noise analysis has developed into a science with multiple applications in the field of nuclear reactors. One of the most important and comprehensive studies of the present status of the reactor noise theory can be found in reference 4 (see note below).

To measure a reactor's transfer function, the only available tool during the early years of experimentation with reactors was the control rod - oscillator experiments, which in general are laborious and expensive in required hardware, and necessitate access to the reactor's core. Reactor noise analysis came in favor in the reactor experiment field for the following reasons among others: a) normally required instrumentation for operating reactors is sufficient; b) core accessibility not required; c) from direct analysis of the linear output of

(Note: In order to easily introduce the reader to the specific formulae theoretically derived by others and used in this dissertation the author has selected in Sections II and III to follow the derivations as presented by Dr. J.A. Thie in his book, Reactor Noise, pages 12-15, 96-98, and 102-104. The author obtained written permission of the copyright owner, as well as of Dr J.A. Thie.)

the power recorder the Fourier spectrum of the core can be obtained, which is a rather direct measure of stability and safety in high power reactors and permits evaluation of certain core parameters at low power, as it will be discussed herein later.

The fluctuations of the neutron population, as recorded by the associated nuclear instrumentation, once proper filtering of equipment background or interference has been performed, has several major sources in the reactor core: a) the natural statistical variation of the neutron chain reaction; b) reactor core coolant temperature and density variations, which affect directly or indirectly the neutron chain reaction; c) perturbation of the core, i.e., control rod oscillation, mechanical vibration of the core elements due to coolant flow, voids in the coolant, etc.

In this dissertation we shall concern ourselves only with the direct usage of noise analysis in low or zero-power reactor, like the UMR, where core heating does not occur and consequently the reactor noise relates exclusively with the intrinsic characteristics of the core and its neutronic fluctuations.

B. Zero-Power Reactor Noise Analysis

Zero-power level in the reactor field normally defines the range from a few milliwatts to approximately 100 watts. At this power level, the dynamic behavior of the neutron chain can be completely represented by the neutron-kinetics equations, since at this power level the neutron population is not affected by thermal effects in the core. Hence the

multiplication of the source neutrons by the core fissionable material, and overall core neutron population fluctuations can be determined only by statistical methods.

The atomic fission process itself occurs according to laws of probability. When atomic fission occurs, an integral number of neutrons is emitted per fission, and yet the measurements of $\bar{\nu}$, the average of the total (prompt plus delayed) number of neutrons per fission, do not give an integer, in fact there is a probability distribution for ν, reference 7, for each fissionable material.

C. Fundamental Statistical Processes of the Neutron Chain in Reactors

Assuming a single energy group of prompt neutrons released at fission in a single core region, it is possible to derive the neutron-kinetics equation, without delayed neutrons, from probability considerations, reference 4.

By definition of the prompt neutron lifetime, ℓ, the probability that one neutron will be lost, P_{loss}, by absorption into another atom, or leakage out the core region in same time interval Δt is:

$$P_{loss}\,\Delta t = \frac{\Delta t}{\ell} \qquad (2.1)$$

Also, if the effective neutron population multiplication constant, for the core region under consideration, is K_p, then, there is a probability that when such a prompt neutron loss has occurred, there will be a probability of:

$$P_{gain}\,\Delta t = K_p \frac{\Delta t}{\ell} \tag{2.2}$$

for returning a prompt neutron to the system. Then if M neutrons are present in the system instead of one, as considered above, the net gain ΔM, of neutrons in the system will be represented by:

$$\Delta M = MK_p \frac{\Delta t}{\ell} - M\frac{\Delta t}{\ell} \tag{2.3}$$

and hence, one has a simplified kinetics equation for prompt neutrons,

$$\frac{dM}{dt} = \frac{K_p - 1}{\ell} M = -\alpha M \tag{2.4}$$

where the so-called Rossi alpha is defined as:

$$\alpha = \frac{1 - K_p}{\ell} \tag{2.5}$$

and the solution of equation (2.4) if M_o neutrons are present at $t = 0$, is,

$$M = M_o e^{(-\alpha t)} \tag{2.6}$$

from which it can be seen that the neutron population increases, stays constant, or decreases with a period, α, depending on, respectively, whether K_p, the effective neutron multiplication, exceeds, equals, or is less than 1.

Hence, it can be seen that an experiment can be performed to measure α, if the time behavior of the neutrons having a single ancestor could be determined. Bruno Rossi first suggested this type of experiment and Feynman, de Hoffman, and Serber, reference 8, developed its theory. Essentially the principle in this type of experiment is to

isolate a single chain of related neutrons when many chains are existing simultaneously by delayed coincidence counting.

These types of experiments have been used by Orndoff, reference 9, and Brunson, reference 10, to determine values of the ratio of the effective delayed neutron fraction to the prompt neutron lifetime, β/ℓ, for fast reactors like Godiva-I and ZPR-III.

The Rossi alpha method is generally applicable to fast reactors having a small prompt neutron lifetime $\ell \sim 10^{-7}$ seconds.

The UMR is a low power, thermal reactor, with a prompt neutron lifetime of 45 microseconds, or 4.5×10^{-5} seconds, as calculated in Section VII. E. 8 of this dissertation, and hence, too low counting rate for utilization of the Rossi alpha experiment.

Another statistical method to obtain information about reactor systems with long prompt neutron lifetime was investigated. It was suggested by Feynman, reference 8, and is sometimes called the "Feynman alpha method," or "Variance-to-Mean Ratio," which consists in studying the statistical nature of neutron counts obtained in various time intervals.

This method was selected by the author for application and experiment with the University of Maryland Reactor to measure reactivity in subcritical fuel assemblies, and to measure shutdown margin (degree of subcriticality) with the UMR full core, with the control rods at different degrees of insertion in the core.

SECTION III

DESCRIPTION OF THE VARIANCE-TO-MEAN RATIO TECHNIQUE FOR REACTIVITY MEASUREMENTS

A. Probability

In dealing with the random distribution of the neutron population over a period of time one uses the theoretical equivalent of the relative frequency; that is, the probability of observations of the neutron population falling in a given interval.

In general the probability of occurrence of an event (p) is the ratio of the number of samples that correspond to the event to the total number of samples. The event for which a probability is defined may be the occurrence of a particular value, $c = c_1$. The probability $p(c_1)$ is then the ratio of the number of times c_1 actually occurs in an experiment to the total number of c values encountered.

The random fluctuation of the neutron population about its average at a constant power level and at steady state operation is a random process in which the independent variable, time (t), does not determine in a complete and definite way (as in a casual process) the random variable c (neutron population). Consequently, the neutron population (c), instead of being definitely characterized by an equation, is characterized by a probability density function, p (c).

B. Moments of the Probability Density Function

The concept of taking moments of a function is quite general and applications are found in many fields.

For a stationary random process, having a probability density function p (c), the n-th moment is:

$$\overline{c^n} = \frac{\int_{-\infty}^{\infty} c^n \, p(c) \, dc}{\int_{-\infty}^{\infty} p(c) \, dc} \tag{3.1}$$

and assuming a discrete distribution, i.e., the number of neutrons (c) present in a core at time (t), then,

$$\overline{c^n} = \frac{\sum_i c_i^n \, p(c_i)}{\sum_i p(c_i)} \tag{3.2}$$

Equation (3.2) indicates that $\overline{c^n}$ may be determined experimentally from a sequence of a large number, N, of individual data values, or neutron population counts c_i, since these will tend to distribute themselves according to $p(c_i)$, where,

$$\overline{c^n} = \frac{1}{N} \sum_{i=1}^{i=N} c_i^n \tag{3.3}$$

It is evident that the moments are average values of various powers of the random variable.

The first moment, $\overline{c}$, is the average value, or "mean" value of the random variable. If we consider the variation of c about its mean

value $\bar{c}$, then the moments with respect to $\bar{c}$, are obtained from:

$$\overline{(c - \bar{c})^n} = \frac{\int_{-\infty}^{\infty} (c - \bar{c})^n \, p(c) \, dc}{\int_{-\infty}^{\infty} p(c) \, dc} \tag{3.4}$$

and hence for the second moment, n = 2,

$$\overline{(c - \bar{c})^2} = \frac{\int_{-\infty}^{\infty} (c - \bar{c})^2 \, p(c) \, dc}{\int_{-\infty}^{\infty} p(c) \, dc} \tag{3.5}$$

Equation (3.5) is normally called the "variance." The square root of the variance is termed the standard deviation, σ.

Equation (3.5) for a discrete distribution can be written as:

$$\sigma = \left[\frac{\sum_{i=1}^{i=N} (c_i - \bar{c})^2 \, p(c_i)}{\sum_{i=1}^{i=N} p(c_i)} \right]^{1/2} = \left[\frac{1}{N} \sum_{i=1}^{i=N} (c_i - \bar{c})^2 \right]^{1/2} \tag{3.6}$$

or

$$\sigma = \left[\overline{c}^2 - (\bar{c})^2 \right]^{1/2} \tag{3.7}$$

C. Variance-to-Mean Ratio (Theory)

The fluctuations of the neutron flux in the core can be studied assuming it to be a conglomeration of a very large number of discrete events (counts per unit of time) c in a total of N attempts. If the average number of discrete events or counts, $\bar{c}$, is large, and the number, N, of attempts is also large, then one can obtain a gaussian distribution which can be

written, reference 4, as:

$$p(c) = \frac{e^{-\frac{(c - \overline{c})^2}{2\overline{c}}}}{\sqrt{2\pi\overline{c}}} \qquad (3.8)$$

where:

$p(c)$ = probability of, c, counts obtained per unit time, t, seconds.

c = number of counts per unit time t, seconds.

$\overline{c}$ = average number of counts per unit time, t, seconds.

Then $p(c)\,dc$ is the probability of the result being between c and $c + dc$. The variance of such a distribution equals the mean:

$$\overline{c^2} - (\overline{c})^2 = \int_0^\infty c^2\, p(c)\, dc - \left[\int_0^\infty c p(c)\, dc\right]^2 = \overline{c} \qquad (3.9)$$

However, the variance cannot be expected to equal the mean if there exists correlations between counts that make up a total due to the chain nature of neutrons in a reactor. It is then possible to obtain the variance-to-mean ratio, when this correlation is present, from integration of the coincidence count probability as derived by Feynman, de Hoffman and Serber, reference 8:

$$\epsilon F_0 \int_0^T dt_2 \int_0^{t_2} p(t_1,\ t_2)\, dt_1 \qquad (3.10)$$

$$= \epsilon F_0 \int_0^T dt_2 \int_0^{t_2} \left[\epsilon F_0 + \frac{\epsilon \overline{\nu(\nu - 1)}}{(\overline{\nu})^2} \sum_{i=1}^{i=7} A_i G_0(\alpha_i)\, e^{-\alpha_i(t_2 - t_1)}\right] dt_1$$

$$= \frac{\epsilon^2 F_0^2 T^2}{2} + \frac{\epsilon^2 F_0 \overline{\nu(\nu - 1)}}{(\overline{\nu})^2}\, T \sum_{i=1}^{i=7} \frac{A_i}{\alpha_i} G_0(\alpha_i) \left[1 - \frac{1 - e^{-\alpha_i T}}{\alpha_i T}\right]$$

where:

ϵ = Counter efficiency = $\frac{\text{fissions detected}}{\text{total fissions occurring}}$

F_o = Total fission rate; fissions per second in the reactor.

T = Selected interval of time for counting events (GATE TIME), seconds.

ν = Number of neutrons emitted per fission.

$\overline{\nu}$ = Average number of neutrons emitted per fission.

A_i, G_o and α_i are defined in terms of the zero power transfer function for each delayed neutron fraction.

Integration of equation (3. 10) is the expected number of pairs of counts that occur during the time interval T(namely, $\overline{c\,(c-1)}\,/2$) since the number of pairs at any given trial is half the product of the number of counts and one less than the number of counts. Hence, reference 4,

$$\frac{\overline{c}^2}{2} - \frac{\overline{c}}{2} = \frac{(\overline{c})^2}{2} + \overline{c}\,\frac{\epsilon\overline{\nu(\nu-1)}}{(\overline{\nu})^2}\sum_{i=1}^{i=7}\frac{A_i}{\alpha_i}G_o(\alpha_i)\left[1 - \frac{1 - e^{-\alpha_i T}}{\alpha_i T}\right] \tag{3.11}$$

and since the average number of counts is:

$$\overline{c} = \epsilon F_o T \tag{3.12}$$

the desired expression for the variance-to-mean ratio of the number of counts is:

(3. 13)

$$\frac{\overline{c}^2 - (\overline{c})^2}{\overline{c}} = 1 + \frac{2\epsilon\,\overline{\nu(\nu-1)}}{(\overline{\nu})^2}\sum_{i=1}^{i=7}\frac{A_i}{\alpha_i}G_o(\alpha_i)\left[1 - \frac{1 - e^{(-\alpha_i T)}}{\alpha_i T}\right]$$

This relation is seen to become unity for $\epsilon = 0$, which is to be expected since the lower the efficiency of the detector, the less likely are correlated counts, and for a purely random source the variance equals the mean (see Section VI).

Substituting the values given by Bennett (reference 5) into equation (3.13), it is found that the contribution from the delayed neutron terms, i = 2 to 7, is negligible for $T < 0.1$ seconds, and hence equation (3.13), becomes, reference 4,

$$\frac{\overline{c}^2 - (\overline{c})^2}{\overline{c}} = 1 + \frac{\epsilon\,\overline{\nu(\nu - 1)}}{(\overline{\nu})^2} \frac{(1 - \beta)^2}{(\beta - \rho)^2} \left[1 - \frac{1 - e^{\left(-\frac{\beta - \rho}{\ell} T\right)}}{\frac{\beta - \rho}{\ell} T} \right] \tag{3.14}$$

where:

$\frac{\overline{\nu(\nu - 1)}}{(\overline{\nu})^2}$ = 0.795 for U-235

ρ = Constant core reactivity = $1 - \frac{1}{K_{eff}}$

β = Effective delayed neutron fraction

ℓ = Prompt neutron lifetime

From equation (3.14), the reactivity ρ and hence the effective multiplication constant can be obtained by solving the equation for $(\beta - \rho)/\ell$ and applying the measured values for the variance-to-mean ratio for several counting times, T, which must be of the order of $\ell/(\beta - \rho)$ seconds, the second term of equation (3.14) becomes approximately equal to $0.7 \times 10^4\ \epsilon$ seconds. Consequently, the counting

efficiency, ϵ, must be of more than 10^{-4} counts per reactor fission.

Bennett, reference 5, has pointed out that if the variance-to-mean ratio experiment is performed on a just critical reactor (i.e., $K_{eff} = 1.00$ and hence $\rho = 0$), then the variance-to-mean ratio would be infinite for any time interval T. Consequently, the variance-to-mean ratio experiments should be conducted in subcritical assemblies (i.e., $K_{eff} < 1.0$), at constant reactor power, and with a source multiplication of $1/(-\rho)$, or, $\bar{\nu} F_o$ = (source neutrons/sec) $\times$ $1/(-\rho)$.

In equation (3.8) and hence in the derivation of equation (3.14), the fluctuations of the neutron flux detected have been considered as a function of time only, c(t). The effect of the energy of the detected particle (neutron or gamma-ray), c(t, E), in the determination of β/ℓ, has been investigated experimentally by Kenney (reference 15). He obtained the same value for β/ℓ in a zero power reactor with two different and extreme energy levels of the detected particle: thermal neutrons in one test, and fission photons in another test (the fission photons or the prompt 2 Mev. neutrons can be equally useful in checking the energy of the neutrons counted). Also Natelson et al. (reference 16) gave the theoretical proof that the space and energy independent model, such as equation (3.14), is valid and gives correct results even though various particle energies are not measured. Further Natelson el al. (reference 16) demonstrate that the characteristics (shape or location) of the detector used in the variance-to-mean measurements have no effect on the characteristic frequency and time behavior of the results.

SECTION IV

DESCRIPTION OF EQUIPMENT

A. General Description

The arrangement of the equipment used during the performances of the different runs is shown in schematic form in Figure 1 and can be described as follows: A boron trifluoride (BF_3) neutron detector is placed inside a leak proof aluminum tubing. The tubing was placed in the center irradiation space, "Glory Hole," of the University of Maryland reactor (UMR) core, as shown in Figures 2 and 3. A high voltage power supply located on the pool bridge, as shown in Figure 4, served the neutron detector. The electrical impulses from the neutron detector were amplified by a preamplifier located on the bridge of the pool, as shown in Figure 5. The amplified signal was then transmitted by a high voltage coaxial cable, as shown in Figure 6, to a TMC Model 214 gate scaler located in the counting room, Figure 7. The gate scaler is a plug-in linear amplifier/pulse height analyzer, which accepts pulses during calibrated time intervals. The pulses accepted per interval of time were accumulated and stored in a TMC Model CN110 Digital Computer. This is comparable to counting in a series of scalers by opening them consecutively for a preset time.

The stored data was retrieved and recorded on a Hewlett-Packard Digital recorder, Model J44561B, which provided the output in a printed

paper tape. The gate scaler, computer, and printer were installed in a controlled humidity and temperature instrumentation room as shown in Figure 7.

A Radiation Instrument Development Laboratory Scaler, Model 49-55, shown in Figure 4 was also used to obtain statistical data prior to each experiment to verify that the conditions of the equipment and position of the neutron detector were equivalent to those of previous runs for the same core conditions.

An Electronics Instruments and Data Systems, Model PG-1, square wave pulse generator was used for generating an external signal to the gate scaler to trigger the gate opening for times less than 0.001 seconds.

B. Test Equipment

1. University of Maryland Reactor, UMR. The UMR, Figures 2 and 3, is a pool training reactor licensed for 10 KW, moderated and cooled by light water and partially reflected by graphite. The fuel is fully enriched (93.5%) uranium in an uranium-aluminum alloy in the form of flat, aluminum clad plates.

The mechanical and nuclear parameters of the reactor are discussed in Section VII.

The permanent instrumentation of the reactor consists of one BF_3 startup channel, one log-N channel, one linear channel and a linear safety channel. The outputs from all the instrumentation are indicated and recorded on the reactor console shown in Figure 8.

2. Aluminum Tubing - BF_3 Arrangement. An aluminum tube,

shown in Figure 9, was used to contain the in-core neutron detector. The tube was 11 feet long, one inch inside diameter and one-sixteenth inch wall. The material was aluminum, Alcoa 6061. This type of aluminum was selected because of its low impurity content which minimized the activation of the tube during its exposure to the neutron flux in the reactor. Because of its thin walls, a difficulty was encountered when capping the tube end. A conical aluminum plug was press fitted into the tube. Several attempts were made to weld the plug to the walls of the tube, but microscopic openings remained, probably due to the porous structure of the weld. Such capping of the tube was abandoned, and a rubber stopper centrally perforated and containing a bolt with a washer and nut was used. After inserting the stopper in the tubing, the rubber was compressed by tightening the nut; complete leak tightness was obtained with quick access to the neutron detector.

To compensate for the reactivity loss in the core by the presence of the neutron detector, the boron of which acts like a control element from reactivity point of view, two cylindrical pieces of graphite, 4 inch long and 12 inch long, by 7/8 inch diameter were inserted in the tubing below the neutron detector.

The proper amount of graphite to balance the negative reactivity of the detector was determined by performing reactor criticality experiments with the aluminum tubing containing the neutron detector and graphite cylinders.

Placement of graphite, instead of water, in a slightly overmoderated reactor, adds reactivity to the core since graphite has a lower absorption

cross-section than water. Also, placement of graphite in the aluminum tube, instead of void, adds reactivity to the core, since graphite is a better material to obtain fast neutron slowing down to thermal energies.

The selected dimensions of the graphite were based on obtaining a compensation of the negative reactivity inserted in the core by the presence of the detector, against the positive reactivity of the graphite.

Careful and controlled position of the detector in the Glory Hole was insured by a guide which was designed to fit the dimensions between the outer plate of the fuel assembly and the aluminum walls of the container. The tube and detector were placed in the core with all the control rods fully inserted.

The control rods were then withdrawn by normal reactor start-up procedures and a critical position was recorded.

After control rods insertion, the detector assembly was withdrawn from the Glory Hole, and critical position of the rods checked. Repetition of this procedure showed an accuracy of ± 0.01 percent $\Delta K/K$ in reproducing the critical settings.

The upper end of the aluminum tube was tight fitted to a plastic tubing ("Tygon"), which extended above the water level, to the pool bridge. The coaxial cables were run through the Tygon tubing and aluminum tube combination from the neutron detector to the preamplifier.

A smaller Tygon tubing accompanied the other tubing and was connected to the service air of the reactor building. This flow of dry

air eliminated moisture and condensation on the cables and neutron detector.

3. Neutron Detector. The manufacturer's specifications are listed below:

Manufacturer	Nuclear-Chicago Corporation
Type Detector	BF_3 thermal neutron detector
Model Number	NC-252
Dimensions and Mechanical Data	
Overall length	15-5/32"
Outside diameter	1.0"
Active length	12.0"
Wall thickness of envelope	0.020" ± 0.002
Material of envelope	Heliarc-welded stainless steel
Insulating material	Alumina ceramic
Neutron absorber material	Enriched BF_3 (96% B^{10})
Weight	8 ounces
Filling gas pressure	120 cm Hg
Active volume	142.4 cm^3
Operational Characteristics	
Operating voltage	3900 volts
Operating plateau	Approx. 300 volts
Sensitivity	12.1 counts/sec per $n/cm^2/sec$

The anode termination of the detector is a 3/4 in-20 HN connector with Teflon insulator which was connected to an Amphenol 82-38 (MIL-

UG 59 A/V) cable fitting. The BF_3 in the aluminum tube was maintained dry during all the experiments. The power supply for the BF_3 was a standard pulse amplifier high voltage supply RIDL Model 14 with a voltage range from 1000 volts DC to 5000 volts DC; the operating voltage of 3900 volts was set by response to a one Curie plutonium-beryllium (Pu-Be) source. The calibration technique is described in detail in Section V.

4. Pre-Amplifier. The manufacturer's specifications are listed below:

Manufacturer	Hamner Electronics Co., Inc.
Type of Pre-Amplifier	Fast rise feed back
Model Number	N-354
Dimensions and Mechanical Data	
Length	7-1/4"
Width	4-3/8"
Depth	4-3/8"
Material	Aluminum
Operational Characteristics	
Gain - Unloaded	24
Gain - Into 1 K load	Down 10%
Rise time	< 0.1 microseconds
60 cycle hum	Approx. 10 mv. peak-to-peak maximum
Noise	2 mv. peak-to-peak

Input	Positive or negative
Output Impedance	Approx. 170 Ohms

Power Requirements

B+ - Approx. 300 volts DC @ 21 ma, ripple less than 1 mv. RMS

Filament supply - 6.3 volts AC at 1.2 ampere, one side of filament grounded.

The pre-amplifier used was a fast rise feed back amplifier adapted for an ionization chamber; it was in an aluminum mounting and was located on the floor of the pool bridge; the power supply for the pre-amplifier was a RIDL Scaler, Model 49-55.

5. Multi-Scaler Logic Unit. The manufacturer's specifications are listed below:

Manufacturer	Technical Measurement Corporation (TMC)
Multi-Scaler Logic Unit	Model 214
Digital Computing Unit	Model 220
Digital Recorder	Hewlett-Packard Model J44.561.B

Input Signal Requirements:

Polarity	Negative
Amplitude	Between 1 and 30 millivolts
Rise time	0.3 microseconds, approximately
Fall time	3 microseconds, approximately
Channel Counting Times	0.001, 0.01, 0.1, and 1.0 second,

Channel Counting Times (cont'd)	plus external timing signals with a repetition rate of up to 10 kc. Wave shape is not critical.
Attenuators	Coarse gain -- A seven-position logarithmic attenuator which divides by a factor of 2 with each successive step.
	Fine gain -- A linear attenuator continuously variable from 50% to 100% of amplitude selected by coarse gain control.
Discriminators	Upper and lower level; both are 10-turn calibrated controls. Upper level control may be switched out.
Pulse Pair Resolution (Resolving Time)	5 microseconds.
Dead Time	20 microseconds per channel.
Start Program	Pushbutton for manual operation. A negative, 3-10 volt trigger pulse is required for automatic or remote operation.
Maximum Count Rate	250, 000 counts per second.

6. Control and Connector Functions.

Name	Function
ΔT Switch	Selects channel time duration internally or from an external source.
COARSE GAIN Control	Permits logarithmic attenuation increasing by a factor of two with each successive step.
FINE GAIN Control	Permits continuously variable linear attenuation covering 50% to 100% of amplitude selected by COARSE GAIN Control setting.
UPPER LEVEL Control	Restricts upper limit of amplitude range in reference to base line setting. Used for differential counting.
BASE LINE Control	Establishes lower limit of amplitude range.
UPPER LEVEL IN/ OUT Switch	Switches out UPPER LEVEL Control for integral counting.
AMP. INPUT Connector	Accepts low-level, negative pulses from a detector or pre-amplifier such as the TMC Model DS-12 or DS-13.

EXT. ΔT Connector	Accepts timing signals from external source up to 10-Kc repetition rate (wave shape not critical).
START PROGRAM Connector	Accepts negative trigger pulse to start analysis cycle.
START PROGRAM MANUAL Pushbutton	Permits start of analysis cycle without use of external trigger.

A maximum of 1023 calibrated time intervals are available with pulses per interval accumulated and stored in the computer memory. This amounts to counting with a series of scalers by opening them consecutively for a pre-set time. Base line and upper discriminator controls enable the operator to select a particular energy region ("window") allowing only events of interest to be counted.

The computing unit has two output options: normal and integrating. The normal output allows for the individual number of events per selected unit time per individual channel to be sent to the digital recorder. The integrating output adds the number of events per selected unit time to that of the previous channels. This integrated output is used to find the average number of events per unit time per channel, dividing the integrated count by 1023, the number of channels available. For gate openings smaller than 0.001 seconds an external triggering signal was obtained from a Electronic Instruments and Data Systems, PG-1 square wave and pulse generator.

7. Square Wave and Pulse Generator. The manufacturer's specifications are listed below:

Manufacturer	Electronic Instruments and Data Systems
Model	PG-1
Dimensions and Mechanical Data	
Height	7 in.
Width	5 in.
Depth	12 inch
Weight	7 lbs.
Operational Characteristics	
Voltage	115 volts AC
Frequency	50/60 CPS
Pulse amplitude	± 20 volts from 50 Ohms
Pulse shape	Rise time less than 12 ns. Fall time less than 10 ns
Pulse polarity	Positive or negative
Frequency range	1 cps to 10×10^6 cps

SECTION V

CALIBRATION OF THE NUCLEAR INSTRUMENTATION

A. Objective

The objective of the calibration was the selection of the optimum settings for the instrumentation to measure the neutron population in the UMR core. This test also included the calibration to compensate for gamma radiation signal.

The procedure was to plot the voltage and pulse height distribution curves; from these, the optimum voltage and pulse height settings were determined.

B. Calibration Principles

The neutron detection instrumentation must be calibrated to ensure that the system will provide an accurate neutron count in the presence of the gamma rays from the fission process and fission products decay. The approximate instrument settings from manufacturers' specifications were used as preliminary. The available instruments adjustments include: detector voltage, amplifier gain, and pulse height selector of discriminator.

Increasing detector voltage increases the pulse height in the detector. The discriminator bias setting cuts off all pulses below that setting. It can be seen that there is considerable choice in these adjustments and one (of the three) may compensate for another, for

example, increased voltage may be compensated by decreased gain or by increased pulse height setting.

The pulses seen at the multichannel analyzer, gate scaler, originate from several sources. Neutron pulses are large because of the intense ionization from alpha particles released from the neutron-boron reaction in the BF_3 detector. Other ionizations due to gamma radiation yield much smaller pulses. The main source of very small pulses is the noise in the input resistor and input tube of the preamplifier. The discriminator, or pulse height selector, screens out all the small pulses from noise and gamma rays and allows only the large neutron pulses to pass through to the gate scaler.

Noise and gamma-ray pulses are statistically random in their size distribution, i. e., the number above a certain pulse height setting is proportional to the number at the setting. Such a distribution is exponential, giving a straight line on a semi-log graph. Thus, a plot of the logarithmic count rate against pulse height setting is a straight line and can be extrapolated to predict the "noise background" at any higher setting.

Neutron pulses, however, are much larger and more uniform in size; therefore, the curve will flatten out to show a plateau above the pulse height settings, and an elimination, cut off, of the noise pulses. At a much higher setting, even neutron pulses are cut off. Therefore, it is desirable to operate near the middle of this plateau where the ratio of total counts to the extrapolated noise background is high (above 100

to 1). This means that more than 99 percent of the pulses counted are from neutrons.

The plot of count rate against voltage or gain is very similar, but reversed (as a mirror image). At low voltage or gain, almost all pulses are too small to pass the discriminator; at high voltage or gain, most of the neutron pulses are counted, giving a broad plateau or fairly constant count rate. At still higher voltage or gain, the noise pulses pass the discriminator, giving a steep rise in count rate. Too high a voltage, which might cause a continuous discharge in the gas-filled detector chamber, should not be applied.

C. Detailed Procedure

1. Voltage Curve (Neutrons Only from the Pu-Be Source). A plutonium-beryllium (Pu-Be) source which has an emission rate of approximately 10^6 neutrons per second was placed inside a block of paraffin. The neutron detector was placed in the same plane as the source, and at a distance of 3 inches from it. The same length of coaxial cable as that required for in-core measurements was used between the detector and the preamplifier.

The voltage and gain control on the high voltage supply were set as per detector manufacturers' suggested settings.

The pulse height discriminator on the gate scaler was set at 0.50 to bias all electronic noise and gamma induced chamber response.

The high voltage or gain was changed from 3300 volts to 4100 volts

at increments of 100 volts. At each voltage increment 1023 one-second counts were taken. The average counts per second for increment in voltage were plotted in Figure 10.

2. Pulse Height Distribution (Neutrons Only from the Pu-Be Source). From the data obtained from the voltage curve, a voltage of 3900 volts was selected as the optimum voltage.

Maintaining the voltage constant at 3900 volts, the pulse height settings were varied from 0.20 to 5.0 at small increments. At each increment 1023 one-second counts were taken. The average counts per second for each increment in voltage were plotted in Figure 11.

3. Voltage Curve (Neutrons from the Pu-Be Source in the Presence of a Cobalt 60 Gamma Source). While maintaining the same neutron source and detector geometry as in the tests mentioned above, a Cobalt 60 gamma source was placed near the neutron detector. The gamma radiation at the detector was measured to be two roentgens per hour. With the discriminator setting at 0.50, and utilizing the same procedure as Section V. C. 1 above, a plot of average counts per second versus voltage was obtained, and is shown in Figure 12.

Upon examination of the curve a voltage of 3900 volts was selected as the optimum to perform the final pulse height distribution curve.

4. Pulse Height Distribution (Neutrons from the Pu-Be Source in the Presence of a Cobalt 60 Gamma Source). Maintaining the voltage constant at 3900 volts, and the same detector - source geometry as in Section V. C. 3 above, the pulse height settings were varied from 0.20

to 5.0 at small increments. At each increment 1023 one-second counts were obtained. The average counts per second for each increment in pulse height were plotted in Figure 13.

D. Results - Final Instrument Settings

From the results of the calibration procedures mentioned in Sections V. C. 1 through V. C. 4 the following final equipment settings were obtained and used throughout the performance of this research:

High Voltage Setting: 3900 volts

Discriminator (Pulse Height) Setting: 0.50 volts

Coarse Gain: 32

Fine Gain: 0.95

SECTION VI

RANDOM SOURCE STATISTICS

A. General Criteria

Once the nuclear instrumentation has been calibrated as shown in Section V, it is necessary to demonstrate that the instrumentation and system is functioning properly. A convenient way to demonstrate the soundness of the counting system and data reduction methods is to perform an experiment with the Pu-Be neutron source alone, which is a perfect random source, and hence, the variance-to-mean ratio must be unity for all counting times selected.

B. Theory

Assuming a typical Poisson distribution for random series of events as:

$$P(x) = e^{-\mu}\mu^{x}/x\,!\;; \quad x = 0, 1, 2, \ldots \tag{6.1}$$

It may be shown that,

$$\sum_{x=1}^{x=\infty} P(x) = 1 \tag{6.2}$$

$$\bar{x} = \mu \tag{6.3}$$

and:

$$\sigma^2 = \mu \tag{6.4}$$

consequently the variance-to-mean ratio is:

$$\frac{\bar{x}^2 - (\bar{x})^2}{\bar{x}} = \frac{\sigma^2}{\bar{x}} = 1 \tag{6.5}$$

C. Experiment to Check Out Equipment

With the equipment as described in Section V. C. 1, and as shown in Figure 1, but with the BF_3 detector out of the core and placed next to the Pu-Be neutron source inside of a paraffin block, 1023 separate counts were taken for each gate opening, and gate openings ranged from one decimillisecond (10^{-4} sec) to 1.0 second.

The data obtained were reduced by the computer program described in Section X, and by the methods used during the actual variance-to-mean experiment with the UMR core. The results of this test are listed in Table I, and the value for the variance-to-mean is in the range of 1.1077 to 0.8913 with a confidence of 99 percent.

This experimental checkout of the equipment was performed repeated times throughout the duration of the experiments, and in particular prior to actual experimentation with the UMR core, in cases when, due to reactor availability needs for other experimenters, the author was required to remove his equipment from the UMR core for several weeks.

SECTION VII

CALCULATION OF THE PHYSICS PARAMETERS FOR THE UNIVERSITY OF MARYLAND REACTOR

A. General

Included in this research are the analysis of presently available computational techniques to calculate the reactivity of the University of Maryland Reactor (UMR). For the purpose of analysis and calculation of the main core parameters, two UMR core configurations were studied, namely, the first critical core, and the present core.

In general, after the calculation of the core volume fractions for the different core regions, an iterative procedure computer code PDQ-2 was used in conjunction with two spectral codes for cross section data: TEMPEST-II for the one thermal neutron group and GAM-1 for the fast three groups.

By means of the iterative procedure, which will be discussed later in detail, the multigroup cross-section data were obtained. A detailed geometrical mock-up of the core, Figure 14, was made and programmed for use with the PDQ-2 multigroup, multiregion, diffusion code.

The iterative technique for the PDQ calculations gave the critical eigen value, $\lambda = K_{eff}$, for the just critical mass of the first core.

The same parameters were used in the calculation of the present UMR core. The calculated eigen value, K_{eff}, was in agreement with the

measured core K_{eff} within 0.20% $\Delta K/K$.

The present UMR core physics parameters calculated in this section, were obtained from the cross section data used in the final PDQ-2 computer calculation mentioned above.

B. Volume Fractions and Atomic Densities for the Different Core Compositions

The physical data of the University of Maryland Reactor were obtained from the as-built reactor drawings, Table II, prepared by the Allis-Chalmers Manufacturing Company, manufacturer of the UMR.

The physical and mechanical features and dimensions of the UMR are listed in Table III. The description of the location of the reactor fuel cans and their contents as arranged in the UMR full core are listed in Table IV.

From the information given in Tables III and IV the composition mixtures for the different core regions were obtained as listed in Table V and their respective core locations are shown in Figure 14.

The actual composition definition and distribution for the UMR used with the PDQ-2 calculations are indicated in Figure 15, which shows the actual computer print-out of the material compositions for the different regions of the fully loaded UMR core.

The volume fractions for the different core compositions were obtained on a per unit height basis, assuming that the core has no axial discontinuities of its cross sectional layout, and that no appreciable fuel burn-up or fission product accumulation has taken place, since it is a

fresh core.

The composition volume fractions and atomic densities used with the spectral code calculations are listed in Table VI.

C. Calculation of the Cross Sections for the UMR Core Material Compositions

As indicated, the atomic densities given in Table VI were used as input for the thermal spectral code TEMPEST-II and the fast spectral code GAM-I.

Both codes were used on the University of Maryland IBM-7094 computer. TEMPEST-II calculates the thermal neutron flux spectra for each individual composition based upon the Wigner Wilkins equation for light moderators, the Wilkins equations for heavy moderators, and the Maxwellian distribution. After arriving at the neutron spectrum, TEMPEST-II calculates and provides effective one group microscopic and macroscopic cross section averaged over that spectrum (from 0 ev. to 0.414 ev.) for each material in the composition assuming a homogeneous mixture.

To account for the heterogeneity of the material in the core, an independent calculation of the disadvantage factors for the regular fuel and the spiked fuel elements was performed by means of a transport calculation using a P-3 transport computer code on the Allis Chalmers Manufacturing Company Bendix G-15 computer. The following values were obtained:

	Regular Fuel Plate	Spiked Fuel Plate
Moderator Disadvantage Factor		
$\bar{\Phi}$ Moderator/$\bar{\Phi}$ Fuel	= 1.036	1.018
Clad Disadvantage Factor		
$\bar{\Phi}$ Clad/$\bar{\Phi}$ Fuel	= 1.040	1.020

Where: $\bar{\Phi}$ = average neutron flux in the moderator, clad or fuel.

The final disadvantage-factor-weighted thermal cross sections used in PDQ were obtained by multiplying the disadvantage factors shown above, times the TEMPEST-II cross sections, which assumed homogeneity of the materials.

The neutron-spectrum for the core-fuel mixture, as obtained from the TEMPEST-II code, is plotted in Figure 16. The most probable energy, E_o, of this spectrum is 0.028 ev. A Maxwell-Boltzmann spectrum with a most probable energy, E_o, of 0.028 ev. was calculated and found to fit this spectrum almost exactly. The average energy of this spectrum, E, is thus:

$$\bar{E} = (4/\pi) \times E_o = 0.03565 \text{ ev.} \qquad (7.1)$$

and the effective neutron temperature, Tn, is:

$$T_n = \frac{\overline{E}\,(\text{ev.})}{k} = \frac{0.03565 \text{ ev.}}{8.61 \times 10^{-5} \text{ ev/K}^\circ} = 413^\circ\text{K} \qquad (7.2)$$

where k is the Boltzmann constant.

The GAM-I code was used to obtain three group effective macroscopic cross sections for the spectral range from 0.414 ev. to 10 Mev.

The selected groups were:

Group 1 - from 10 Mev. to 454 ev.

Group 2 - from 454 ev. to 3.93 ev.

Group 3 - from 3.93 ev. to .414 ev.

The cross section library, which is stored in the GAM-I, contains 68 energy or lethargy groups for each nuclide.

In order to obtain an accurate set of fast cross section data, the following iterative procedure was as follows:

A preliminary GAM-I run was performed utilizing the atomic densities of composition 1 (regular fuel). A fast axial buckling, B_z^2, was hand calculated, assuming an extrapolation length, L, based on the fast transport cross section for the fuel-water mixture, Σ_{tr}^{fast}. Utilizing the B-1 approximation option in the GAM-I slowing down code, which required as input a value for square root of the fast buckling, B_z, an initial run was performed and the three group macroscopic cross-sections were obtained for all the core compositions. An X-Y PDQ calculation was performed on the just critical core configuration (which was composed of regular fuel only) utilizing the preliminary calculations

of the fast group cross-section, and the independently (TEMPEST-II) calculated thermal cross-section. The axial buckling input to the PDQ-2 was based on the fast transport cross section obtained from the preliminary GAM-I run, by the following relation:

$$B_z^2 = \left[\frac{\pi}{60 + 2 \times \frac{0.71}{\sum_{tr}^{fast}}} \right]^2 \qquad (7.3)$$

After three iterations of the value of B_z^2, an eigen value $\lambda = 1.0$, solution of the multiregion, multigroup diffusion equations by means of PDQ-2 was obtained. Placing the final value for the fast buckling of 0.00255 cm^{-2} as input to GAM-I and utilizing the B-1 option, the final three group core cross section data were obtained, and the final PDQ calculations performed to verify these data on the critical core and the fully loaded core. The computer calculated cross sections for the different core compositions of the UMR core are given in Table VII.

D. Calculation of the UMR Full Core Cold Clean K_{eff}

The cross-section data described in Table VII were then utilized as input to the PDQ-2 computer code. PDQ-2 is a code programmed to solve the neutron diffusion equations for one to four lethargy groups over a rectangular region of the x-y plane or cylindrical r-z plane. Figure 14 shows the selected geometrical mock-up of the core and

Figure 15 the PDQ-2 print out of the distribution of the core compositions. A total of 74 mesh points were utilized in the x-direction (west-east) and 60 in the y-direction (north-south). An axial buckling of 0.00255 cm^{-2} was used as calculated from the cross section data obtained from the GAM-I code. The effect of the axial buckling in the calculations is to represent the core size for leakage purposes in the axial direction.

The output of PDQ-2 calculation gave a value of K_{eff} of 1.0144. Given in Table VIII is a list of the composition integrated areas and composition integrated fluxes for all the groups and all the regions, as well as composition averaged fluxes, as obtained from the final PDQ-2 calculations of the UMR full core. These values of the fluxes were used to obtain effective cross-sections to calculate the individual UMR core physics parameters, as shown in the following sections.

E. Calculation of the UMR Core Parameters

1. η - The Average Number of Neutrons Produced Per Thermal Neutron Absorbed in the Fuel.

$$\eta = \frac{\sum_{i,j} (\nu \Sigma_f)^{i,j} \Phi^{i,j} V^j}{\sum (\Sigma_a^{fuel})^{i,j} \Phi^{i,j} V^j} \qquad (7.4)$$

where:

i = number of energy groups = 4

j = number of core regions = 28

ν = effective number of neutrons liberated per fission in each energy group

Σ_f = effective fission cross-section for each group and region

Σ_a = effective absorption cross-section for each group and region

Φ = effective flux for each group and region

V = effective volume for each region

η was calculated from the output of GAM-I and TEMPEST-II, since these codes give individual microscopic cross sections for each material and each region. The number densities cancel.

$\nu\Sigma_f$ values are also obtained from the spectral codes and they are given as integral values. The volume weighted fluxes were obtained from the PDQ-2 output, as given in Table VIII. A value of $\eta = 2.0371$ was thus calculated.

2. K$_\infty$ Infinite Multiplication Factor. The infinite multiplication factor for the UMR cold clean full core was obtained from the following formula:

$$K_\infty = \sum_{i,j} (\nu\Sigma_f)^{i,j} \Phi^{i,j} V^j / \sum_{i,j} \Sigma_{a_{total}}^{i,j} \Phi^{i,j} V^j \qquad (7.5)$$

Where: Σa_{total} = absorption cross-section for each group and for each region for all the materials of the core. A value of $K_\infty = 1.712$ was thus calculated.

3. f - Thermal Utilization. The thermal utilization was obtained

simply by the ratio K_∞/η since the fast fission factor, ϵ, and the escape resonance probability, p, are equal to 1.0 for the fully enriched fuel. Hence f = 1.7120/2.0371 = 0.8404.

4. τ - Fermi Age. The effective Fermi Age, τ, for the UMR cold clean full core was obtained from the formula:

$$\tau = \frac{\sum_{i,j} (\Phi^{i,j} V^i / 3\Sigma_{tr}^{i,j} \Sigma_R^{i,j})}{\sum_{i,j} \Phi^{i,j} V^j} \qquad (7.6)$$

Where:

$\Sigma_{tr}^{i,j}$ = effective macroscopic transport cross-section for each group and each region

$\Sigma_R^{i,j}$ = effective macroscopic removal cross-section for each group and each region.

The value of τ = 49.2 cm^2 was thus calculated for the cold clean full core Fermi Age.

5. L^2 = Thermal Diffusion Area. The effective diffusion area was obtained from the following equation:

$$L^2 = 1/3\ \overline{\Sigma}_{tr}\ \overline{\Sigma}_a \qquad (7.7)$$

A value of L^2 = 3.425 cm^2 was obtained from the cross-section data.

6. B^2 Buckling. From the parameters described and calculated above, one can obtain an effective one group buckling for the cold clean full core from the following relation:

$$K_{eff} = \frac{K_\infty \, e^{-\tau B^2}}{1 + L^2 B^2} \qquad (7.8)$$

K_{eff} was obtained from the PDQ-2 calculated excess reactivity of the core, namely 1.0144. Solving equation (7.8) for B^2, the value of 0.00996 cm^{-2} was obtained for the UMR full core one group buckling. Figure 17 shows the one group buckling for different UMR core sizes, i.e., buckling as a function of the effective core multiplication constant, since K_∞, τ and L^2 are independent of core size.

7. β_{eff} - The Effective Delayed Neutron Fraction. The effective delayed neutron fraction (β_{eff}) is the main factor to correlate measured reactivity with calculated values; hence all correlation between calculated and measured values are always subject to the accuracy of β_{eff}. Since delayed neutrons are born with a lower average energy than that of prompt neutrons, they will have a smaller age to thermal and, hence, a smaller probability of leaking while slowing down than the prompt neutrons. The ratio of the effective delayed neutron fraction to the delayed neutron fraction for infinitely large reactors is given in reference 11, as:

$$\frac{\beta_{eff}}{\beta} = \frac{1}{(1 - \beta) \, e^{-(\tau_p - \tau_d) B^2} + \beta} \qquad (7.9)$$

or for six groups of delayed neutrons:

$$\beta_{eff} = \sum_{i=1}^{i=6} \beta_{eff_i} = \sum_{i=1}^{i=6} \frac{1}{\frac{1 - \beta_i}{\beta_i} \, e^{-(\tau_{p_i} - \tau_{d_i}) B^2} + 1} \qquad (7.10)$$

Where:

B^2 is the buckling = 0.00996 cm^{-2}

β_i = fraction of delayed neutrons of the i-th group for an infinite reactor.

τ_{p_i} = age to thermal of prompt neutrons of the i-th group.

τ_{d_i} = age to thermal or the delayed neutrons of the i-th group.

The values for the delayed neutron fraction for six groups are listed in Table IX and were obtained from reference 11.

The values of the thermal age for the different delayed neutron energies were obtained by means of the GAM-I code. This code has the option of calculating the spectrum of a monoenergetic source in a given material mixture. Figure 18 shows τ, the Fermi Age to thermal energy, as a function of neutron energy for the UMR core and for water. From these values and from equation (7.10) shown above one gets the corresponding K_{eff} for the different core sizes. Figure 17 shows the effective delay neutron fraction for different core sizes. The value obtained for the full UMR core β_{eff} is 0.008693 and for the just critical UMR core β_{eff} is 0.008758.

8. ℓ^* Prompt Neutron Lifetime. The effective prompt neutron lifetime ℓ^*, for the thermal range was obtained from the following relation:

$$\ell^* = \frac{1}{\overline{V} \sum_a^{core} (1 + L^2 B^2)} = 45 \text{ microseconds} \qquad (7.11)$$

Where:

$\overline{V}$ = effective average neutron velocity

= 2.6×10^5 cm/sec (obtained from the core spectrum, Figure 16).

$\sum_a^{core}$ = effective total core macroscopic absorption cross-section

= 0.08709 cm^{-1}

L^2 = thermal diffusion area = 3.425 cm^2

B^2 = the total core buckling = 0.00996 cm^{-2}

F. Summary of the UMR Core Physics Parameters

The following is the summary of the calculated UMR cold clean core physics parameters:

η = 2.0371

ϵ = 1.0000

p = 1.0000

f = 0.8404

L^2 = 3.4250

τ = 49.2000

K_∞ = 1.7120

K_{eff} = 1.0144

β_{eff} = 0.008693 (full core)

β_{eff} = 0.008758 (critical core)

ℓ^* = 45 microseconds

SECTION VIII

CONTROL ROD CALIBRATION IN THE FULL UMR CORE

A. General Theory

The variation of the neutron flux with time at a point $\underline{r}$ in a reactor, upon the introduction of a step reactivity $\Delta k/k$ at time $t = 0$, can be written (reference 12) as:

$$\Phi(\underline{r}, t) = A_o e^{tw_o} + A_1 e^{tw_1} + \ldots A_i e^{tw_i} + \ldots A_m e^{tw_m} \tag{8.1}$$

where:

$w_o, w_1 \ldots w_m$ are the $m + 1$ roots of the equation

$$\frac{\Delta K}{K_{eff}} = \frac{\ell^* W}{\ell^* W + 1} + \frac{1}{\ell^* W + 1} \sum_{i=1}^{i=m} \frac{W \beta_i \epsilon_1}{W + \lambda_i} \tag{8.2}$$

A_o, A_1 etc. are constants determined by the initial conditions of the reactor,

ℓ^* = effective lifetime of the thermal neutrons in the reactor

β_i = fraction of the total number of neutrons which are delayed neutrons of the i^{th} group in an infinite medium

λ_i = the decay constant of the i^{th} group of delayed neutrons

$\epsilon_i \beta_i$ = effective fraction of delayed neutrons of group i in the reactor

For positive reactivities, w_0 is positive, and w_1, $w_2 \ldots w_m$ are negative. As t increases, the contributions of all terms beyond the first on the right of equation (8. 1) decrease rapidly to zero - i. e., these terms make a transient contribution to the neutron flux and soon become negligible compared to the first term. Hence, after a very short time interval, equation (8. 1) reduces to:

$$\Phi(\underline{r}, t) = A_0 e^{t w_0} \tag{8. 3}$$

and since w has the dimensions of the reciprocal time:

$$\Phi(\underline{r}, t) = A_0 e^{t/T} \tag{8. 4}$$

Thus, T is the reactor period after the lapse of sufficient time to permit the contributions of the transient terms to damp out, and is called the stable reactor period.

Upon the introduction of $T = 1/w$ in equation (8. 2) the following relationships between reactivity and stable period are obtained:

For the infinite core:

$$\rho = \frac{\ell^*}{T K_{eff}} + \sum_{i=1}^{i=6} \frac{\beta_i}{1 + \lambda_i T} \tag{8. 5}$$

For the finite core:

$$\rho = \frac{\Delta K}{K_{eff}\, \beta_{eff}} = \frac{\ell^*/\beta_{eff}}{T K_{eff}} + \sum_{i=1}^{i=6} \frac{\beta_i}{\beta} \frac{1}{1 + \lambda_i T} \tag{8. 6}$$

where:

$$\beta = \sum_{i=1}^{i=6} \beta_i \tag{8.7}$$

and,

$$\beta_{eff} = \sum_{i=1}^{i=6} \epsilon_i \beta_i \tag{8.8}$$

or,

$$\beta_{eff} = \epsilon \sum_{i=1}^{i=6} \beta_i \quad \text{if} \quad \epsilon_1 = \epsilon_2 = \text{---} \; \epsilon_6 = \epsilon \tag{8.9}$$

i. e., if all delayed neutron groups have the effectiveness (ϵ)

$$\beta_{eff} = \epsilon\beta \tag{8.10}$$

The neutron flux behavior after the introduction of a step change of reactivity at time t = 0, i. e., equation (8. 1), is shown in Figure 19, and indicates the transient and stable behavior of the neutron flux.

Equations (8. 5) and (8. 6) are useful to determine small step reactivities, if it is possible to measure the stable period shortly after the step change in reactivity. Figure 20 is a graphical representation of the stable period term of this equation solved with the constants (reference 11) appearing in Table IX (Section VII), and indicates reactivity in percent $\Delta K/K$ versus stable reactor period in seconds for an infinite size reactor and the finite UMR full core.

B. Control Rod Calibrations - Single Rod Calibrations

Prior to the calibration of a particular rod, the reactor was brought critical on the three rod bank at the lowest power possible. All control rod calibration experiments were performed in the 0.1 to 10 watts range, so as to assure a power level above source range interference, and low enough so that no significant heating of the UMR core occurs, thus eliminating any reactivity losses due to the negative temperature coefficient.

With criticality maintained at approximately the same power level, the rod being calibrated was placed in a nearly fully inserted position, and the reactor was maintained critical by simultaneously compensating for reactivity reduction by withdrawing the other two rods as a bank.

A critical position was carefully established and the control rod positions, time, and water temperatures were recorded. The reactor power was then reduced to about one decade below the critical range by further insertion of the control rod being calibrated, and immediately thereafter the rod was withdrawn to a predetermined position to make the reactor supercritical and induce a stable period of the order of 40 seconds.

After the transient power increase ceased, the reactor stable period was obtained by recording the doubling time of the reactor power increase, as indicated on the linear power recorder. This procedure was repeated to give at least three calibration points in that range of the control rod. The procedure was repeated for other rod positions over its entire

range of withdrawal.

The reactor period T, in terms of the doubling time t_d is given by:

$$T = \frac{t_d}{0.693} \text{ seconds} \qquad (8.11)$$

The reactivity in % ΔK/K, corresponding to a period of T seconds, was obtained from Figure 20.

The worth of the rod applied to the mid-interval of the control rod travel between the critical and supercritical withdrawal positions is therefore:

$$\text{rod worth} = \frac{\rho}{x_2 - x_1} \text{ \% } \Delta K/K \text{ per cm, at } \frac{x_2 + x_1}{2} \text{ cms} \qquad (8.12)$$

where x_1 is the critical and x_2 is the supercritical withdrawal position of the rod.

A plot of control rod worth in % ΔK/K per cm versus average withdrawal position was obtained for each rod in the range of its maximum insertion in the critical core to its full withdrawal. Symmetry was assumed for the total control rod worth. By integrating under the area of each of these curves, the integral control rod worth curves were obtained.

The actual control rod worths for the UMR full core can be obtained from the values plotted in Figures 21, 22, and 23 for the infinite core, multiplied by the ratio of:

$$\frac{\beta \text{effective UMR full core}}{\beta \text{infinite core}} = \frac{0.008693}{0.006398} = 1.358 \qquad (8.13)$$

For reactivity measurements on smaller cores during the loading and unloading of the core, the following ratio was applied to obtain rod worths:

Rod worth in small core = rod worth infinite core x.

$$x \frac{\beta \text{effective for small UMR core}}{\beta \text{ infinite core}} \qquad (8.14)$$

where the effective delayed neutron fraction for small UMR cores was obtained from equation (7.10), which is plotted in Figure 17 for the different UMR core sizes to be studied in Sections IX and X.

SECTION IX

REACTIVITY MEASUREMENTS OF UMR SUPERCRITICAL CORES BY CONVENTIONAL METHODS AND COMPARISON WITH CALCULATED VALUES

A. Objective

The reactivity of the UMR full core and two smaller supercritical core were to be measured by conventional methods and results compared with calculated values obtained by the analytical technique described in Section VII.

B. Prerequisite Conditions

During the performance of the measurements of the reactivity of the core encountered during the unloading and loading of the UMR, all the safety criteria applicable to the UMR was enforced.

The Plutonium - Beryllium startup source was located in core position B-3, see Figure 2. The reactor water level was at seven inches below the top of the tank, and the reactor pool water purity was as specified in the UMR operating manual. Reactor water temperature was at ambient conditions. The BF_3 detector was positioned in the Glory Hole, and in order to verify that it was always placed in the same core location, rods were pulled by the normal startup procedure to the just critical core condition. The rod bank position was verified before data taking.

The UMR console equipment was checked by the normal pre-startup procedures before startup and the special statistics equipment was also checked prior to any reactor startup and data taking. The UMR experimental facilities were filled with paraffin as needed to simulate the flooded condition desired.

All the nuclear instrumentation remained in operation at all times during the loading and unloading operations and tests. Any abnormal response or behavior of any of the nuclear instrumentation, i.e., the startup channel, log N channel, linear channel and safety channel required an immediate discontinuation of the loading or unloading operations until a clear understanding was had of the abnormal behavior, and continuation of the test was not started until after proper corrective action had been taken. All reactor scram circuitry was routinely tested.

Also the concept of "cocked safety" was utilized as an added safety factor during the tests. Shim rod #2 was withdrawn to 20 cm from the bottom of the core and held at that position while shim rod #1 and the regulating rod were maintained fully inserted. This technique allowed the insertion of negative reactivity in case of scram signal requirements.

A complete record was kept at all times of each fuel element movement from the core to storage and back to the core.

One licensed UMR operator was at the reactor control console at all times during the performance of all the tests, see Figure 8. The operator determined the mode of operation, and in particular limited and directed the unloading and loading of the fuel and reflector elements.

One operator, experienced in the handling of the UMR fuel handling tool, moved the fuel and reflector elements from the pool bridge, following instructions by the console operator. The author was an UMR reactor licensed operator and was aided in the performance of all the tests by the UMR reactor operations staff. The experimental facilities of the UMR, i.e., the through tube and the east and west beam ports (see Figure 2) were maintained filled with paraffin plugs as needed during the tests with small cores to simulate fully reflected conditions.

C. General Procedures for Reactivity Measurements by Conventional Techniques

After all the prerequisite conditions discussed in Section B had been met, and once a desire core full configuration had been obtained, three five minute counts were taken with the startup chamber, and the average count per minute was calculated and recorded.

The control rods were pulled out of the core one at a time, approximately 3 centimeters. At all times were maintained in a bank, i.e., their respective distance from the core bottom was maintained to within 3 cm. of each other. When criticality was obtained, at approximately 0.8 watts power level, the control rods were adjusted so as to maintain criticality with all the rods at the same distance from the core bottom. This was done to maintain a normal core flux radial distribution, and hence the rod worth was not affected.

The final positions of the control rods were recorded and the excess reactivity of each core was obtained from the worths of the control rods

calibrated in Section VIII.

During the performance of the tests, the last core configuration reactivity that was measured any one day, was again measured first the following day of experimentation, to verify that all core conditions were equal, and thus continuity of the data was insured.

D. Measurement of the UMR Full Core Reactivity and Comparison With the Calculated Values

By the procedures outlined in Section C above, the UMR full core with the experimental facilities empty was made critical at a power level of 0.8 watts, at 70°F reactor water temperature, and all the control rods withdrawn to 46.135 cm. from the bottom of the core.

Hence, with all the rods at 46.135 cm., the excess reactivity of the UMR full core was as follows:

	Reg. Rod	Rod #1	Rod #2
Total Worth	0.358% ΔK/K	2.00% ΔK/K	3.60% ΔK/K
Worth at 46.135 cm	0.314% ΔK/K	1.80% ΔK/K	3.23% ΔK/K
Core Reactivity Controlled by the Rods	0.044% ΔK/K	0.20% ΔK/K	0.37% ΔK/K

Hence, the total excess reactivity in the core was:

$$\rho_{total} = 0.0440 + 0.20 + 0.37 = 0.614\% \Delta K/K$$

The value corrected by the ratio of the UMR effective delayed neutron fraction to the infinite core delayed neutron fraction was:

$$\rho_{UMR_{core}} = 0.614 \times \frac{0.008693}{0.006398} = 0.834\% \ \Delta K/K$$

And, therefore,

$$K_{eff} = 1.00841$$

Now, this value of $K_{eff} = 1.00841$ corresponds to the full UMR core with the beam ports and through tube empty and nothing but water in the two irradiation spaces. As pointed out in Section IV. B. 2, the detector in the Glory Hole was arranged so as to not increase or decrease reactivity in the UMR core. Flooding (or filling) the experimental facilities with water (or highly hydrogeneous material) was measured (reference 2) to increase the core excess reactivity by 0.368% ΔK/K. Therefore the value of the excess reactivity of the UMR assuming fully flooded experimental facilities is 1.202% ΔK/K and hence, $K_{eff} = 1.0121$.

As reported in reference 2, the excess reactivity of the UMR with the fully flooded experimental facilities would be 1.22% ΔK/K, and hence, the K_{eff} of the core was 1.0124. The difference in values of reactivities is 0.018% ΔK/K. This difference can be attributed, perhaps, to slight fission product accumulation, slight difference in the core temperature during the two measurements, slight difference in the positioning of the fuel elements in the core when they have been removed and placed back in the core, or ultimately, difference of positioning of the rods in the core, or different tachometer reading for the same rod positions.

Hence, finally a value of K_{eff} = 1.0121 is accepted as the present K_{eff} value for the UMR operating core with the experimental facilities full of hydrogenous material.

Full Core with Facilities Flooded

K_{eff} = 1.0121 ρ = 1.202% $\Delta K/K$

Full Core with Facilities Empty

K_{eff} = 1.00841 ρ = 0.834% $\Delta K/K$

The calculated K_{eff} for the UMR with fully flooded experimental facilities utilizing the technique and methods outlined in Section VII, is 1.0144, and ρ = 1.42% $\Delta K/K$. Consequently, the difference between the calculated and measured reactivities is 0.218% $\Delta K/K$ for the present UMR core.

Since the analytical calculation of K_{eff} was based on fresh fuel (new fuel) and exact mathematical core positioning of fuel it appears that the calculational value of ρ = 1.42% $\Delta K/K$ approaches the earlier experimentally indicated value of the UMR core of 1.22% $\Delta K/K$, and hence an accuracy of calculated and experimental value are thus obtained to within 0.2% $\Delta K/K$, which is within the accuracy of the analytical model.

E. Reactivity Measurements with Smaller UMR Supercritical Cores and Comparison with Calculated Values

To further demonstrate the predictability of the UMR core reactivity by the calculational methods described in Section VII, two slightly supercritical smaller UMR cores were measured by the technique

described in Section D above and compared with the calculated results.

The actual steps leading to the smaller UMR supercritical cores are listed in Table X and shown in Figures 24 and 25. The results of measured and calculated values are shown in Tables XI and XII.

It was concluded that the analytical parameters and methods used to calculate the reactivity of the UMR cores is satisfactory to within 0.2% $\Delta K/K$. Consequently, the analytical prediction of the UMR subcritical cores can be obtained to within the same accuracy of 0.2% $\Delta K/K$, since in the utilization of the PDQ-2 computer technique, the neutron leakage in the x-y plane is accurately calculated, and the axial neutron leakage remains constant for smaller cores, since the fuel element height is constant.

SECTION X

REACTIVITY MEASUREMENTS BY STATISTICAL PROCESSES

A. Description of Statistical Data Measurements

1. Obtainment of Raw Statistical Data. With the experimental equipment as described in Section IV, and after calibration of the equipment as described in Sections V and VI, the same procedure was followed to obtain statistical data for each UMR core condition studied.

A period of about 15 minutes after each change in the UMR core condition was allowed to achieve neutron flux stability and equilibrium core conditions before statistical data were gathered.

The pulses from the BF_3, located in the center Glory Hole of the UMR, were counted with the TMC Model 214 gate scaler. Gate openings of 0.0001, 0.0005, 0.001, 0.01, 0.1 and 1.0 seconds were selected. Each gate opening was repeated 1023 times, and the number of pulses per opening was recorded in the Hewlett-Packard Digital Recorder.

The recorder had two modes of output: a) direct paper-tape print-out of the number of pulses recorded for each gate opening of the gate scaler, or b) paper-tape print-out of the sum of the pulses recorded for each gate opening, i.e., sum from i = 1 to i = 1023 of C_i, where C_i is the number of pulses recorded for each gate opening. Both recorder outputs were utilized.

2. Processing of Statistical Data. As it is evident from what is stated above, the amount of data gathered for each UMR core condition was of large proportions, actually a minimum 6138 pieces of data for each case, and consequently, great care of coordination and recording was needed to maintain adequate records.

To process the data to obtain the variance-to-mean ratio defined in Section III, for each case, a FORTRAN-II program was written, see Appendix 1, for use with the University of Maryland IBM-7090.

The data were transferred from the paper-tape to IBM computer cards. To quickly ascertain that all the statistical data for each gate opening had been accurately recorded in the IBM cards, each case was identified in the computer by a title card which described the case condition studied, the gate opening for which data was being analyzed, and the average number of pulses for that particular case, see Appendix 2. The average number of pulses was obtained by dividing the integral number of pulse output from the recorder by the number of gate openings (1023).

If the IBM-7090 calculated average number of pulses was equal to the prior calculated average, the computer proceded to calculate the standard deviation and the variance-to-mean ratio as defined in Section III.

The computer program also allowed calculation of the standard deviation and variance-to-mean ratio for gate openings in between those measured with the equipment. Data for the in-between gate openings

were generated by the computer by summing sequential number of counts for each gate opening. This technique is valid for the range of gate openings from0.001 seconds and above, since the scaler dead counting time between two consecutive gate openings is of the order of 20 micro-seconds. The error is of the order of 2.0% for 0.001 seconds gate opening, 0.2% for 0.01 seconds gate opening, etc. For example data for 2.0-second gate opening, were obtained by adding consecutive 1.0-seconds counts, thus obtaining 1023/2 bits of data for 2.0-seconds gate opening, see Appendix 3.

The IBM-7090 computer program was checked by actual hand calculation of one complete case.

B. Determination of Counting Equipment Efficiency - ϵ

It is evident from equation (3.14) that to obtain reactivity, ρ, directly from the variance-to-mean measurements, one must determine the value for the counting equipment efficiency, ϵ, which is a constant for all cases, since the BF_3 detector was always located in the center Glory Hole of the UMR core and the same equipment was used in all the experiments, see Appendix 4.

To obtain, ϵ, statistical data were obtained and processed as described above for three UMR full core subcritical conditions, (see Figures 31, 32, and 33) namely with the control rods banked at 45 cm, 42 cm, and 35 cm from the core bottom. The degree of subcriticality or negative reactivity ($-\rho$) for each was obtained from the calibration of the control rods.

For example with the rods banked at 45.0 cm, shim rod #1 controls 0.24% $\Delta K/K$ (see Figure 21), shim rod #2 controls 0.42% $\Delta K/K$ (see Figure 22) and the regulating rod controls 0.05% $\Delta K/K$ (see Figure 23). All shim rods control 0.71% $\Delta K/K$. Multiplying this value by the ratio of β_{eff} full core/$\beta_{infinite\ core}$, or 1.358 for the full UMR core, one obtains the actual reactivity controlled by the shim rods, i.e., 0.964% $\Delta K/K$.

Subtracting 0.834% $\Delta K/K$, the UMR core excess reactivity with the experimental facilities empty (since this experiment was done without paraffin simulation in the experimental facilities), one gets the actual degree of subcriticality with the rods at 45 cm i.e., ρ at 45 cm = -0.13% $\Delta K/K$.

Hence, by the same technique one gets:

ρ at 42 cm = -0.563% $\Delta K/K$

ρ at 35 cm = -1.822% $\Delta K/K$

Equation (3.14) was solved for ϵ, for various values of the variance-to-mean ratio and gate openings shown in Figure 31 through 33 for each core condition mentioned above, and an average value of $\epsilon = 2.4 \times 10^{-4}$ was obtained.

C. Reactivity Measurements from Statistical Data

1. Shutdown Margin Measurements. Normally the shutdown margin of a core represents the degree of subcriticality, $-\rho$, of the core with the rods at different levels of insertion in the core, and most frequently represents the degree of subcriticality of a core with all rods fully inserted.

There are several conventional methods of measuring shutdown margins. One method normally used during the first loading of a reactor, and prior to having performed full control rod calibrations, is the inverse multiplication method. This method consists of normalizing the inverse multiplication constant, M, to reactivity, and is described in Chapter 4 of reference 13.

Utilizing this method, the average count per second was determined with all rods banked at 45 cm, where $\rho = -0.13\%\ \Delta K/K$. Plotting this value, ρ, versus counts per minute in a log-log graph, one obtains a normalization of counts per second, versus reactivity (see Figure 34) by drawing a line at 45° angle through the plotted point since $\rho = -(1/M - 1)$. The values of ρ for rods banked at 45 cm, 42 cm, 35 cm were obtained from Figure 34, and are listed in Table XV.

Another method is the Schulz rod drop method, described in Chapter 5 of reference 13, first developed by H. F. Schulz, and applied to the UMR core by R. Weiner, reference 14.

Both of the above mentioned methods are highly sensitive to the neutron detector location in the core.

Another method to measure shutdown margins is used in this study by means of the variance-to-mean relation to reactivity as shown in equation (3.14), which is independent of core detector geometry.

The variance-to-mean minus one was plotted for various gate openings for the UMR rods banked at different core elevations, as shown in Figures 31, 32, and 33.

The shutdown margin, $-\rho$, for each case of rod banks was obtained by solving equation (3.14) at two different gate openings.

For example, from Figure 32, with all rods at 42 cm, the variance-to-mean minus one at 0.1 seconds gate opening is 0.85, and at 0.005 seconds gate opening is 0.425. Hence,

$$\frac{\left[V/M - 1\right]_{T = 0.005}}{\left[V/M - 1\right]_{T = 0.1}} = \frac{0.425}{0.85} = \frac{1 - \frac{1 - e^{-0.005\chi}}{0.005\chi}}{1 - \frac{1 - e^{-0.1\chi}}{0.1\chi}} \qquad (10.1)$$

where

$$\chi = \frac{\beta - \rho}{\ell} \qquad (10.2)$$

Equation (10.1) was solved by iteration, and since β and ℓ are known, ρ can be determined (see Appendix 5), independent of the counter efficiency ϵ.

Repeating the same technique for various gate openings, an average value of $\rho = -0.00502$ was obtained that satisfied equation (3.14) for the measured data for all rods at 42 cm.

Utilizing the same method, the shutdown margins, or negative reactivities, were obtained for rods banked at 45 cm, 42 cm, and 35 cm. The results are listed in Table XV and plotted in Figure 34.

Although statistical data were gathered for the case of all rods at 30 cm and $\rho = -3.00\%\ \Delta K/K$, the variance-to-mean obtained for gate

openings between 0.0001 and 0.1 seconds was of the order of one, which indicates that approximately -3.0% ΔK/K is the maximum negative reactivity that can be measured with the overall counting efficiency for the instrumentation used in this study.

Further accuracy could have been obtained with the same instrumentation if a larger number of gate openings would have been used. An error of 12 percent in the variance-to-mean obtained from 1023 gate opening per gate time, represented an error of 1.0% ΔK/K in reactivity in the case of all rods at 30 cm. The standard deviation of measured variance-to-mean values was of the order of 6 percent. Consequently, in order to obtain an accuracy of the variance-to-mean such that reactivity can be obtained to within 1.0% ΔK/K, approximately 36,000 gate openings are needed for each gate time, since error is inversely proportional to the square root of the number of data points.

The results shown in Table XV and Figure 34 indicate that the measurements of the shutdown margin by the variance-to-mean method are in agreement with the values obtained from the rod calibration method for negative reactivities of less than -1.00% ΔK/K, and within ten percent for negative reactivities of approximately -2.0% ΔK/K.

2. Small UMR Core Reactivity Measurements. Several subcritical UMR cores were obtained following the steps shown in Tables XIII and XIV, and in Figures 26 through 30, and according to the procedures outlined in Section IX.

Statistical data were gathered after each completed unloading step

in the same manner as described above.

The variance-to-mean ratio was obtained and plotted as a function of the gate opening time.

The results for cases 3-B and 4-B are shown in Figures 35 and 36. For core cases 5-B through 7-B, the variance-to-mean ratio obtained had values of less than one, indicating that the limits of the counting equipment efficiency had been reached, and consequently, the error in the statistical data collected was such that it did not permit resolution of the variance-to-mean equation for reactivity.

The subcriticality, or negative reactivity, of cores 3-B and 4-B was obtained by solving equation (3.14) for ρ (see Appendix 5), utilizing a value of $\epsilon = 2.4 \times 10^{-4}$. The corresponding effective delayed neutron fraction for the actual core size was obtained from Figure 17, and various values of variance-to-mean ratio and gate openings from Figures 35 and 36 respectively.

The calculated reactivities and effective multiplication constants for cores 3-B and 4-B are listed in Tables XVI and XVII, and compared with PDQ-2 calculated values for the same core conditions.

It is evident from Table XVII that the step in negative reactivity between cores 4-B and 5-B($\simeq$2.5% $\Delta K/K$), gives a total subcriticality of $\simeq$ -4.8% $\Delta K/K$, which is beyond the accuracy of the equipment and number of data points selected for this study as indicated above.

Examination of the results (see Appendix 6 and Table XVII) show that for UMR cores 3-B and 4-B the PDQ-2 calculated reactivities fall

within the range of the experimental reactivities for 99 percent confidence in the reactivity estimates. The mean of the experimental reactivities agrees with the PDQ-2 calculated values to within 6% for core 3-B and 8% for core 4-B.

D. Comparison of the Variance-to-Mean Method with Present Methods Used During Initial Reactor Fuel Loadings

The methods presently used for the safe determination of criticality during initial nuclear reactor fuel loadings have not changed from the performance of the first reactor fuel loading, Chicago Pile 1, CP-1, in 1942, by Dr. Enrico Fermi, to the fuel loading of modern large nuclear power plants (see note below).

In essence the methods consist in plotting the relative inverse counting rate of each neutron detector as a function of the total number of fuel assemblies loaded in the reactor core, or as a function of the moderator height in cases where the fuel is batch loaded without moderator material present in the core.

The form of the critical approach curves mentioned above depend in great extent on the neutron start-up source used and its location in

---

(Note: The author has directly participated in the initial fuel loadings of various nuclear reactors. Further, the author, in order to support the above statement, has checked the procedures used for initial fuel loading of a recent large nuclear power plant, Dresden Unit 2, which was initially fuel loaded by the General Electric Co. during the last quarter of 1969.)

the core, as well as on the position of the neutron detectors used to determine counting rates (flux levels). Normally the initial reference counting rate is that obtained from the detectors in the presence of the neutron source only in the core. The subsequent counting rates obtained after fuel addition to the core are normalized as multiples of the reference counting rate. This normalized count is called the multiplication factor of the neutron population.

Usually the neutron source is placed in the center of the core and fuel assemblies are added around it. The neutron detectors must be located where they can sample the over-all neutron flux of the fuel assembly obtained during the different steps in fuel loading. Further, the detectors must be located in such a manner as to be able to detect the changes in the neutron flux multiplication. However, due to the harmonic content of the neutron flux in the fuel assembly the critical approach curves can take two different shapes as shown below:

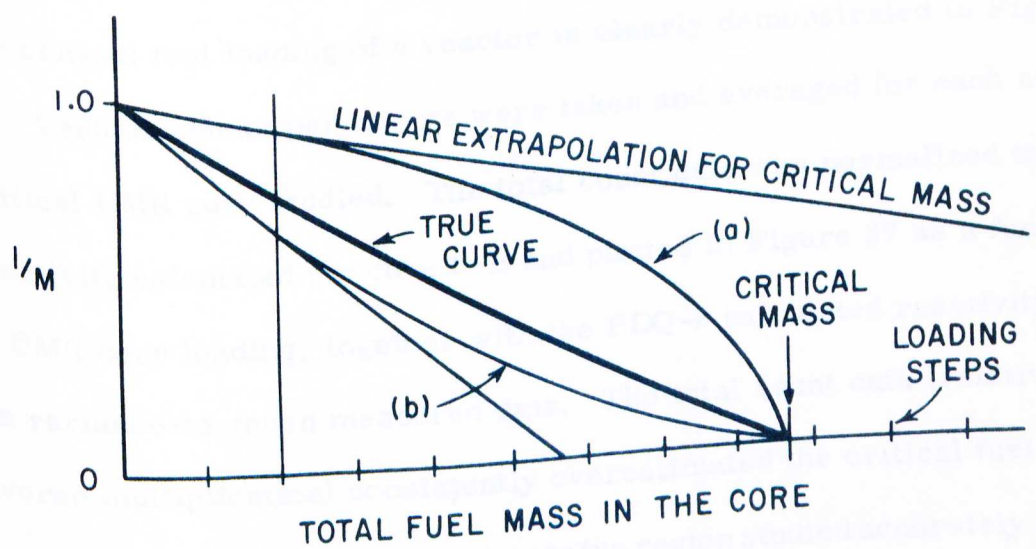

Curve (a) represents a highly undesirable arrangement of source and detectors, whereby linear extrapolation of the inverse multiplication factor (1/M) of neutron flux predicts an overestimate of the fuel loading required for criticality, and obviously this can lead to adding too much fuel between loading steps, thus creating a potentially hazardous condition. Normally, when such a curve is obtained during initial reactor loading, the loading is discontinued and the detectors relocated, after which the reactor loading is reinitiated.

Curve (b) represents a safe approach to criticality, since the linear extrapolation of the 1/M factor conservatively estimates critical fuel loading.

The true curve of 1/M factor is hard to achieve by these methods primarily because of the inherent inefficiencies in the detector sampling of the true neutron flux multiplication.

The superiority of the variance-to-mean method presented in this research over the relative inverse multiplication in safely determining the critical fuel loading of a reactor is clearly demonstrated in Figure 37.

Various counts per minute were taken and averaged for each subcritical UMR core studied. The total count data was normalized to the reactivity calculated for core 6-B and plotted in Figure 37 as a function of UMR core loading, together with the PDQ-2 calculated reactivity and the variance-to-mean measured data. The total count data (relative inverse multiplication) consistently overestimated the critical fuel mass; however, the variance-to-mean data in the region studied accurately predicted the critical loading of the UMR core.

SECTION XI

SUMMARY

The University of Maryland reactor core physics parameters have been calculated and measured in great detail in this study.

Agreement to within 0.2% $\Delta K/K$ has been obtained between the control rod measured and PDQ-2 calculated reactivities for the UMR full core, and smaller supercritical cores.

The statistical technique of the variance-to-mean ratio of the number of counts for various gate openings as a means to determine the degree of subcriticality, or shutdown margin, has been shown an effective method.

An accuracy of approximately 0.3% $\Delta K/K$ has been obtained between the negative reactivities measured by statistical methods and the PDQ-2 calculated values.

SECTION XII

CONCLUSIONS

It appears from this study that greater overall counting efficiency for the same amount of statistical data would permit more accurate measurements at larger degrees of subcriticality, perhaps in the region of -4.0% $\Delta K/K$ to -5.0% $\Delta K/K$.

The system utilized for the statistical data processing is exact, however cumbersome, due to the amount of data to process and the amount of peripheral hardware to be utilized in the reduction of the data.

It is the author's opinion that a system to measure negative reactivity continuously and directly could be devised by designing a small computer capable of accepting the output of a multichannel scaler similar to the one used in this study. The computer would have a fixed internal logic capable of calculating the variance-to-mean ratio for a fixed number of counts per gate opening, for various fixed gate openings from 0.0001 to 1.0 seconds. Also programmed in the computer logic would be the correlation between the variance-to-mean ratio and $(\beta - \rho)/\ell$. The counting efficiency, ϵ, would be determined for each specific counting system in a particular reactor, and would be a fixed parameter to the computer logic.

For reactivity measurements with a fixed core, i.e., shutdown margin measurements, changes in the control rod worth, or core

characteristics with fuel burnup, β and ℓ, would be approximately constant, and consequently, negative reactivity could be measured directly. It is important to point out that the variance-to-mean ratio technique allows reactivity measurements without the measurements being affected by the source-detector geometry.

The technique described herein should be an asset in determining the criticality of the small core assemblies obtained during normal initial reactor core fuel loadings, and hence would allow safe and accurate prediction of criticality.

APPENDIX I

FORTRAN II - COMPUTER PROGRAM TO CALCULATE THE VARIANCE-TO-MEAN RATIO

```
$EXECUTE        IBJOB
$ID   DIAZ,A.   *302/65/017*60M*800P$
$IBJOB          GO,SOURCE
$IBFTC MAIN     LIST,REF,DECK
      DIMENSION X(6000),Y(6000),TITLE(60)
2     WRITE(6,1)
1     FORMAT(50X,37HCALCULATION OF VARIANCE TO MEAN RATIO)
      READ(5,9)(TITLE(I),I=1,12)
9     FORMAT(12A6)
      WRITE(6,9)(TITLE(I),I=1,12)
      READ(5,10) N,N1
10    FORMAT(2I5)
      READ(5,20)(X(I),I=1,N)
20    FORMAT(12F5.0)
      DO 40 J=1,N1
      NUM = N/J
      DO 30 I=1,NUM
      Y(I) = 0.
      II=(I-1)*J+1
      III=I*J
      DO  30 K=II,III
30    Y(I)= Y(I)+X(K)
      XBAR = 0.
      DO 70 I=1,NUM
70    XBAR=XBAR+Y(I)
      XNUM=NUM
      XBAR=XBAR/XNUM
      WRITE(6,80) J
80    FORMAT(1H0,8HTIME IS ,I4,10H   SECONDS)
      WRITE(6,90) XBAR
90    FORMAT(1X,12HAVERAGE IS  ,F12.7)
      SIGMA = 0.
      DO 100 I=1,NUM
100   SIGMA = SIGMA + (Y(I)-XBAR)*(Y(I)-XBAR)
      SIGMA = SIGMA/XNUM
      VAR = SIGMA
      SIGMA = SQRT(SIGMA)
      WRITE(6,110) SIGMA
110   FORMAT(1X,22HSTANDARD DEVIATION IS ,F12.6)
      WRITE(6,120) VAR
120   FORMAT(1X,12HVARIANCE IS ,F12.2)
      RATIO=VAR/XBAR
      WRITE(6,130) RATIO
130   FORMAT(1X,26HVARIANCE TO MEAN RATIO IS ,F12.8)
40    CONTINUE
      GO TO 2
      END
$DATA
```

133971367013418132531346013444134441316413385133391337213324	36
132881334513174132661329813258131491329613391132241335613396	37
135041337813434132911335813258134041313513321133441351613292	38
133811334413440135831338313608133491330513528133631329813204	39
134911354313386133471349113463133711339413443132671347713463	40
134511359113397133591347113201133571333313345135001346313499	41
136491332213433135741343113310134511338513360134921333113244	42
135531341513419134931353713358133781315613226135811325413348	43
134551339813436133721343613407134741328913426134361323513332	44
133471327313431132341324713456134281340513446132441327213373	45
132101334713376131221329813247133211335813355132511322913275	46
133261328613380134351321513165133751325013423131841316213446	47
131471339913196133211337713336130281323313389131971344513144	48
133111338213380132851313913226132981316313321132131330813236	49
133101354013164132121328813345132731323513251132361342413306	50
133611330713316132621338413301133431341111335213324133371337	51
134481335113401133801344313260135211328613194132171326213304	52
133901328413138133221332113183133291323213221133581331213285	53
133431349313460133501315713203134831340713272136011334813440	54
132891332113304134011326513434135091317713386133871344413381	55
134511330313430132511337513274133101328513238133111329113423	56
132361338113386132941333613407135781346913396131711358213432	57
134341341613508133061335413414134011334813523132451325613415	58
133651337113285133211319113407132851327913269132661338513190	59
134771320813416133061335913215133261324713304133251336313391	60
132641320613491133861330513418134021336713457131501323113247	61
132961349413384133421342413193134391336313405133991349213327	62
134321359513420133651326713271131501333513596134441321313389	63
132631329713368134341322613061134971326213238132541338113292	64
132381316113290133901336813286135691341913477133401343213317	65
135211334613330133531326913406134781334513281133821327513438	66
134571324813309133051330313264133061343313391133001329513277	67
132731343213414132231324313434130191332113532133741332313260	68
134111301813127131781323213272134831331413471133731333613464	69
134271351613324135101351413467134581340813317134221341313385	70
133791342513249133641330113202132341338113277134301337613404	71
133741336313433133391329813406132021327413518132911323513385	72
133881354613142133221331513586135231351313371133131333313317	73
131751325513144134061346413379132701329113506133451331413302	74
133151329513480134571334113262130921327413260134031337513372	75
132291330013327134581331013452134081342213524134281346613565	76
133031344413311133671346813612135681339213254132981340113549	77
136151331813512133141338013384134101346013435131721332013273	78
132621319813249130461346913372131321318813463133441355313272	79
134641355313430133111323013341132871334813271133731319213196	80
132591335913212132361342113161133031314813275133491312413319	81
133381325813236133471346713381132581343613053133201347313226	82
133791335413190132941330913349134101319813344133151335813228	83
133561337213289132441348713341132841341413469132361334113330	84
134511353513168133741340413157134131341913178132551339313278	85
133521322513279	86

APPENDIX 3
TYPICAL IBM-7090 COMPUTER OUTPUT

```
CALCULATION OF VARIANCE TO MEAN RATIO


*E=13399.75 TIME=1.0000 SEC- CASE 5-B - 3-16-66

TIME IS     1   SECONDS
AVERAGE IS 13399.7526855
STANDARD DEVIATION IS   137.044283
VARIANCE IS     18781.14
VARIANCE TO MEAN RATIO IS   1.40160312

TIME IS     2   SECONDS
AVERAGE IS 26799.7414551
STANDARD DEVIATION IS   234.9C3383
VARIANCE IS     55179.6C
VARIANCE TO MEAN RATIO IS   2.05896011

TIME IS     3   SECONDS
AVERAGE IS 40199.2578125
STANDARD DEVIATION IS   326.771118
VARIANCE IS     106779.36
VARIANCE TO MEAN RATIO IS   2.65625212

TIME IS     4   SECONDS
AVERAGE IS 53600.3564453
STANDARD DEVIATION IS   421.937283
VARIANCE IS     178031.07
VARIANCE TO MEAN RATIO IS   3.32145309

TIME IS     5   SECONDS
AVERAGE IS 67COC.4453125
STANDARD DEVIATION IS   5C8.C96672
VARIANCE IS     258162.23
VARIANCE TO MEAN RATIO IS   3.85314193

TIME IS     6   SECONDS
AVERAGE IS 80400.5351563
STANDARD DEVIATION IS   596.1C8688
VARIANCE IS     355345.57
VARIANCE TO MEAN RATIO IS   4.4196915C
```

APPENDIX 4

EFFECTS OF MEASUREMENT ERRORS ON V/M COUNTING EQUIPMENT SYSTEM DEAD TIME

In the derivation of Equation (3.14) for V/M a necessary condition was that the counting equipment system response be independent of the number of neutrons available for counting during any specific gate opening time, T. This condition cannot be justified if the efficiency of the counting equipment system, ϵ, is dependent on the rate at which neutrons are recorded. The limitation in the rate is determined by the counting equipment system dead time, which is defined as the time period following the recording of a neutron pulse by the gate scaler, during which, a second neutron pulse in the neutron detector will not be recorded by the gate scaler.

In a counting system such as the one used in this research and described in Section IV, the dead time of the system is basically that of the pulse pair resolution time of the gate scaler.

The technique normally used for the determination of the counting equipment system dead time requires a double pulse generator which permits adjustment of the polarity, amplitude, width and time between subsequent pulses. By adjusting polarity, amplitude and width of the generated pulse one can simulate the shape of the pulse of the amplifier discriminator of the counting equipment. Then by feeding the simulated signal to the gate scaler at various pulse separation times, one can determine the counting equipment system dead time, which would be that

separation time below which two subsequent individual pulses would be counted as one.

Since the pulse pair resolution (resolving time) of the gate scaler used in this research, TMC-Model 214, is given by the manufacturer specification to be 5 microseconds (see page 24), to verify this measurement a double pulse generator with a pulse separation time of one to ten micorseconds would have been needed. The author was not able to obtain such a generator.

Although the determination of the counting equipment efficiency, ϵ, obtained in Section X. B, inherently includes the effects of the counting system dead time, they are not included in a manner consistent with the theoretical derivation of Equation (3.14).

The effects of the counting equipment system dead time on the measured variance-to-mean can be determined (reference 6) from:

$$\bar{c} = \bar{C}\, e^{-\bar{C}\, T_d} \qquad (1)$$

where:

$\bar{c}$ = measured average count rate

$\bar{C}$ = true average count rate

T_d = counting equipment system dead time

and assuming that $\bar{C}$ is large, T_d is small and the distribution is normal, then approximately:

$$(\bar{c}^2 - (\bar{c})^2) \approx (\bar{C}^2 - (\bar{C})^2)\, e^{-2\, \bar{C}\, T_d} \qquad (2)$$

where:

$(\bar{c}^2 - (\bar{c})^2)$ = measured variance of count rate

$(\bar{C}^2 - (\bar{C})^2)$ = true variance of count rate

hence, for any gate opening time, T seconds, the ratio of the variance-to-mean measured to the true variance-to-mean is:

$$\frac{(\bar{c}^2 - (\bar{c})^2)}{\bar{c}} \Big/ \frac{(\bar{C}^2 - (\bar{C})^2)}{\bar{C}} \approx e^{-\bar{C} T_d} \qquad (3)$$

From Equation (3) above the following measured to true error correction tabulation for the variance-to-mean can be obtained for various measured average count rates, $\bar{c}$, for a counting equipment system dead time, T_d, of 5 μ-seconds.

Measured Average Counts Per Second $\bar{c}$	Measured to True Variance-to-Mean Percent Error %
100	0.05
1000	0.50
2000	1.00
5000	2.47
10000	4.88

Consequently the error introduced by the loss of counts due to the counting equipment system dead time is of the order of 2.00 percent or less, since the measured average counts obtained were of the order of 5000 cps or less.

APPENDIX 5

EFFECTS OF SECOND ORDER TERMS IN THE VARIANCE-TO-MEAN EQUATION

Examination of Equation (3.13) of Section III reveals that from the variance-to-mean ratio of the neutron count, information can be obtained about various fundamental physics parameters, namely:

$\frac{\overline{\nu(\nu-1)}}{(\overline{\nu})^2}$	the relative width of the probability distribution of the fission neutron emission for the fissionable core material
α_1	the prompt neutron population decay eigenvalue
$\alpha_2 \rightarrow \alpha_7$	the delayed neutron population decay eigenvalue for delayed groups

Of the physics parameters mentioned above, only the relative width of the probability distribution of the fission neutron emission can be independently determined (see reference 7). However, information about the other parameters can be obtained by analyzing the results of the measurements of the variance-to-mean ratio according to the ranges of the values of αT, in which the experiments have been made, by analyzing the data on a selected range.

In this research the author is primarily interested in the measurement of the prompt neutron population decay eigenvalue α_1. Consequently, in analyzing the results of the experiments (Figure 31 through 34 and Figures 35 and 36), which implies the necessary conditions that:

$$\alpha_1 >> |\alpha_2| > |\alpha_3| > \ldots \quad (1)$$

and:

$$|\alpha_2| T << 1 \quad (2)$$

Consequently, the second order terms α_2, α_3, ... etc. can be disregarded since their contribution is negligible for $T < 0.1$ seconds, and hence Equation (3.13) can be represented by Equation (3.14). Further, it can be said that since the variance is the autocorrelation function evaluated at zero time lag, the terms with larger decay constants become negligible, in the application of the Equation (3.13) the spatial effects on the core parameters are also negligible.

Ultimately it is evident from Equation (3.14) that the measurement of the variance-to-mean provides with an independent and unique measurement of α_1, and it does not allow for the independent direct measurment of the core reactivity, ρ, since $\alpha_1 = \alpha = (\beta - \rho)/\ell$.

However, let us examine the possible error that can be introduced in the solution of Equation (3.14) directly for ρ, by inserting in Equation (3.14) the theoretically calculated values of the prompt neutron lifetime, ℓ, and the effective (one group) delayed neutron fraction, for the different UMR cores studied in this research.

The value of the prompt neutron lifetime [Equation (7.11)] is affected by the core temperature, core lifetime, and core size. Since the experiments were performed on the cold, clean, UMR core, only the core size change during fuel loading would affect the value of the prompt neutron lifetime.

The prompt neutron lifetimes calculated for the full size UMR core and the smallest core considered in this research, core 4-B, are 45 μ - seconds, and 42 μ - seconds respectively. Consequently, the error introduced in the measurement of reactivity directly from Equation (3.14) by fixing the prompt neutron life to 45 μ - seconds is of the order of 6% for the smaller core studied, core 4-B, and less than 6% for the larger cores.

The effective delay neutron fraction is discussed in Section VII. 7.8 and its values for the different core sizes given in Figure 17. Taking a maximum expected error band on the calculated values of β_{eff} of 3.5 percent (the range between the UMR full core β_{eff} and the smaller UMR core considered, core 4-B), the error introduced in the measurement of reactivity directly from Equation (3.14) by fixing the value of β_{eff}, as given in Figure 17 for different core sizes, would be in the order of 3.5 percent. However, this possible error was minimized to less than 3.5 percent by using the corresponding delayed neutron fraction from Figure 17 for the actual core size considered.

Consequently, because of the above reasoning, it appears that the uncertainty in the second order terms in Equation (3.14) would allow the measurement of reactivity directly from the variance-to-mean measurement with an accuracy of 6 percent of its actual value for a UMR type core.

APPENDIX 6

CONFIDENCE LIMITS FOR THE REACTIVITY OF UMR CORES 3-B AND 4-B

The confidence limits for the value of the reactivity as function of the variance-to-mean minus one obtained from experiments and plotted in Figures 35 and 36 for UMR cores 3-B and 4-B, were calculated as follows:

UMR Core 3-B

Gate Time Seconds	(V/M)-1	Calculated Reactivity % ΔK/K
1.0	1.000	-0.489
1.0	1.100	-0.425
1.0	1.067	-0.450
0.1	1.023	-0.450
0.1	1.082	-0.415
0.1	0.977	-0.485
0.01	0.691	-0.486
0.01	0.745	-0.424
0.01	0.720	-0.450
		$\bar{\rho}$ = -0.4527

Where the reactivity was obtained directly from Equation (3.14) by solving ρ for the measured value of (V/M)-1 for the 9 data points selected randomly from the data in the range of 0.01 to 1.0 seconds gate opening.

The calculated standard deviation of the reactivity is 0.02688% ΔK/K and consequently, assuming a normal distribution, it can be said with 99% confidence that the mean of the measured reactivity for the UMR core 3-B lies in the interval -0.4846% ΔK/K to -0.4208% ΔK/K.

By the same approach for UMR Core 4-B the mean of the measured reactivity can be expected to lie with a 99% confidence in the interval -2.464% ΔK/K to -1.714% ΔK/K.

UMR Core 4-B

Gate Time Seconds	(V/M)-1	Calculated Reactivity % ΔK/K
1.0	0.280	-1.71
1.0	0.300	-1.61
1.0	0.275	-1.73
0.1	0.235	-1.91
0.1	0.220	-2.01
0.1	0.202	-2.15
0.01	0.120	-2.83
0.01	0.168	-2.20
0.01	0.110	-2.97
0.001	0.062	-1.90
0.001	0.058	-2.05
0.001	0.059	-2.00
		$\bar{\rho}$ = -2.089

REFERENCES

1. Duffey, D., et al., "Safeguards Evaluation of the University of Maryland Reactor," Allis Chalmers Manufacturing Company, Nuclear Power Department, Washington, D.C., February, 1960.

2. Diaz, A. and Fisher, J.R., "Criticality Experiments with the University of Maryland Reactor," Nuclear Engineering Department of the University of Maryland, October 1962.

3. de Hoffman, F., "Intensity Fluctuation of a Neutron Chain Reactor," MDDC-382, LADC-256, 1946.

4. Thie, J.A., "Reactor Noise," Prepared under the auspices of the Division of Technical Information, United States Atomic Energy Commission, 1963.

5. Bennett, E.F., "The Rice Formulation of Pile Noise," Nuclear Sci. and Eng., 8:53 (1960).

6. Albrecht, R.W., "Measurement of Dynamic Nuclear Reactor Parameters by Methods of Stochastic Processes," Doctor of Philosophy Thesis, U. of Michigan, 1961.

7. Diven, B.C., et al., "Multiplicities of Fission Neutrons," Phys. Rev., 101: 1012 (1956).

8. Feynman, R., de Hoffman, F., and Serber, R., "Dispersion of the Neutron Emission in U-235 Fission," J. Nuclear Energy, 3:64 (1956).

9. Orndoff, J.D., "Prompt Neutron Periods of Metal Critical Assemblies," Nuclear Sci. and Eng., 2:450 (1957).

10. Brunson, G.S., et al., "Measuring the Prompt Period of a Reactor," Nucleonics, 15, 11:132 (1957).

11. Keeping, G.R., et al., "Delayed Neutrons from Fissionable Isotopes of Uranium, Plutonium and Thorium," LA-2118, July 1957.

12. Glasstone, S., "Principles of Nuclear Reactor Engineering," 223:236, D. Van Nostrand Company Inc., 1955.

13. Stehn, J.R., Naval Reactors Physics Handbook, Volume III,

REFERENCES (cont.)

The Physics of Intermediate Spectrum Reactors, U.S. Government Printing Office, Washington 25, D.C., September 1958.

14. Weiner, R., "Experimental Determination of the Correction for the Effect of Axial Flux Shift on the Measurements of Shutdown Reactivity of the University of Maryland Reactor," Master of Science Thesis, U. of Maryland, 1965.

15. Kenney, E.S., "Noise Analysis of Nuclear Reactors with the Use of Gamma Radiation," 9th AEC Symposium Series, CONF-660206, May 1967.

16. Natelson, M., Osborn, R.K., and Shure, F., "Recent Developments in the Analysis of Neutron Noise Experiments," 9th AEC Symposium Series, CONF-660206, May 1967.

TABLE I

Random Source Statistical Measurements to Checkout Instrumentation

Gate Time Δt (sec)	$\sum_{i=1}^{i=1023} c_i$	Mean $\overline{c}$	Standard Deviation σ	Variance $\overline{c^2} - (\overline{c})^2$	Variance-to-Mean Ratio
0.0001	203	0.1998	0.44160	0.19562	0.9789
0.001	1986	1.9413	1.40397	1.97001	1.0153
0.01	20155	19.7018	4.39963	19.35674	0.9824
0.05	97867	95.6664	9.41427	88.62851	0.9264
0.1	200768	196.2549	15.10206	228.07001	1.1621
0.5	994392	972.0355	30.93410	956.91202	0.9844
1.0	2030455	1984.7965	43.34640	1878.87300	0.9466

TABLE II

As-Built Drawings Used in the Preparation
of the Core Mock-Up (Grid Mesh)
Input to the PDQ Code

Item No.	Drawing No.	Description
1	15-D-04600	Grid Plate
2	15-D-0500-B	Graphite Source Holder and Weldment Assembly
3	15-C-05003-A	Graphite Reflector
4	15-D-03004	Shim Rod
5	15-D-03006-D	Shim Rod and Reg. Rod Guide
6	15-D-03003	Regulating Rod
7	15-D-02000	Fuel Element Assembly
8	15-D-02001	Fuel Element Container

TABLE III

Physical Features of the
University of Maryland Reactor

Core Components	Material Description
Fuel	Highly enriched (93.5% U-235) aluminum alloy
Cladding	Aluminum
Moderator	Ordinary water
Reflector	Graphite in the four lateral sides of the core and ordinary water above and below the core
Control Rods Shims #1 and #2	B_4C contained in aluminum cans
Regulating Rod	Perforated hollow stainless steel rod
Neutron Source	Pu-Be - one Curie

Core Components	Dimensions	
Fuel Layer Per Plate	Length	2.469 in.
	Width	0.026 in.
	Height	23.625 in.
Aluminum Cladding Per Plate	Length	2.775 in.
	Width	0.027 in.
	Height	25.125 in.
Aluminum Fuel Container	Length	2.827 in.
	Width	2.827 in.
	Height	26.250 in.
	Thickness of Can	0.064 in.

TABLE III (cont.)

Physical Features of the
University of Maryland Reactor

Core Components	Dimensions
Spacing Between Fuel Cans (Center to Center)	Along west-east axis 3.189 in. (X-axis in PDQ calculation) Along north-south axis 3.035 in. (Y-axis in PDQ calculation)
Spacing Between Fuel Plates (Pitch)	0.262 in.
Reflector Elements, (Including Aluminum Clad)	Length 2.807 in. Width 2.807 in. Height 25.125 in.
Fuel Loading Per Plate	Regular Fuel Plate 15.84 g. of U-235 Spiked Fuel Plate 18.00 g. of U-235
Total Number of Fuel Plates in the Fuel Core	Spiked 19 Regular 147
Critical Present UMR Core Loading	2581 gms of U-235
Present UMR Full Core Loading	2671 gms of U-235

TABLE IV

Description of Location of the Fuel Cans and Their Contents as Arranged in the UMR Core

Can No.	Contents	Core Location (See Figure 2)
102	4 - 18.0 g fuel plates 1-aluminum plate	B-5
30	9 - 15.8 g fuel plates 1-aluminum plate	C-4
20	10 - 15.8 g fuel plates	C-5
19	10 - 15.8 g fuel plates	C-6
10	6 - 15.8 g fuel plates Regulating Rod	C-7
14	10 - 15.8 g fuel plates	D-4
100	5 - 18.0 g fuel plates 1-aluminum plate	D-5 (Glory Hole)
17	10 - 15.8 g fuel plates	D-6
15	10 - 15.8 g fuel plates	D-7
29	6 - 15.8 g fuel plates Shim Rod #1	E-4
8	10 - 15.8 g fuel plates	E-5
13	16 - 15.8 g fuel plates Shim Rod #2	E-6
16	10 - 15.8 g fuel plates	E-7
18	10 - 15.8 g fuel plates	F-3
9	10 - 15.8 g fuel plates	F-4
11	10 - 15.8 g fuel plates	F-5
12	10 - 15.8 g fuel plates	F-6
7	10 - 15.8 g fuel plates	F-7
101	10 - 18.0 g fuel plates	F-8

TABLE V

List of UMR Core Regions
Composition Descriptions

Region	Composition Description
1	Regular fuel plates (15.8 g of U-235) plus water moderator.
2	Spiked fuel plates (18.0 g of U-235) plus water moderator.
3	Aluminum shroud can and water in mixture in areas surrounding the core and between fuel elements.
4	Aluminum and water mixture in the area between the core and the thermal column and areas between the reflector elements.
5	Aluminum and water mixture in the control rod area of the core.
6	Aluminum, graphite and water mixture for the graphite element containing the start-up source.
7	Graphite reflector elements
8	Water moderator
9 through 13	Regular fuel and water mixture equal to composition 1.
14	Spiked fuel and water mixture for the center Glory Hole, and fuel element equal to composition 2.
15 through 27	Regular fuel and water mixture equal to composition 1.
28	Spiked fuel and water mixture for the fully loaded spiked element.

TABLE VI

UMR Core Volume Fractions and Atomic Densities

Composition No.	Material	Volume Fraction	Atomic Densities $\times 10^{-24}$
1, 9 through 13 &15 through 27	U-235	.00298	.000144 atoms/cm^3
	U-238	.00019	.000009 " "
	Al	.30098	.018134 " "
	H_2O	.69585	.023265 O- " "
			.046530 H- " "
2, 14, 28	U-235	.00338	.000164 atoms/cm^3
	U-238	.00022	.000010 " "
	Al	.30055	.018106 " "
	H_2O	.69585	.023205 O- " "
			.046410 H- " "
3	Al	.30900	.018650 " "
	H_2O	.69100	.023100 O- " "
			.046200 H- " "
4	Al	.61500	.037200 " "
	H_2O	.38500	.021850 O- " "
			.043700 H- " "
5	Al	.10800	.006530 " "
	H_2O	.89200	.029800 O- " "
			.059600 H- " "
6	C	.66900	.053700 " "
	Al	.12700	.007700 " "
	H_2O	.20400	.003420 O- " "
			.006840 H- " "
7	C	1.00000	.076700 " "
8	H_2O	1.00000	.017100 O- " "
			.034200 H- " "

TABLE VII

Four Group Calculated Cross Section Data for the UMR Full Core

Group	Comp.	Diffusion Coefficient D (cm.)	Absorption Cross Section Sigma A (cm^{-1})	Removal Cross Section Sigma R (cm^{-1})	Fission Neutrons Per Fission Times Fission Cross Section Nu x Sigma F
1	1	1.425877	0.000660	0.042710	0.000847
1	2	1.425536	0.000710	0.042685	0.000961
1	3	1.427507	0.000250	0.042713	0.
1	4	1.576380	0.000270	0.023008	0.
1	5	1.364920	0.000250	0.054876	0.
1	6	1.579018	0.000050	0.007187	0.
1	7	1.354609	0.000001	0.002641	0.
1	8	1.336414	0.000240	0.061303	0.
1	9	1.425877	0.000660	0.042710	0.000847
1	10	1.425877	0.000660	0.042710	0.000847
1	11	1.425877	0.000660	0.042710	0.000847
1	12	1.425877	0.000660	0.042710	0.000847
1	13	1.425877	0.000660	0.042710	0.000847
1	14	1.425536	0.000710	0.042685	0.000961
1	15	1.425877	0.000660	0.042710	0.000847
1	16	1.425877	0.000660	0.042710	0.000847
1	17	1.425877	0.000660	0.042710	0.000847
1	18	1.425877	0.000660	0.042710	0.000847
1	19	1.425877	0.000660	0.042710	0.000847
1	20	1.425877	0.000660	0.042710	0.000847
1	21	1.425877	0.000660	0.042710	0.000847
1	22	1.425877	0.000660	0.042710	0.000847
1	23	1.425877	0.000660	0.042710	0.000847
1	24	1.425877	0.000660	0.042710	0.000847
1	25	1.425877	0.000660	0.042710	0.000847
1	26	1.425877	0.000660	0.042710	0.000847
1	27	1.425877	0.000660	0.042710	0.000847
1	28	1.425536	0.000710	0.042685	0.000961

TABLE VII (cont.)

Four Group Calculated Cross Section Data for the UMR Full Core

Group	Comp.	Diffusion Coefficient D (cm.)	Absorptoin Cross Sectior Sigma A (cm^{-1})	Removal Cross Section Sigma R (cm^{-1})	Fission Neutrons Per Fission Times Fission Cross Section Nu x Sigma F
2	1	0.795668	0.009830	0.189322	0.013140
2	2	0.794240	0.011080	0.188868	0.014910
2	3	0.809063	0.000450	0.191826	0.
2	4	1.249538	0.000420	0.103631	0.
2	5	0.659240	0.000470	0.248923	0.
2	6	1.065829	0.000090	0.032343	0.
2	7	0.887858	0.000004	0.010222	0.
2	8	0.599742	0.000484	0.279679	0.
2	9	0.795668	0.009830	0.189322	0.013140
2	10	0.795668	0.009830	0.189322	0.013140
2	11	0.795668	0.009830	0.189322	0.013140
2	12	0.795668	0.009830	0.189322	0.013140
2	13	0.795668	0.009830	0.189322	0.013140
2	14	0.794240	0.011080	0.188868	0.014910
2	15	0.795668	0.009830	0.189322	0.013140
2	16	0.795668	0.009830	0.189322	0.013140
2	17	0.795668	0.009830	0.189322	0.013140
2	18	0.795668	0.009830	0.189322	0.013140
2	19	0.795668	0.009830	0.189322	0.013140
2	20	0.795668	0.009830	0.189322	0.013140
2	21	0.795668	0.009830	0.189322	0.013140
2	22	0.795668	0.009830	0.189322	0.013140
2	23	0.795668	0.009830	0.189322	0.013140
2	24	0.795668	0.009830	0.189322	0.013140
2	25	0.795668	0.009830	0.189322	0.013140
2	26	0.795668	0.009830	0.189322	0.013140
2	27	0.795668	0.009830	0.189322	0.013140
2	28	0.794240	0.011080	0.188868	0.014910

TABLE VII (cont.)

Four Group Calculated Cross Section Data for the UMR Full Core

Group	Comp.	Diffusion Coefficient D (cm.)	Absorption Cross Section Sigma A (cm^{-1})	Removal Cross Section Sigma R (cm^{-1})	Fission Neutrons Per Fission Times Fission Cross Section Nu x Sigma F
3	1	0.774501	0.010668	0.384245	0.015361
3	2	0.772945	0.011711	0.383977	0.017434
3	3	0.788791	0.002940	0.384472	0.
3	4	1.224186	0.002560	0.213038	0.
3	5	0.640149	0.003180	0.496239	0.
3	6	1.057105	0.000601	0.071499	0.
3	7	0.887073	0.000032	0.027124	0.
3	8	0.581044	0.003310	0.556578	0.
3	9	0.774501	0.010668	0.384245	0.015361
3	10	0.774501	0.010668	0.384245	0.015361
3	11	0.774501	0.010668	0.384245	0.015361
3	12	0.774501	0.010668	0.384245	0.015361
3	13	0.774501	0.010668	0.384245	0.015361
3	14	0.772945	0.011711	0.383977	0.017434
3	15	0.774501	0.010668	0.384245	0.015361
3	16	0.774501	0.010668	0.384245	0.015361
3	17	0.774501	0.010668	0.384245	0.015361
3	18	0.774501	0.010668	0.384245	0.015361
3	19	0.774501	0.010668	0.384245	0.015361
3	20	0.774501	0.010668	0.384245	0.015361
3	21	0.774501	0.010668	0.384245	0.015361
3	22	0.774501	0.010668	0.384245	0.015361
3	23	0.774501	0.010668	0.384245	0.015361
3	24	0.774501	0.010668	0.384245	0.015361
3	25	0.774501	0.010668	0.384245	0.015361
3	26	0.774501	0.010668	0.384245	0.015361
3	27	0.774501	0.010668	0.384245	0.015361
3	28	0.772945	0.011711	0.383977	0.017434

TABLE VII (cont.)

Four Group Calculated Cross Section Data for the UMR Full Core

Group	Comp.	Diffusion Coefficient D (cm.)	Absorption Cross Section Sigma A (cm^{-1})	Removal Cross Section Sigma R (cm^{-1})	Fission Neutrons Per Fission Times Fission Cross Section Nu x Sigma F
4	1	0.244300	0.087087		0.148185
4	2	0.247400	0.095031		0.164802
4	3	0.227400	0.016960		0.
4	4	0.304800	0.014730		0.
4	5	0.178000	0.018350		0.
4	6	0.681500	0.003769		0.
4	7	0.915300	0.000209		0.
4	8	0.161500	0.019010		0.
4	9	0.244300	0.087087		0.148185
4	10	0.244300	0.087087		0.148185
4	11	0.244300	0.087087		0.148185
4	12	0.244300	0.087087		0.148185
4	13	0.244300	0.087087		0.148185
4	14	0.247400	0.095031		0.164802
4	15	0.244300	0.087087		0.148185
4	16	0.244300	0.087087		0.148185
4	17	0.244300	0.087087		0.148185
4	18	0.244300	0.087087		0.148185
4	19	0.244300	0.087087		0.148185
4	20	0.244300	0.087087		0.148185
4	21	0.244300	0.087087		0.148185
4	22	0.244300	0.087087		0.148185
4	23	0.244300	0.087087		0.148185
4	24	0.244300	0.087087		0.148185
4	25	0.244300	0.087087		0.148185
4	26	0.244300	0.087087		0.148185
4	27	0.244300	0.087087		0.148185
4	28	0.247400	0.095031		0.164802

TABLE VIII

Composition Integrated and Averaged Areas, Fluxes, and Sources for the UMR Full Core, Cold Clean

Composition - Integrated Area (cm^2)				
*0.422157E 02	0.187626E 02	0.390678E 03	0.102469E 03	0.562876E 02
0.496814E 02	0.146048E 04	0.389069E 04	0.469064E 02	0.[illegible]4E 02
0.140719E 02	0.140719E 02	0.469063E 02	0.234532E 02	0.[illegible]063E 02
0.469063E 02	0.140719E 02	0.140719E 02	0.469064E 02	0.140719E 02
0.140719E 02	0.469064E 02	0.496814E 02	0.469064E 02	0.469064E 02
0.469064E 02	0.469064E 02	0.496793E 02		
Composition - Integrated Flux - Group 1				
0.241119E 04	0.892414E 03	0.236068E 05	0.321021E 04	0.422202E 04
0.499788E 03	0.282948E 05	0.139760E 05	0.352092E 04	0.361394E 04
0.865339E 03	0.630189E 03	0.353390E 04	0.243884E 04	0.489976E 04
0.377739E 04	0.919337E 03	0.123245E 04	0.509284E 04	0.150219E 04
0.141236E 04	0.406812E 04	0.189555E 04	0.312703E 04	0.402956E 04
0.404004E 04	0.333380E 04	0.210905E 04		
Composition - Averaged Flux - Group 1				
0.571160E 02	0.475636E 02	0.604252E 02	0.313286E 02	0.750079E 02
0.100599E 02	0.193736E 02	0.359217E 01	0.750626E 02	0.770458E 02
0.614941E 02	0.447835E 02	0.753394E 02	0.103988E 03	0.104458E 03

*Note - All values listed in this table are given for the 28 different Core Regions listed in Table V in numerical order starting with Region Number One. E 02 = x 10^2.

TABLE VIII (cont.)

Composition Integrated and Averaged Areas, Fluxes, and Sources for the UMR Full Core, Cold Clean

Composition - Averaged Flux - Group 1 (cont.)				
*0.805304E 02	0.653313E 02	0.875823E 02	0.108575E 03	0.106751E 03
0.100367E 03	0.867286E 02	0.381542E 02	0.666654E 02	0.859063E 02
0.861298E 02	0.710734E 02	0.424533E 02		
Composition - Integrated Flux - Group 2				
0.491178E 03	0.184047E 03	0.503617E 04	0.724538E 03	0.917340E 03
0.120986E 03	0.665791E 04	0.333589E 04	0.719160E 03	0.736521E 03
0.181714E 03	0.131701E 03	0.721838E 03	0.500255E 03	0.100273E 04
0.773485E 03	0.192506E 03	0.258872E 03	0.104051E 04	0.315174E 03
0.296268E 03	0.832166E 03	0.387173E 03	0.642042E 03	0.828570E 03
0.831076E 03	0.684245E 03	0.428328E 03		
Composition - Averaged Flux - Group 2				
0.116350E 02	0.980926E 01	0.128909E 02	0.707080E 01	0.162974E 02
0.243525E 01	0.455872E 01	0.857403E 00	0.153318E 02	0.157019E 02
0.129132E 02	0.935912E 01	0.153889E 02	0.213299E 02	0.213772E 02

*Note - All values listed in this table are given for the 28 different Core Regions listed in Table V in numerical order starting with Region Number One. E 02 = $\times 10^2$.

TABLE VIII (cont.)

Composition Integrated and Averaged Areas, Fluxes, and Sources for the UMR Full Core, Cold Clean

Composition - Averaged Flux - Group 2 (cont.)				
*0.164900E 02	0.136801E 02	0.183964E 02	0.221828E 02	0.223974E 02
0.210539E 02	0.177410E 02	0.779311E 01	0.136877E 02	0.176643E 02
0.177178E 02	0.145875E 02	0.862187E 01		
Composition - Integrated Flux - Group 3				
0.230877E 03	0.874863E 02	0.240727E 04	0.345380E 03	0.445845E 03
0.595105E 02	0.302277E 04	0.170373E 04	0.339845E 03	0.346134E 03
0.870537E 02	0.630790E 02	0.340466E 03	0.237426E 03	0.473425E 03
0.364460E 03	0.922154E 02	0.124092E 03	0.489951E 03	0.151143E 03
0.142145E 03	0.391619E 03	0.183032E 03	0.303671E 03	0.391563E 03
0.393540E 03	0.322928E 03	0.201678E 03		
Composition - Averaged Flux - Group 3				
0.546897E 01	0.466281E 01	0.616177E 01	0.337058E 01	0.792083E 01
0.119784E 01	0.206971E 01	0.437899E 00	0.724518E 01	0.737926E 01
0.618634E 01	0.448262E 01	0.725843E 01	0.101234E 02	0.100930E 02
0.776994E 01	0.655315E 01	0.881843E 01	0.104453E 02	0.107408E 02
0.101014E 02	0.834895E 01	0.368413E 01	0.647398E 01	0.834775E 01
0.838990E 01	0.688453E 01	0.405961E 01		

*Note - All values listed in this table are given for the 28 different Core Regions listed in Table V in numerical order starting with Region Number One. E 02 = x 10^2.

TABLE VIII (cont.)

Composition Integrated and Averaged Areas, Fluxes and Sources for the UMR Full Core, Cold Clean

Composition - Integrated Flux - Group 4				
*0.138976E 04	0.626506E 03	0.187014E 05	0.369483E 04	0.383952E 04
0.120822E 04	0.349248E 05	0.378278E 05	0.209770E 04	0.196979E 04
0.632866E 03	0.527681E 03	0.204940E 04	0.151318E 04	0.271908E 04
0.206843E 04	0.697784E 03	0.859902E 03	0.267694E 04	0.105512E 04
0.100014E 04	0.215226E 04	0.130087E 04	0.178756E 04	0.220721E 04
0.230818E 04	0.180869E 04	0.132903E 04		
Composition - Averaged Flux - Group 4				
0.329203E 02	0.333913E 02	0.478691E 02	0.360580E 02	0.682125E 02
0.243195E 02	0.239133E 02	0.972265E 01	0.447209E 02	0.419941E 02
0.449737E 02	0.374989E 02	0.436913E 02	0.645191E 02	0.579683E 02
0.440970E 02	0.495870E 02	0.611077E 02	0.570699E 02	0.749806E 02
0.710734E 02	0.458842E 02	0.261842E 02	0.381090E 02	0.470557E 02
0.492082E 02	0.385595E 02	0.267522E 02		
Composition - Integrated Source				
0.217983E 03	0.108376E 03	0.	0.	0.
0.	0.	0.	0.328498E 03	0.309948E 03
0.982389E 02	0.814275E 02	0.321397E 03	0.263317E 03	0.427523E 03

*Note - All values listed in this table are given for the 28 different Core Regions listed in Table V in numerical order starting with Region Number One. E 04 = x 10^4.

TABLE VIII (cont.)

Composition Integrated and Averaged Areas, Fluxes, and Sources for the UMR Full Core, Cold Clean

Composition - Integrated Source (cont.)				
*0.325471E 03	0.108125E 03	0.133776E 03	0.422193E 03	0.164088E 03
0.155478E 03	0.339328E 03	0.202273E 03	0.280638E 03	0.347390E 03
0.362424E 03	0.284794E 03	0.230956E 03		
Composition - Averaged Source				
0.516355E 01	0.577621E 01	0.	0.	0.
0.	0.	0.	0.700327E 01	0.660780E 01
0.698121E 01	0.578653E 01	0.685189E 01	0.112273E 02	0.911441E 01
0.693873E 01	0.768378E 01	0.950658E 01	0.900076E 01	0.116607E 02
0.110488E 02	0.723415E 01	0.407140E 01	0.598294E 01	0.740602E 01
0.772653E 01	0.607155E 01	0.464895E 01		

*Note - All values listed in this table are given for the 28 different Core Regions listed in Table V in numerical order starting with Region Number One. E 03 = $\times 10^3$.

TABLE IX

Delayed Neutron Fraction Data

Group	Mean Energy (KeV)	Decay Constant for the Delayed Neutron of the i/th Group	Fraction Time of Delayed Neutrons for an Infinite Reactor
1	250	0.0124	2.1050×10^{-4}
2	460	0.0305	1.4010×10^{-3}
3	405	0.1110	1.2550×10^{-3}
4	450	0.3010	2.5263×10^{-3}
5	420	1.1300	7.3684×10^{-4}
6	397	3.0000	2.6720×10^{-4}
		$\sum_{i=1}^{i=6} \beta_i$	$= 0.0063984$

TABLE X

Movements of the Core Components for the Unloading of the UMR (Supercritical Cores)

Step #	Description of Core Material Being Moved	From		To		Remarks
		Core Position	Storage Position	Core Position	Storage Position	
1-A	Fuel container #102 with 4-18 g plates and one Al plate	B-5			10	
1-B	Reflector container #21 with solid graphite piece		5	B-5		See Figure 24
2-A	Fuel container #18 with 10-15.84 g plates	F-3			9	
2-B	Reflector container #26 with solid graphite piece		4	F-3		See Figure 25

TABLE XI

K_{eff}'s for Two Small
UMR Supercritical Core Loadings

After Step #	Total U-235 in the Core in Grams	Total No. of Plates in the Core		K_{eff} measured with experimental facilities empty	K_{eff} measured with experimental facilities flooded	K_{eff} calculated with flooded experimental facilities
		15.84 g	18 g			
Full Core	2670.5	147	19	1.00841	1.0121	1.0144
1-B and 14-B	2598.5	147	15	1.00680	1.0109	1.0112
2-B and 13-B	2440.1	137	15	——	1.0023	1.0043

TABLE XII

Reactivities for Two Small UMR Supercritical Loadings

After Step #	Measured Excess Reactivity with Facilities Empty % ΔK/K	Measured Excess Reactivity with Facilities Flooded % ΔK/K	Calculated Excess Reactivity with Facilities Flooded % ΔK/K	Change in the Excess Reactivity from Previous Step % ΔK/K	
				Measured	Calculated
Full Core	0.834	1.202	1.420	0.000	0.000
1-B and 13-B	0.678	1.079	1.107	(-0.123)	(-0.313)
2-B and 12-B	——	0.231	0.428	(-0.848)	(-0.679)

TABLE XIII

Movements of the Core Components for the Unloading of the UMR (Subcritical Cores)

Step #	Description of Core Material Being Moved	From		To		Remarks
		Core Position	Storage Position	Core Position	Storage Position	
3-A	Fuel container #101 with 10-18 g plates	F-8			8	
3-B	Spare reflector container #28 with solid graphite piece		3	F-8		See Figure 26
4-A	Fuel container #7 with 10-15.84 g plates	F-7			7	
4-B	Spare reflector container #28 with solid graphite piece	F-8		F-7		See Figure 27
5-A	Fuel container #16 with 10-15.84 g plates	E-7			6	
5-B	Reflector container #5 with solid graphite piece	E-8		E-7		See Figure 28
6-A	Fuel container #15 with 10-15.84 g plates	D-7			5	

TABLE XIII (cont.)

Movements of the Core Components for the Unloading of the UMR (Subcritical Cores)

Step #	Description of Core Material Being Moved	From		To		Remarks
		Core Position	Storage Position	Core Position	Storage Position	
6-B	Reflector container #4 with solid graphite piece	D-8		D-7		See Figure 29
7-A	Fuel container #9 with 10-15.84 g plates	F-4			4	
7-B	Fuel container #11 with 10-15.84 g plates	F-5			3	
7-C	Fuel container #12 with 10-15.84 g plates	F-6			13	
7-D	Reflector container #1 with hollow graphite piece for the Pu-Be source	B-7		F-4		
7-E	Reflector container #2 with solid graphite piece	B-8		F-5		
7-F	Reflector container #3 with solid graphite piece	C-8		F-6		See Figure 30

TABLE XIV

Movements of the Core Components for the Loading of the UMR (Subcritical Cores)

Step #	Description of Core Material Being Moved	From		To		Remarks
		Core Position	Storage Position	Core Position	Storage Position	
8-A	Reflector container #3 with solid graphite piece	F-6		C-8		
8-B	Reflector container #2 with solid graphite piece	F-5		B-8		
8-C	Reflector container #1 with hollow graphite piece for the Pu-Be source	F-4		B-7		
8-D	Fuel container #12 with 10-15.84 g plates		13	F-6		
8-E	Fuel container #11 with 10-15.84 g plates		3	F-5		
8-F	Fuel container #9 with 10-15.84 g plates		4	F-4		See Figure 29

TABLE XIV (cont.)

Movements of the Core Components for the Unloading of the UMR (Subcritical Cores)

Step #	Description of Core Material Being Moved	From		To		Remarks
		Core Position	Storage Position	Core Position	Storage Position	
9-A	Reflector container #4 with solid graphite piece	D-7		D-8		
9-B	Fuel container #15 with 10-15.84 g plates		5	D-7		See Figure 28
10-A	Reflector container #5 with solid graphite piece	E-7		E-8		
10-B	Fuel container #16 with 10-15.84 g plates		6	E-7		See Figure 27
11-A	Reflector container #28 with solid graphite piece	F-7		F-8		
11-B	Fuel container #7 with 10-15.84 g plates		7	F-7		See Figure 26

TABLE XIV (cont.)

Movements of the Core Components for the Loading of the UMR (Subcritical Cores)

Step #	Description of Core Material Being Moved	From		To		Remarks
		Core Position	Storage Position	Core Position	Storage Position	
12-A	Reflector container #28 with solid graphite piece	F-8			8	
12-B	Fuel container #101 with 10-18 g plates		3	F-8		See Figure 25 Supercritical Core
13-A	Reflector container #26 with solid graphite piece	F-3			4	
13-B	Fuel container #18 with 10-15.84 g plates		9	F-3		See Figure 24 Supercritical Core
14-A	Reflector container #21 with solid graphite piece	B-5			5	
14-B	Fuel container #102 with 4-18 g plates and one Aluminum plate		10	B-5		See Figure 2 UMR Full Core

TABLE XV

Comparison of Shutdown Margins for
Various Positions of the UMR Rod Bank

UMR Rod Bank Position cm.	Shutdown Margin		
	Rod Calibration Method % ΔK/K	1/M Method % ΔK/K	Variance-to-Mean Method % ΔK/K
45	-0.130	-0.13	-0.128
42	-0.563	-0.63	-0.502
35	-1.822	-1.50	-1.620
30	-2.979	-1.80	---

TABLE XVI

K_{eff}'s Calculated from the Statistical Data and it's Comparison with PDQ-2 Calculated Values for UMR Subcritical Cores Listed in Table XIII

After Step #	Total U-235 in the Core in Grams	Total No. of Plates in the Core		Unrodded Core Conditions	
		15.84 g	18 g	K_{eff} Calculated from Statistical Data-(Variance-to-Mean Ratio)	K_{eff} Calculated by Means of PDQ-2 Computer Code
3-B and 11-B	2260.1	137	5	0.9955	0.9952
4-B and 10-B	2101.7	27	5	0.9795	0.9779
5-B and 9-B	1943.3	117	5	------	0.9549
6-B and 8-F	1784.4	107	5	------	0.9343
7-F	1309.7	77	5	------	0.8600

TABLE XVII

Reactivities Calculated from Statistical Data and it's Comparison with PDQ-2 Calculated Values for UMR Subcritical Cores Listed in Table XIII

After Step #	Reactivity calculated from statistical data (Variance-to-Mean ratio) % ΔK/K	Reactivity calculated by means of PDQ-2 Computer Code % ΔK/K	Change in the Excess Reactivity from previous step % Δk/k	
			Measured	Calculated
3-B and 11-B	(-0.45)	(-0.482)	(-0.681)	(-0.910)
4-B and 10-B	(-2.09)	(-2.260)	(-1.550)	(-1.778)
5-B and 9-B	------	(-4.723)	------	(-2.463)
6-B and 8-F	------	(-7.032)	------	(-2.309)
7-F	------	(-16.28)	------	(-9.247)

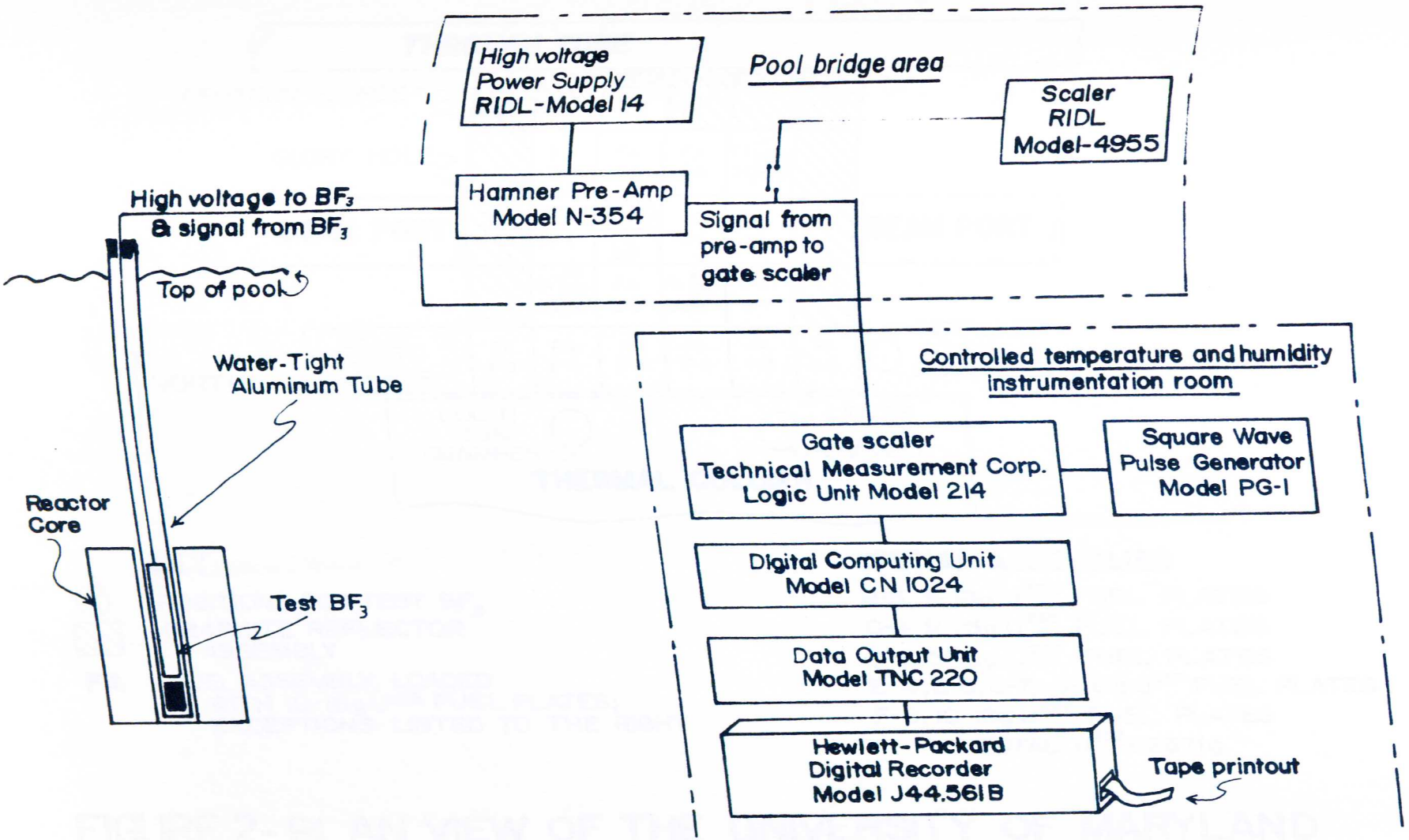

FIGURE1 SCHEMATIC DIAGRAM OF TEST EQUIPEMENT

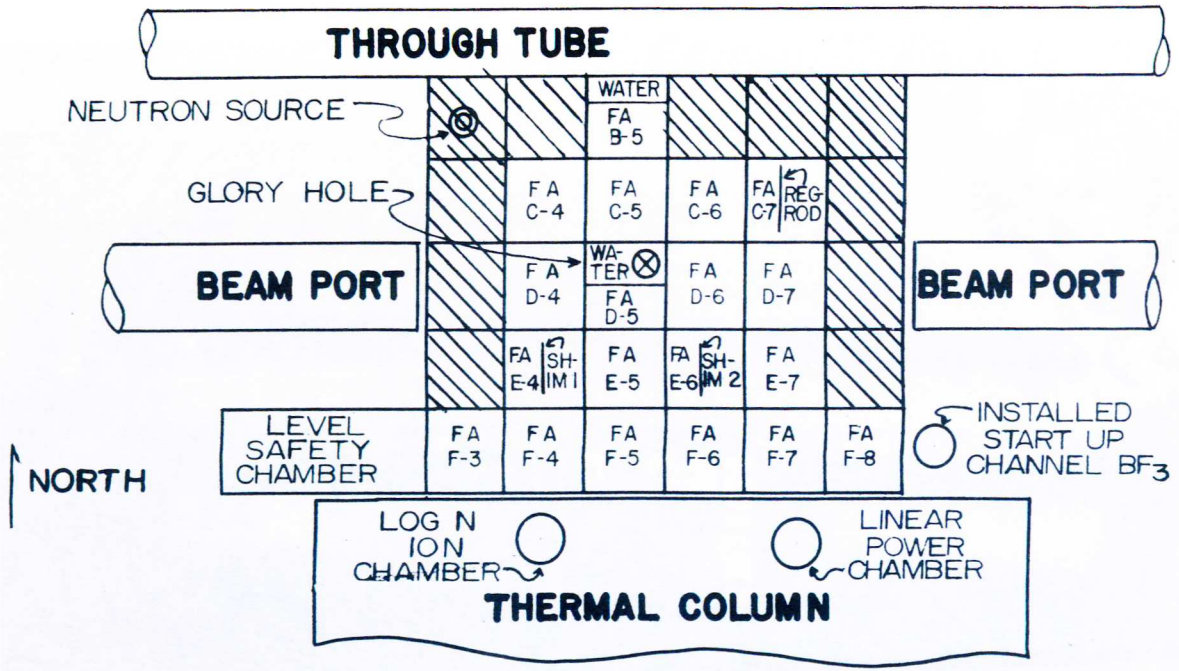

KEY

⊗ POSITIONS FOR TEST BF_3

GRAPHITE REFLECTOR ASSEMBLY

FA FUEL ASSEMBLY, LOADED WITH 10-16g U^{235} FUEL PLATES; EXCEPTIONS LISTED TO THE RIGHT

SPECIAL ASSEMBLIES

B-5, 4-18g U^{235} FUEL PLATES
C-4, 9-16g U^{235} FUEL PLATES
D-5, 5-18g U^{235} FUEL PLATES
E-4, E-6, C-7, 6-16g U^{235} FUEL PLATES
F-8, 10-18g U^{235} FUEL PLATES
TOTAL U^{235} = 267Ig

FIGURE 2- PLAN VIEW OF THE UNIVERSITY OF MARYLAND REACTOR SHOWING LOCATION USED FOR TEST BF_3 DETECTOR

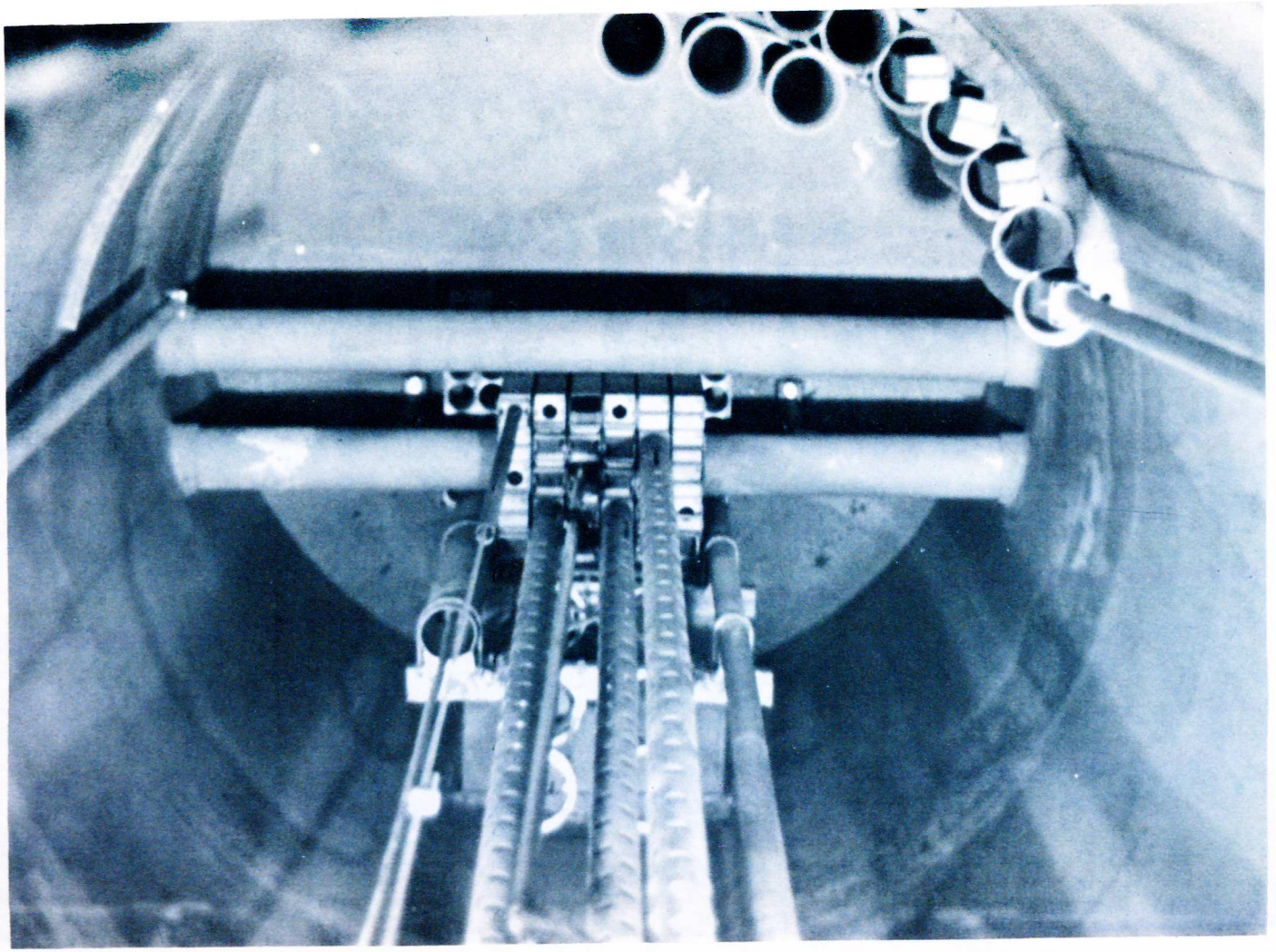

FIGURE 3- GENERAL VIEW OF THE UMR SHOWING ALUMINUM TUBE CONTAINING THE BF_3 INSERTED IN THE CENTER GLORY HOLE

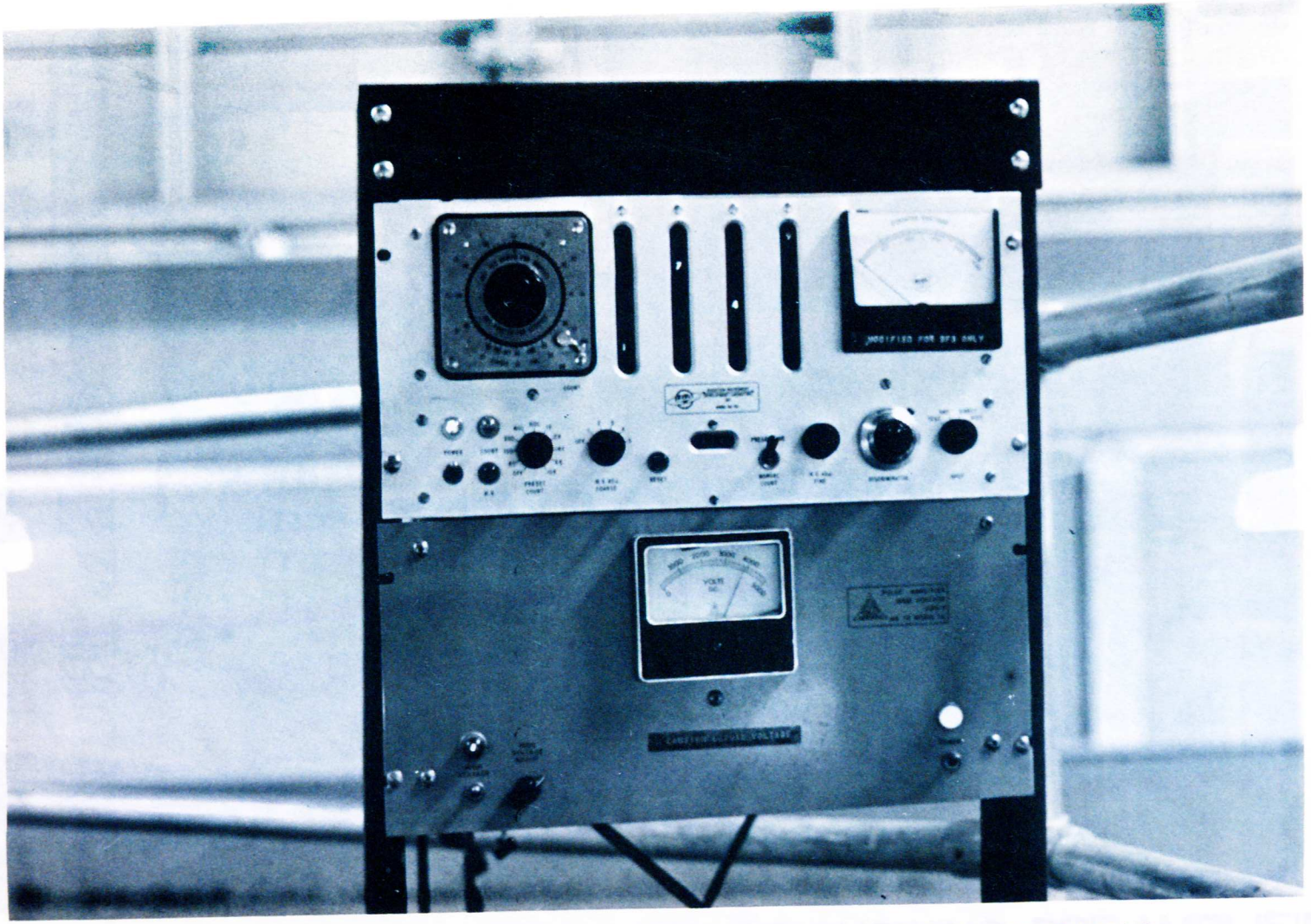

FIGURE 4 - SCALER AND HIGH VOLTAGE SUPPLY LOCATED ON THE POOL BRIDGE

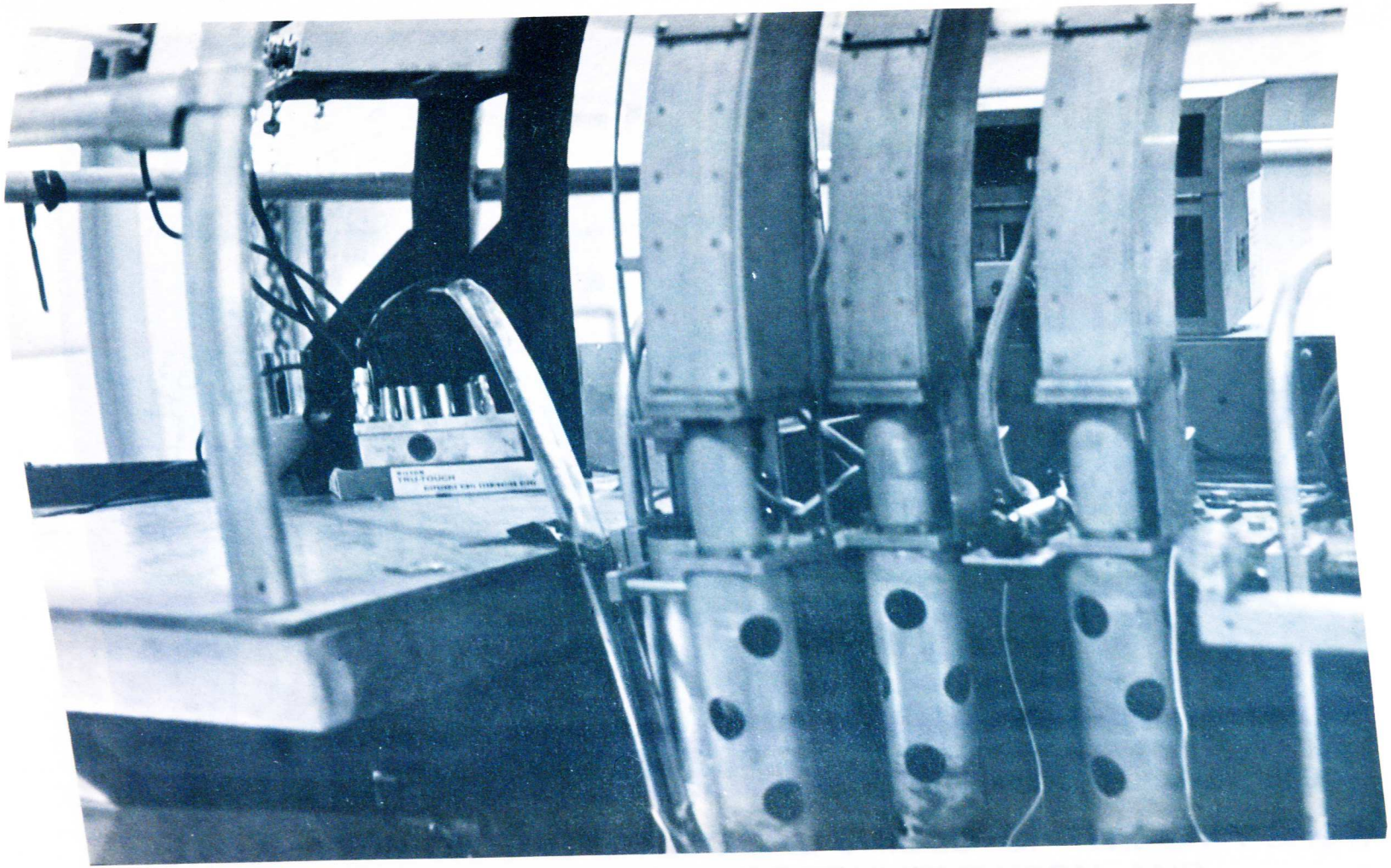

FIGURE 5-VIEW OF THE POOL BRIDGE SHOWING PRE-AMPLIFIER AND TYGON TUBING CONTAINING THE COAXIAL CABLES

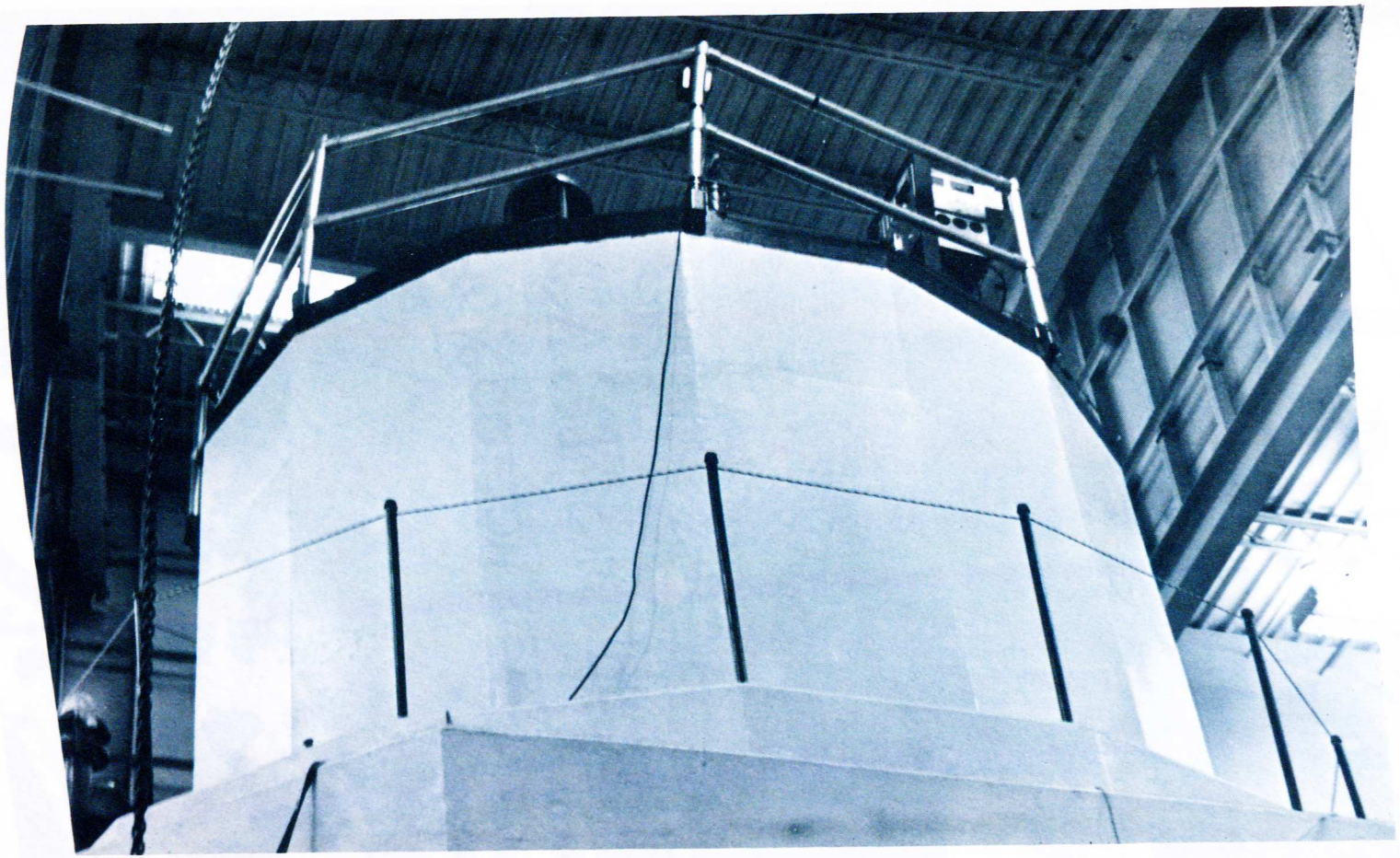

FIGURE 6- VIEW OF THE BIOLOGICAL SHIELD OF THE UMR SHOWING THE POOL BRIDGE INSTRUMENTATION AND CABLE LEADING TO THE COUNTING ROOM

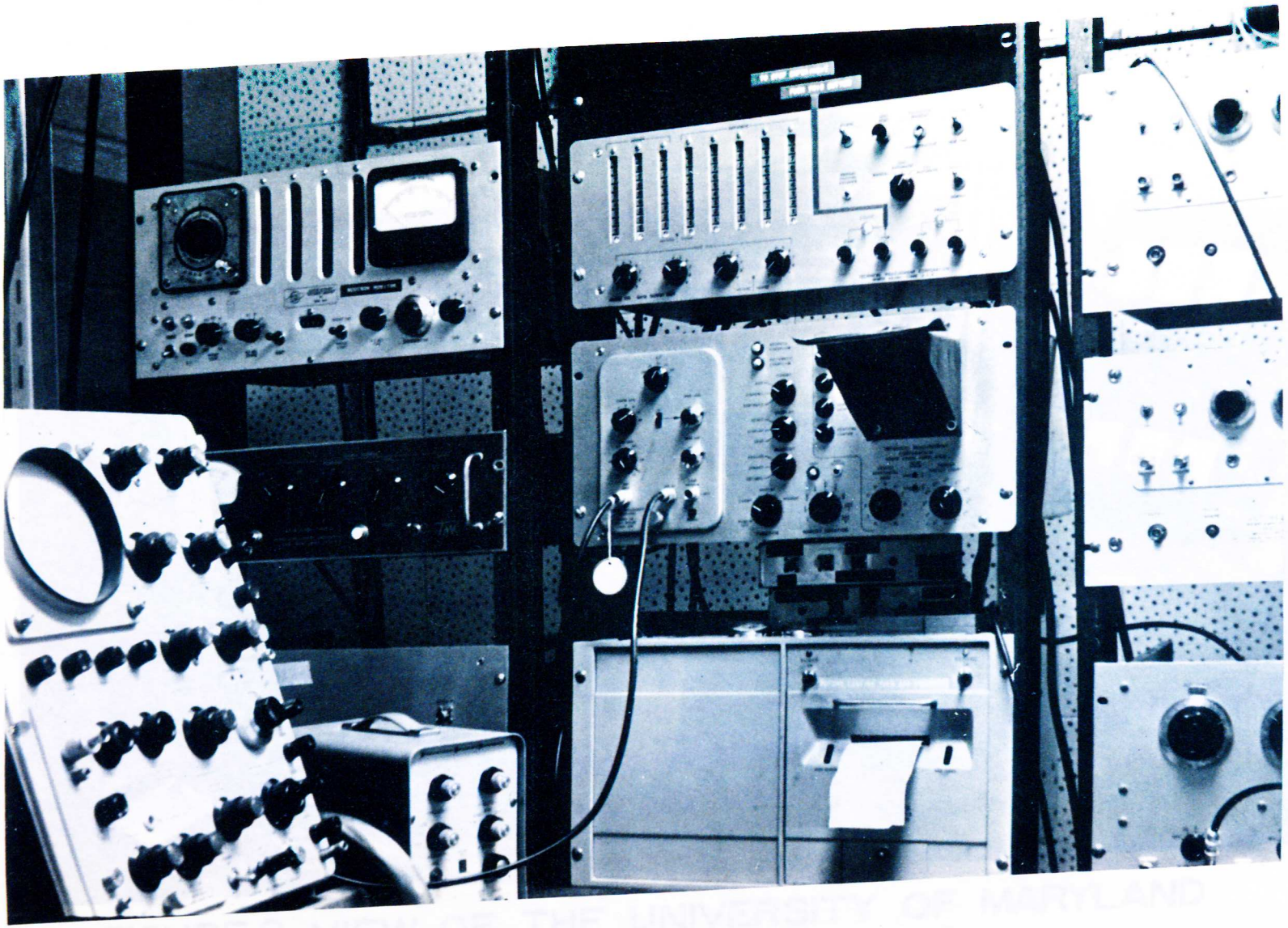

FIGURE 7- VIEW OF THE COUNTING ROOM

FIGURE 8- VIEW OF THE UNIVERSITY OF MARYLAND REACTOR CONSOLE

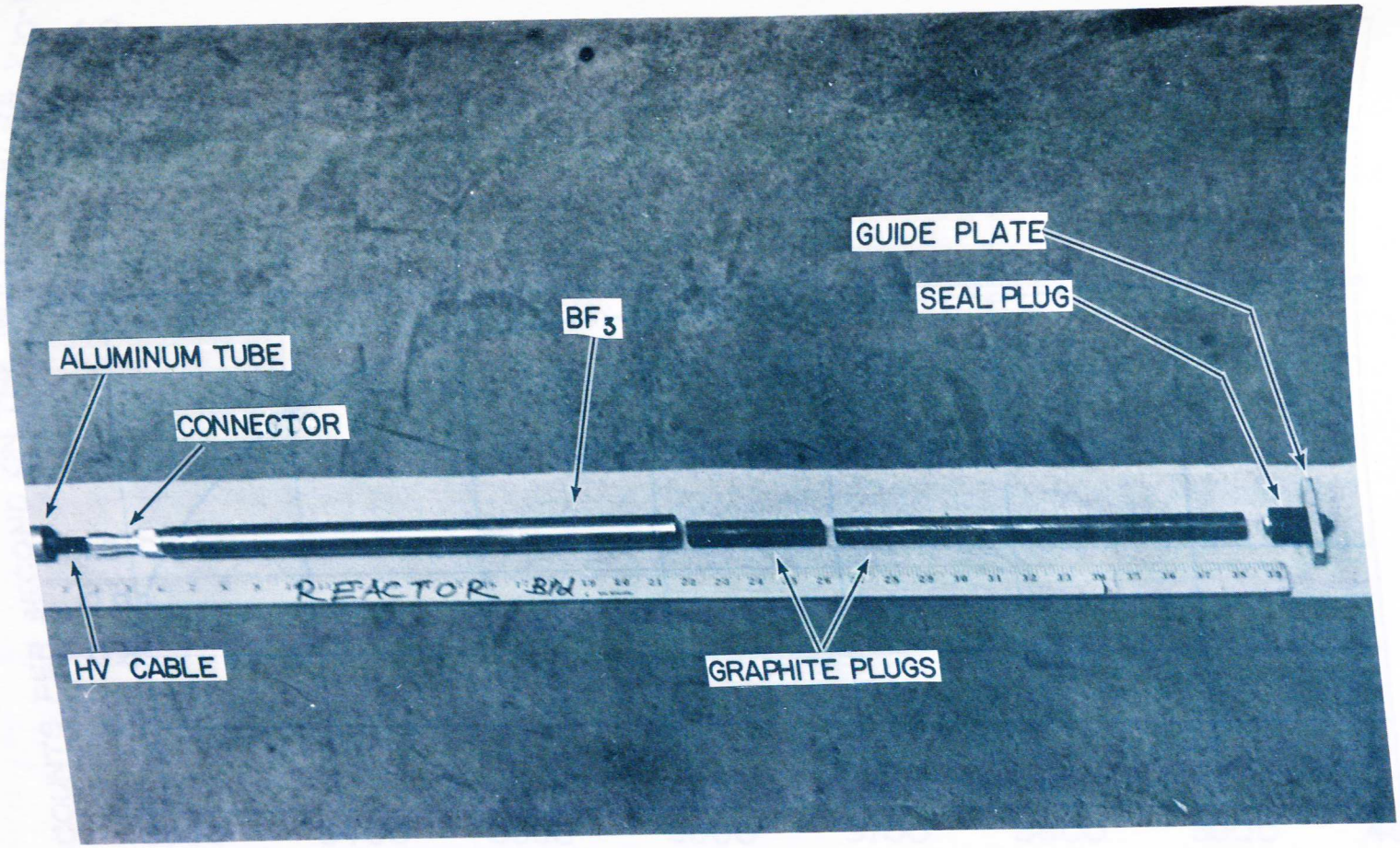

FIGURE 9- DETAIL SHOWING LOWER END OF ALUMINUM TUBE, CABLE, CONNECTOR, BF_3, GRAPHITE PLUG, SEAL PLUG AND GUIDE PLATE

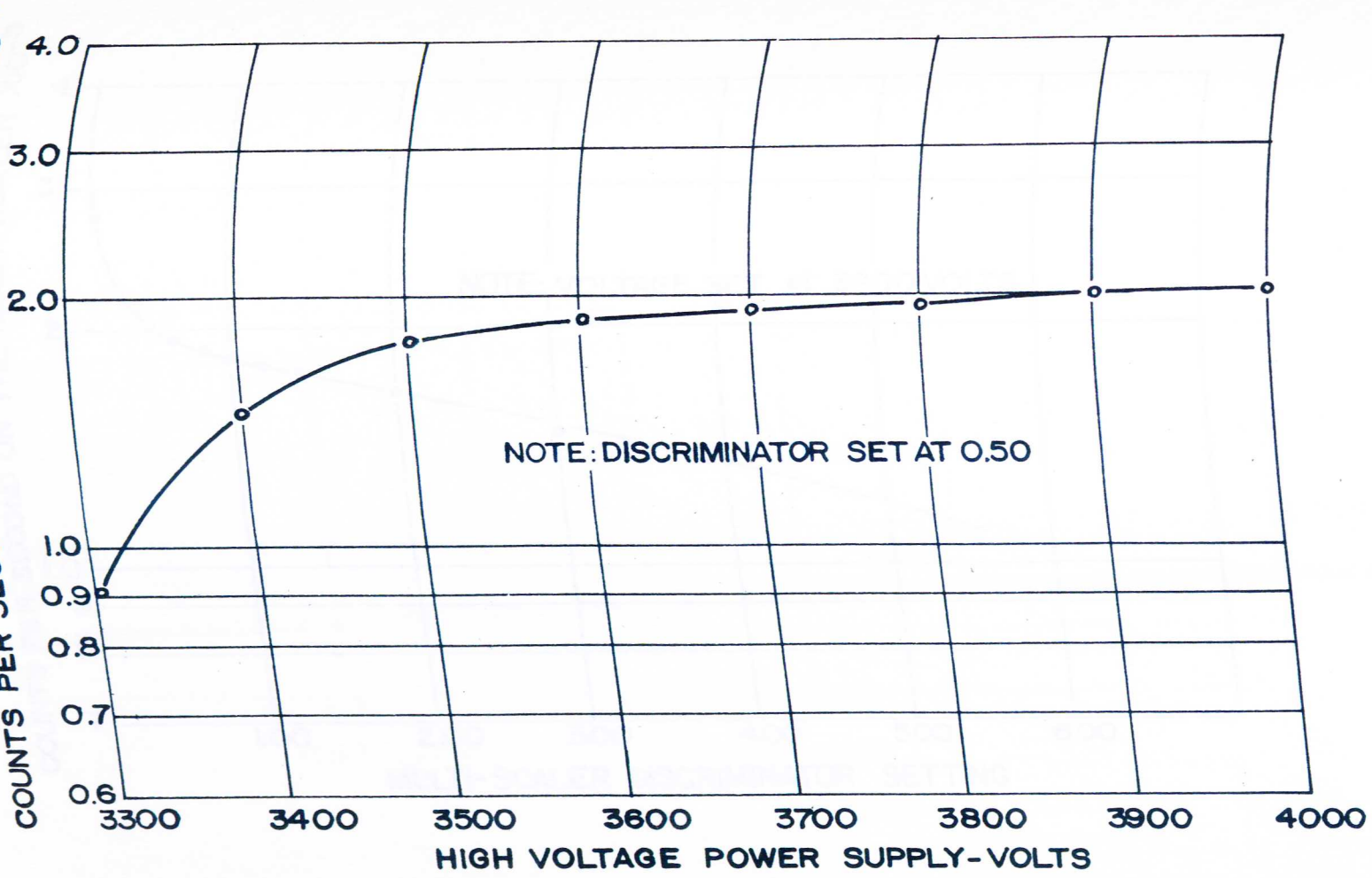

FIGURE 10 VOLTAGE CURVE-NEUTRONS FROM PU-BE ONLY

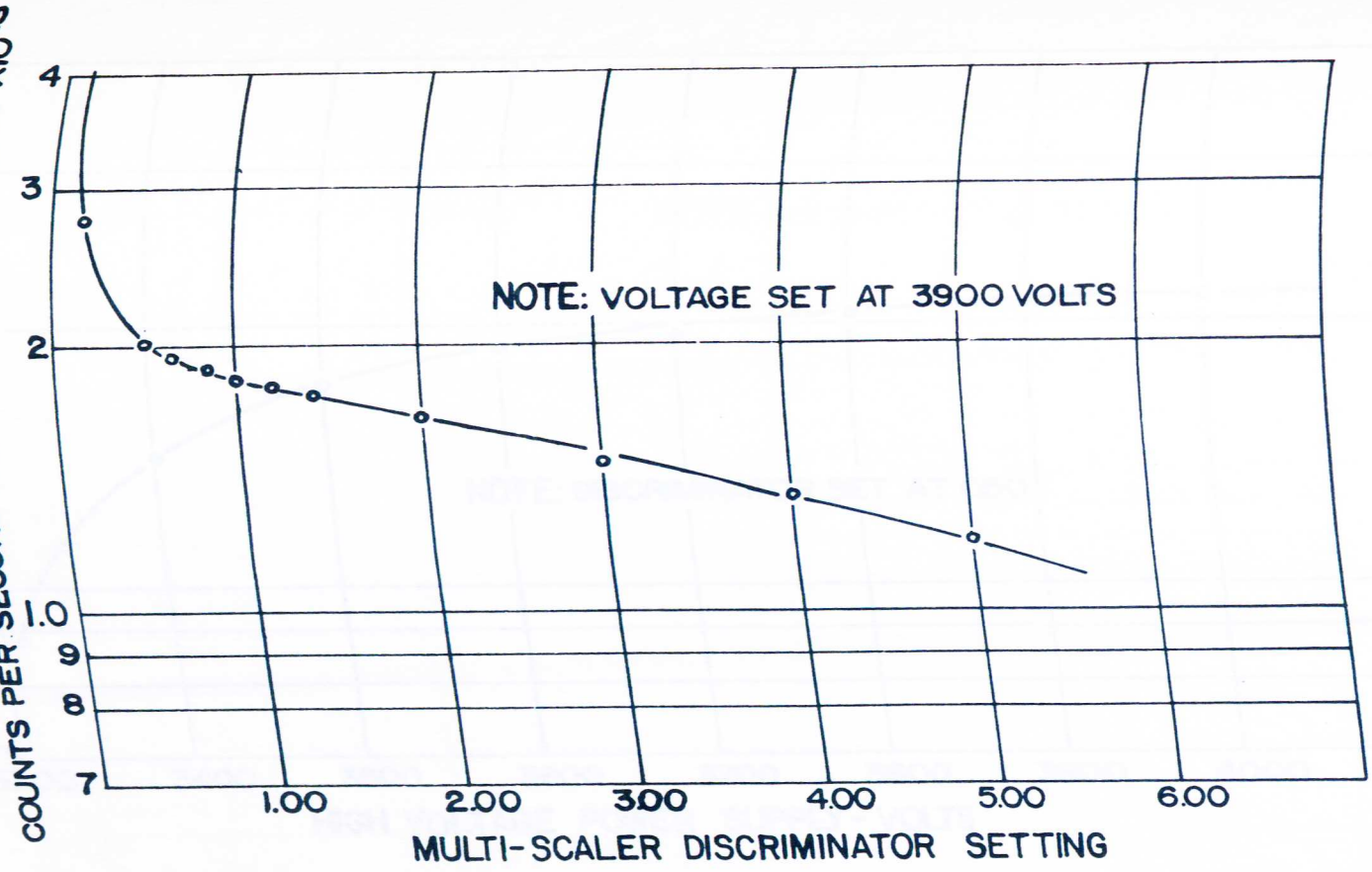

FIGURE II PULSE HEIGHT DISTRIBUTION- NEUTRONS FROM PU-BE ONLY

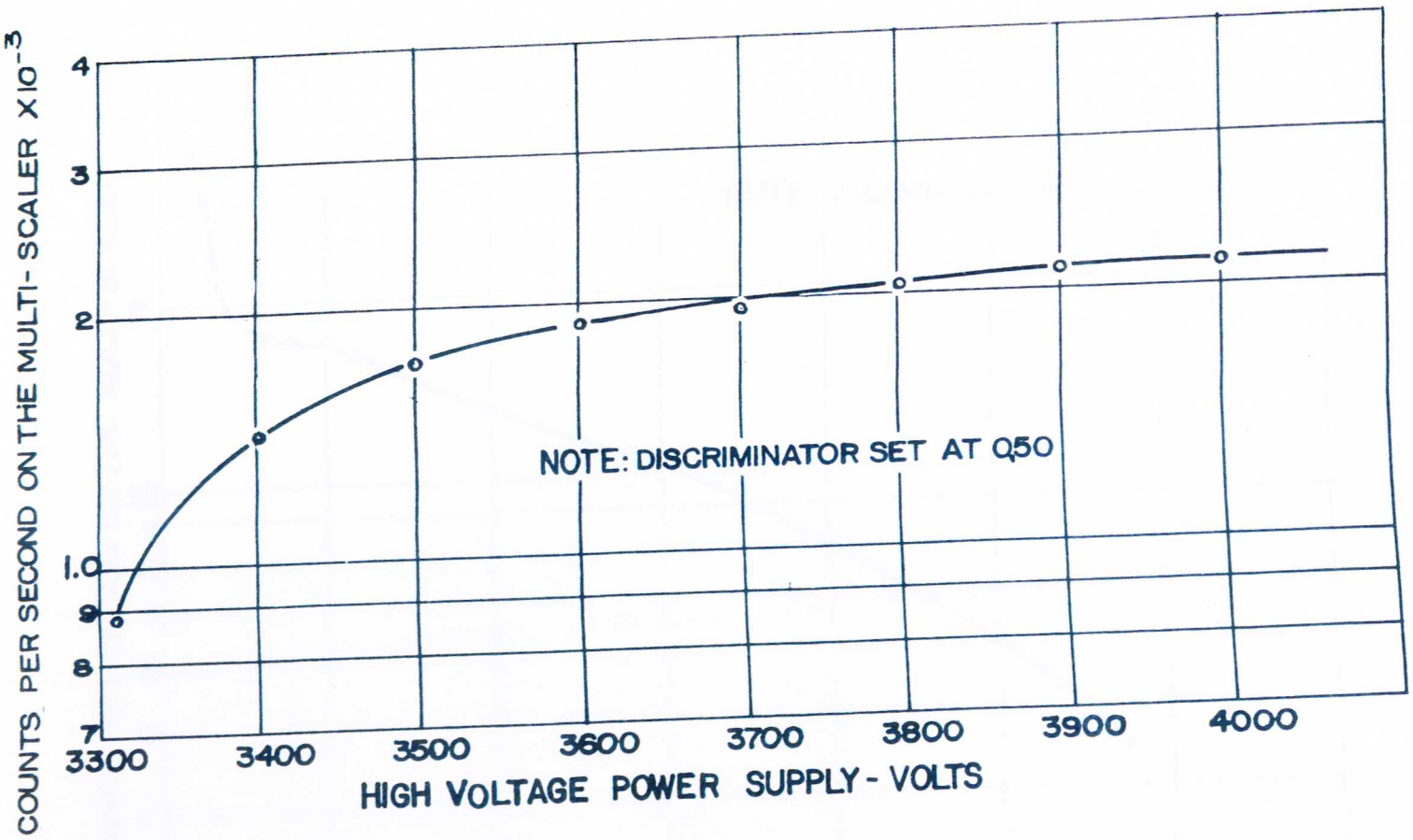

FIGURE 12 VOLTAGE CURVE-NEUTRONS FROM PU-BE, AND GAMMA RADIATION FROM COBALT SOURCE

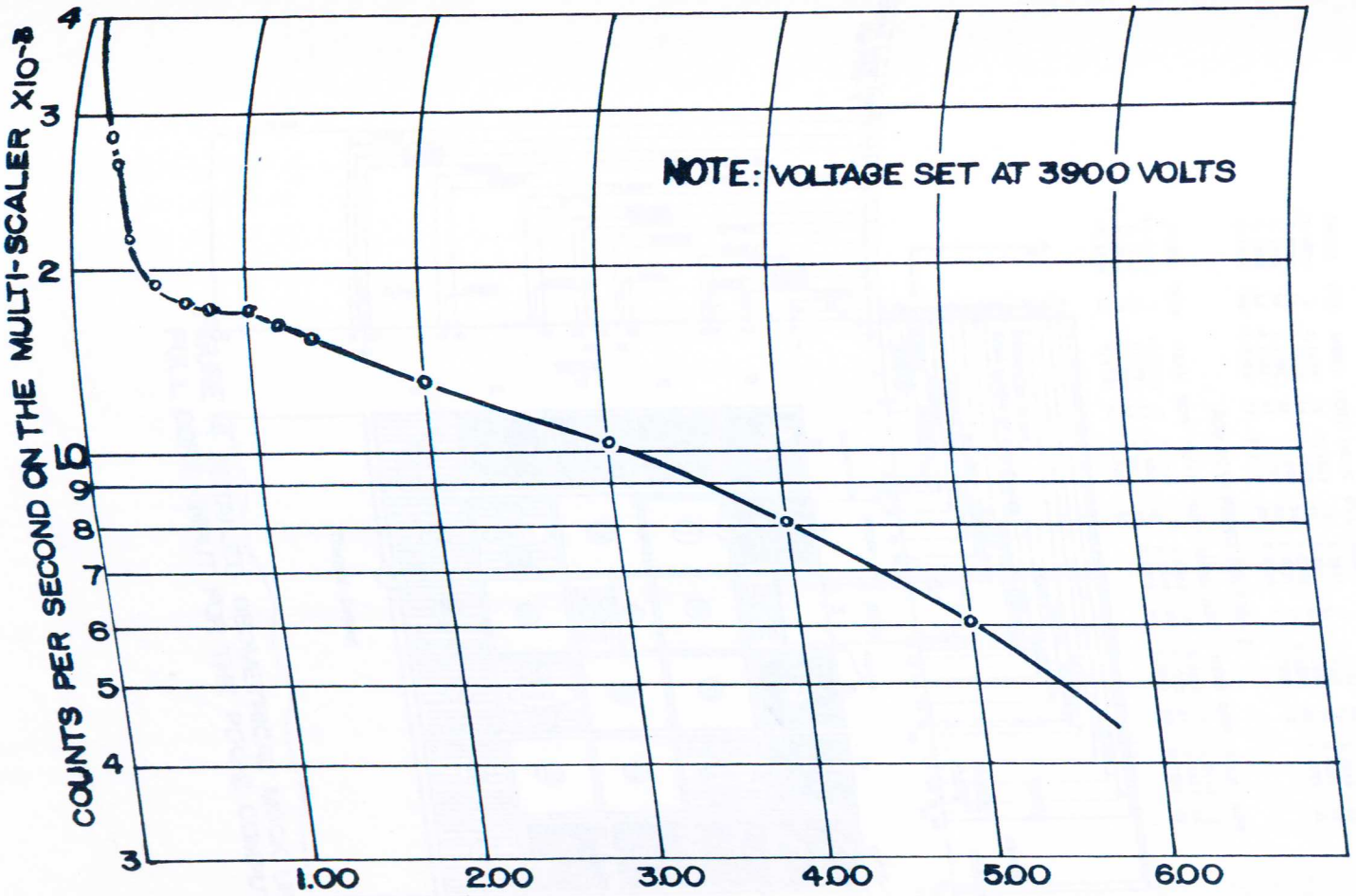

FIGURE 13 PULSE HEIGHT DISTRIBUTION-NEUTRONS FROM PU-BE, AND GAMMA RADIATION FROM COBALT SOURCE

COLUMN MESH POINTS FOR PDQ - 2

MESH	COL	MESH	COL	MESH	COL	MESH	COL	MESH	COL	MESH	COL
10.0000	1	5.0000	3	0.2629	5	2.3495	8	0.2629	10	0.3613	12
0.3327	14	0.6655	16	0.6655	20	0.4991	24	0.7226	25	0.5258	26
0.1968	27	1.1091	33	0.1968	34	0.5258	35	0.7226	36	0.4991	40
0.6655	44	0.4991	48	0.7226	50	0.4991	54	0.6655	58	0.4991	62
0.3613	64	0.2629	66	2.3494	69	0.2629	71	5.0000	74		

ROW MESH POINTS FOR PDQ - 2

MESH	ROW	MESH	ROW	MESH	ROW	MESH	ROW	MESH	ROW	MESH	ROW
10.0000	1	10.0000	2	0.3302	3	1.8605	5	0.6655	6	1.3310	8
0.1651	10	0.1651	12	0.8811	20	0.3302	22	1.5278	24	0.3327	26
0.8318	30	0.3302	32	0.8811	40	0.3302	42	0.8811	50	0.1651	52
0.5295	54	0.4762	56	5.0000	60						

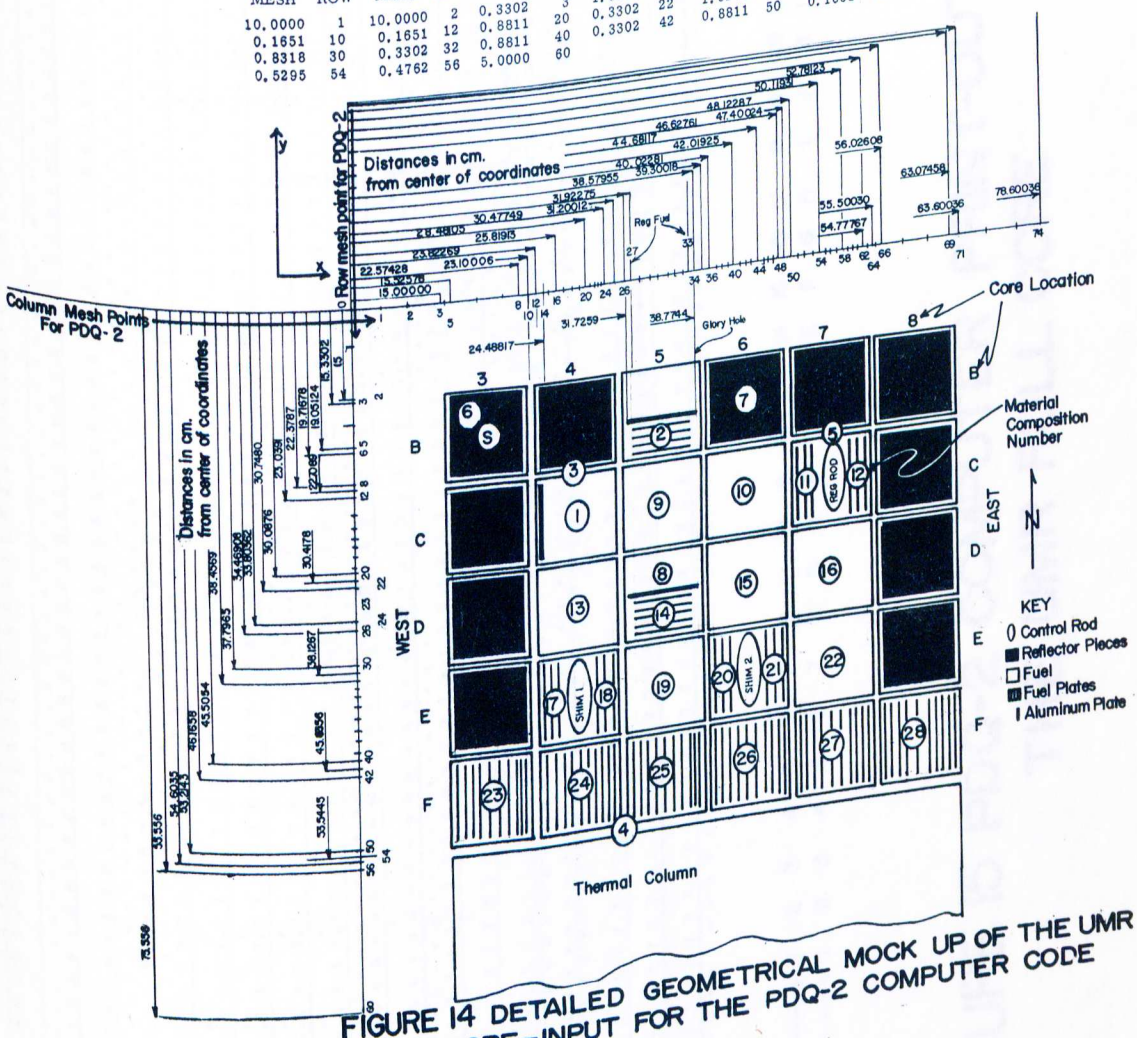

FIGURE 14 DETAILED GEOMETRICAL MOCK UP OF THE UMR FULL CORE-INPUT FOR THE PDQ-2 COMPUTER CODE

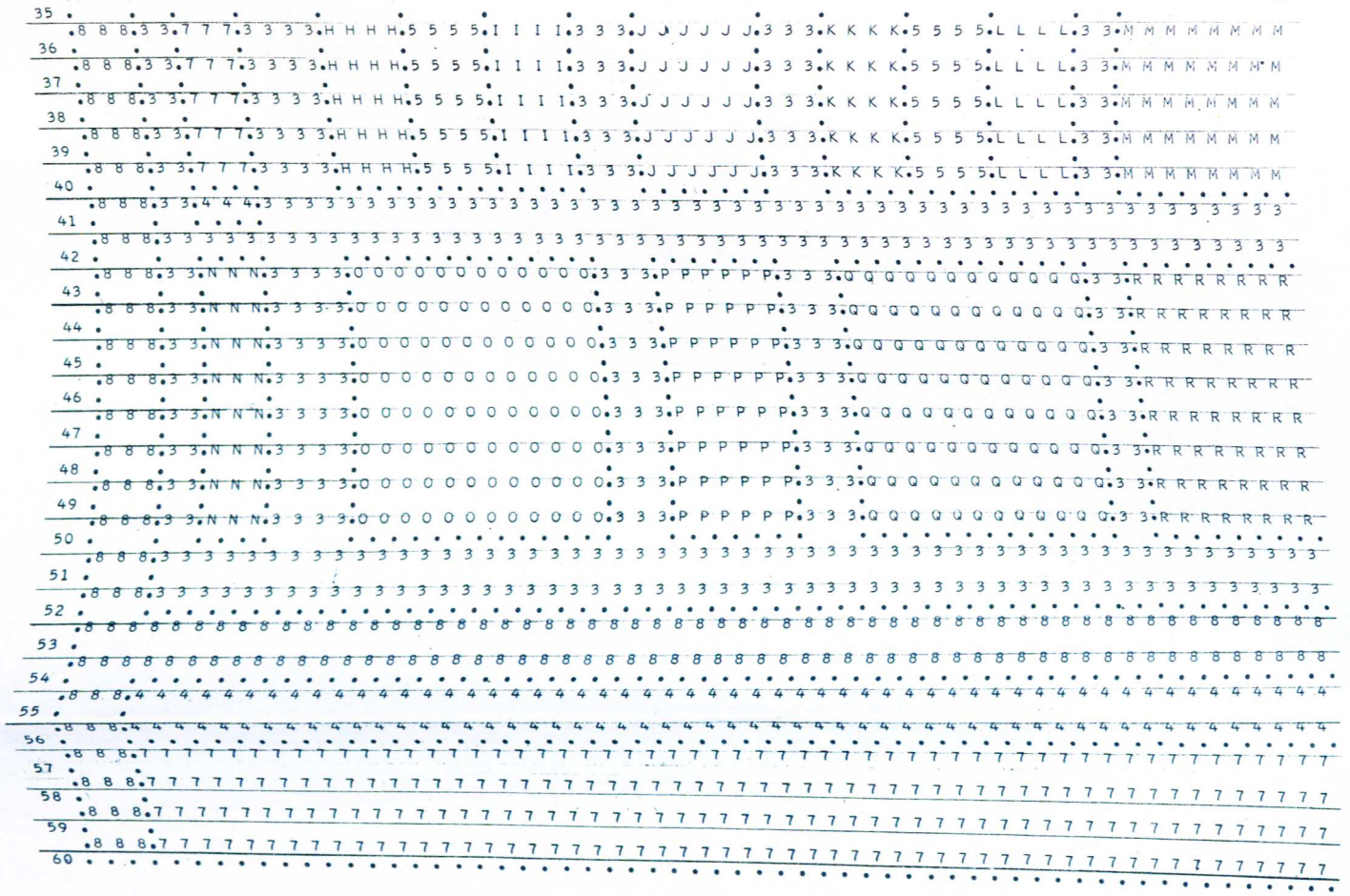

NOTE:

Region No. From Table V ⟶	1	2	3	4	5	6	7	8	9	10	11	12	13	14	15	16	17	18	19	20	21	22	23	24	25	26	27	28
Corresponding PDQ-2 Region ⟶	1	2	3	4	5	6	7	8	9	A	B	C	D	E	F	G	H	I	J	K	L	M	N	O	P	Q	R	S

FIGURE 15 PDQ-2 COMPUTER PRINT-OUT FOR THE UMR FULL CORE

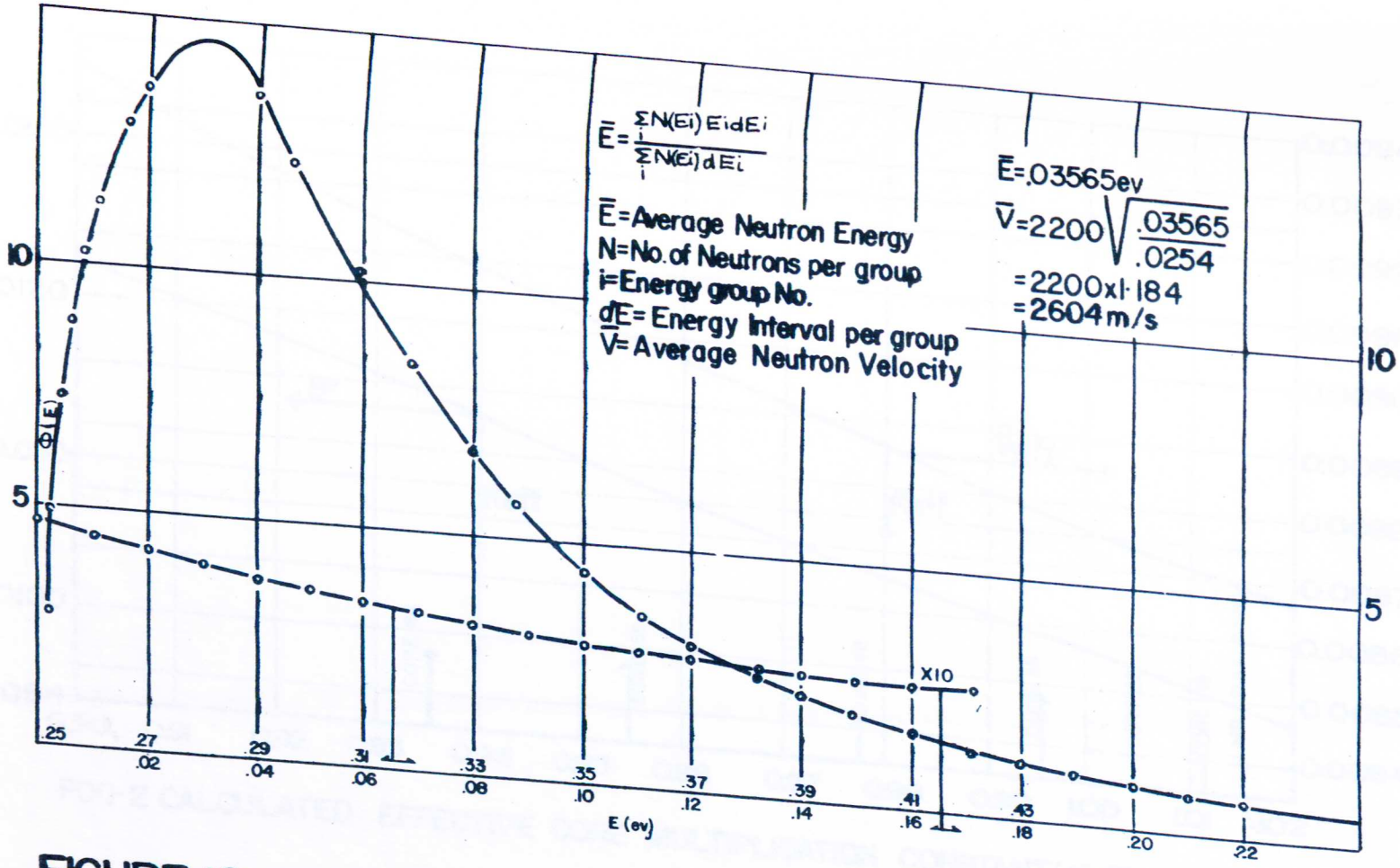

FIGURE 16 NEUTRON FLUX SPECTRUM FOR THE UMR CORE COLD CLEAN AS OBTAINED FROM THE TEMPESTII COMPUTER CODE

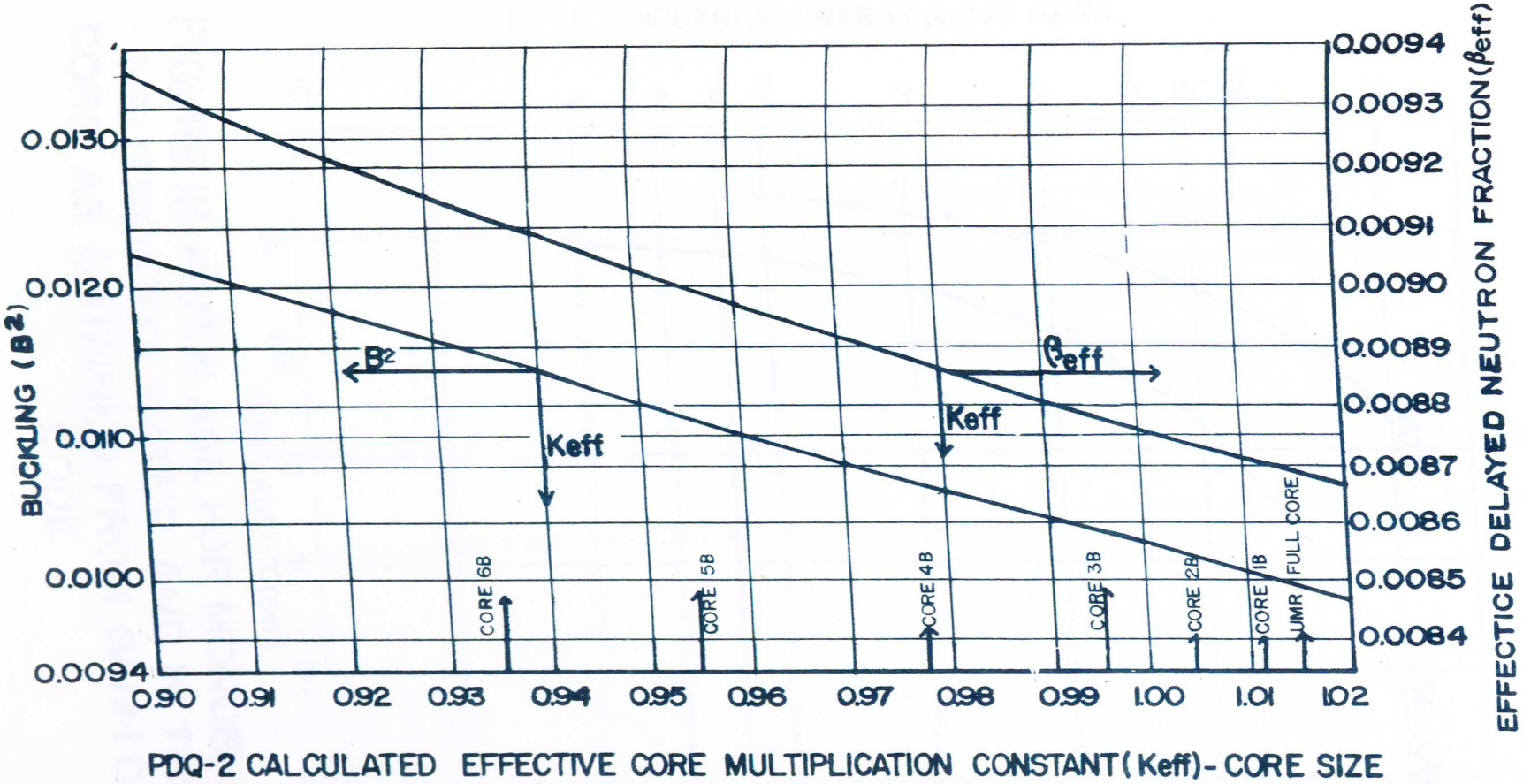

FIGURE 17 BUCKLING AND EFFETIVE DELAYED NEUTRON FRACTION AS A FUNCTION OF THE UMR CORE SIZE

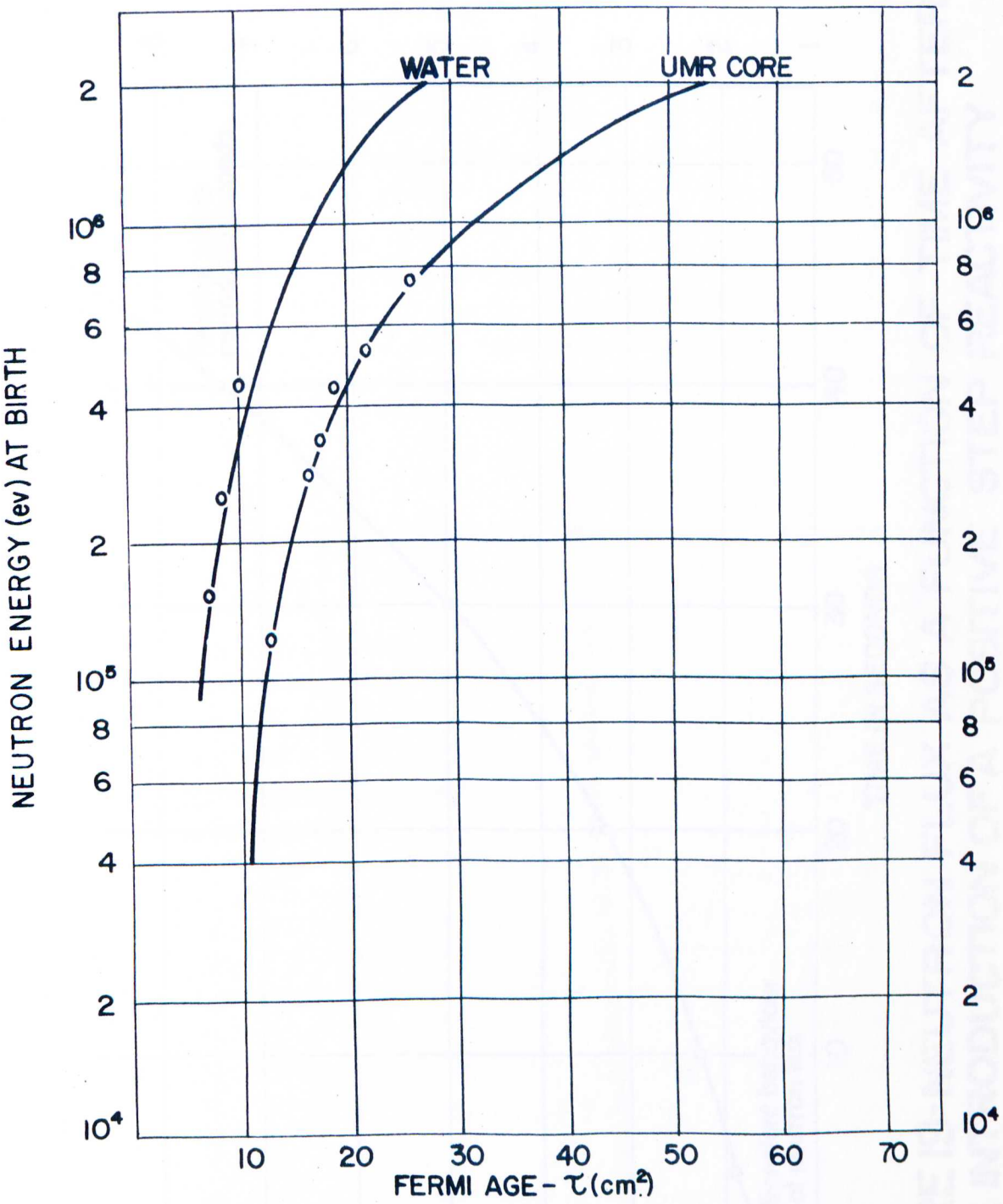

FIGURE 18- FERMI AGE FOR MONOENERGETIC NEUTRONS IN WATER AND IN THE UMR CORE AS OBTAINED FROM GAM-I COMPUTER CODE

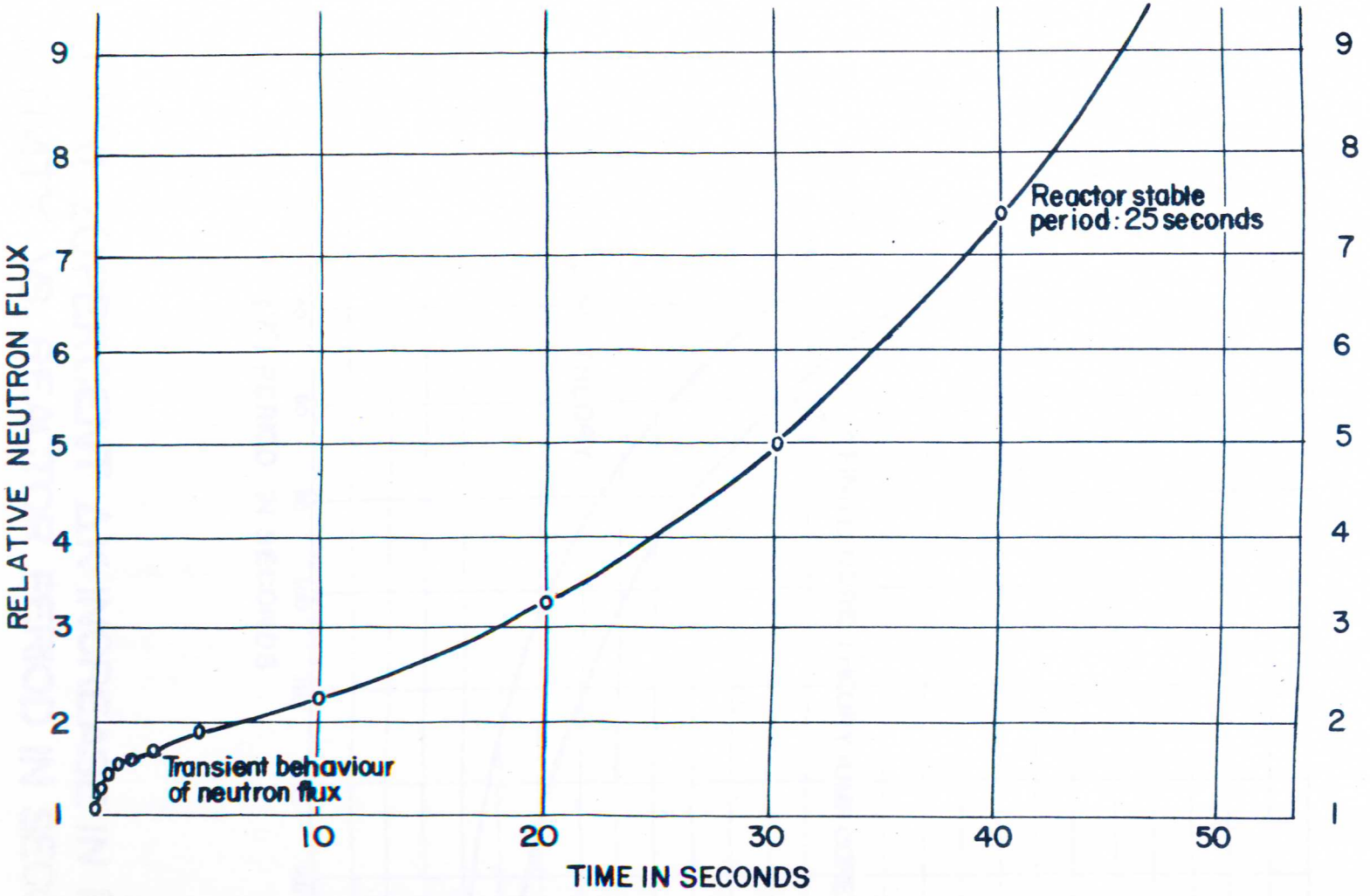

FIGURE 19-NEUTRON FLUX AS A FUNCTION OF TIME AFTER THE INTRODUCTION OF A POSITIVE STEP REACTIVITY

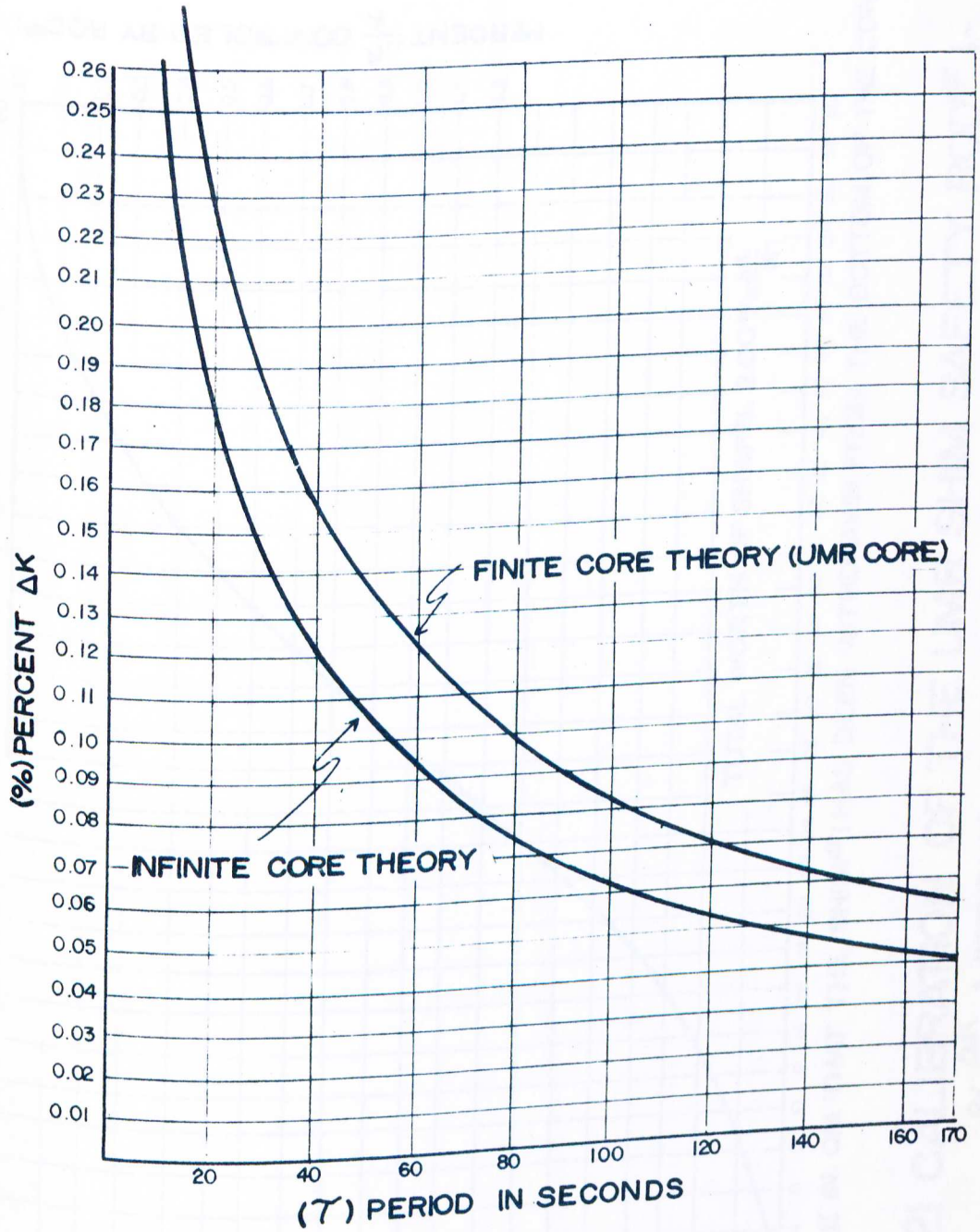

FIGURE 20 PERCENT ΔK INCREASE IN REACTIVITY VS. REACTOR PERIOD IN SECONDS

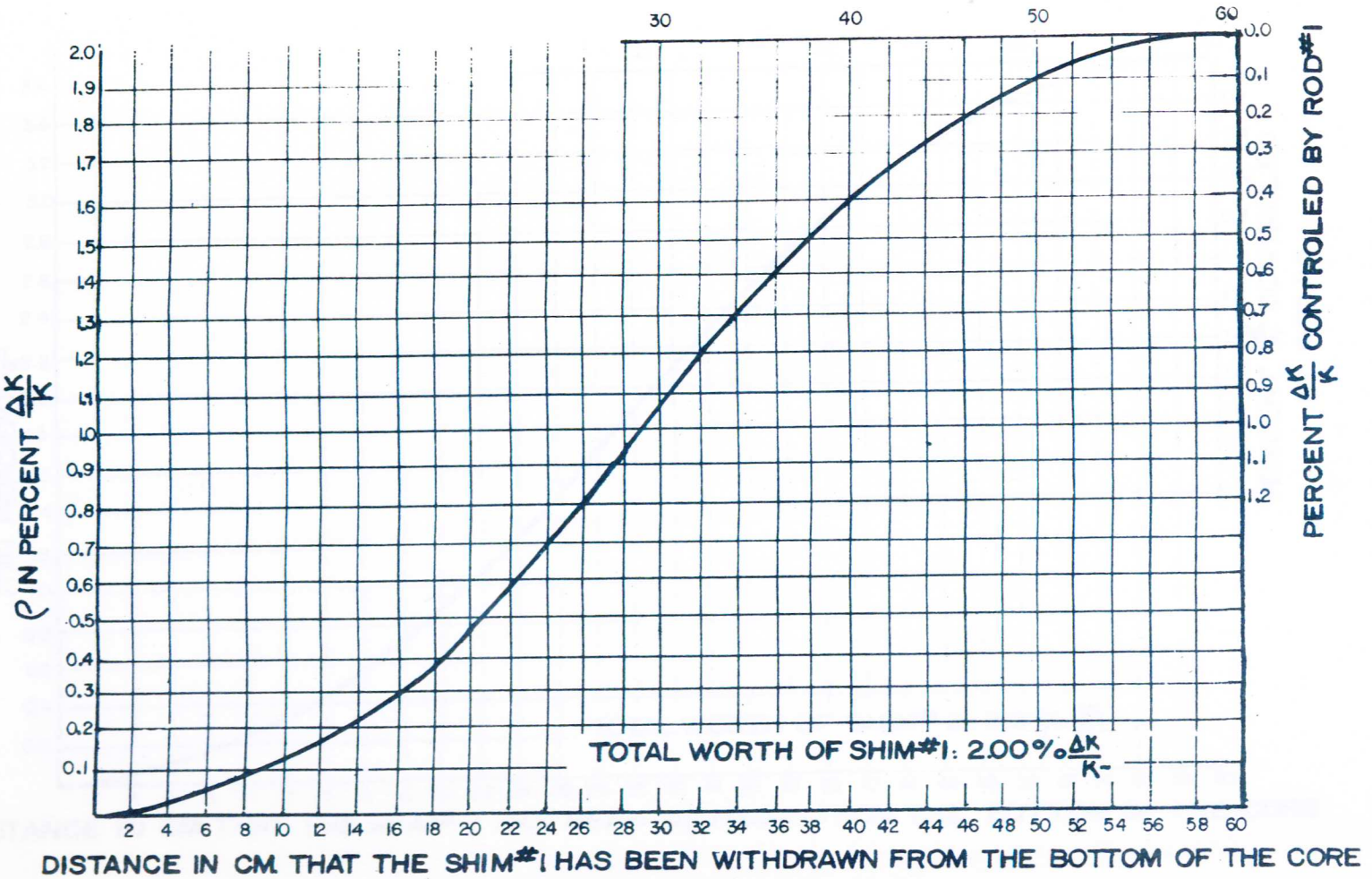

FIGURE 21 CALIBRATION OF THE UMR SHIM SAFETY ROD# 1- $\%\frac{\Delta K}{K}$ VERSUS DISTANCE IN CM.

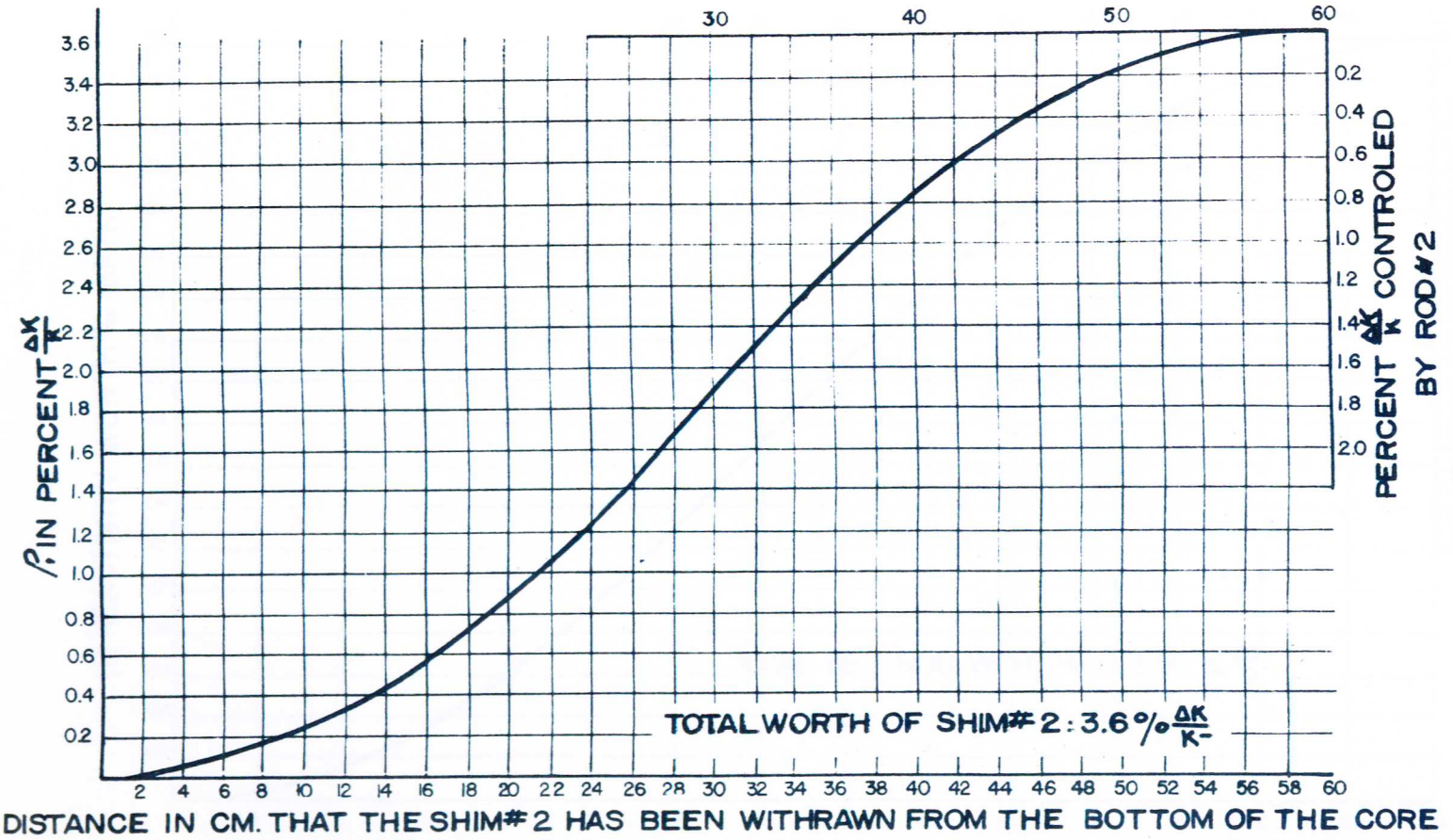

FIGURE 22 CALIBRATION OF THE UMR SHIM SAFETY ROD#2 - %ΔK/K VERSUS DISTANCE FROM CORE BOTTOM IN CENTIMETERS

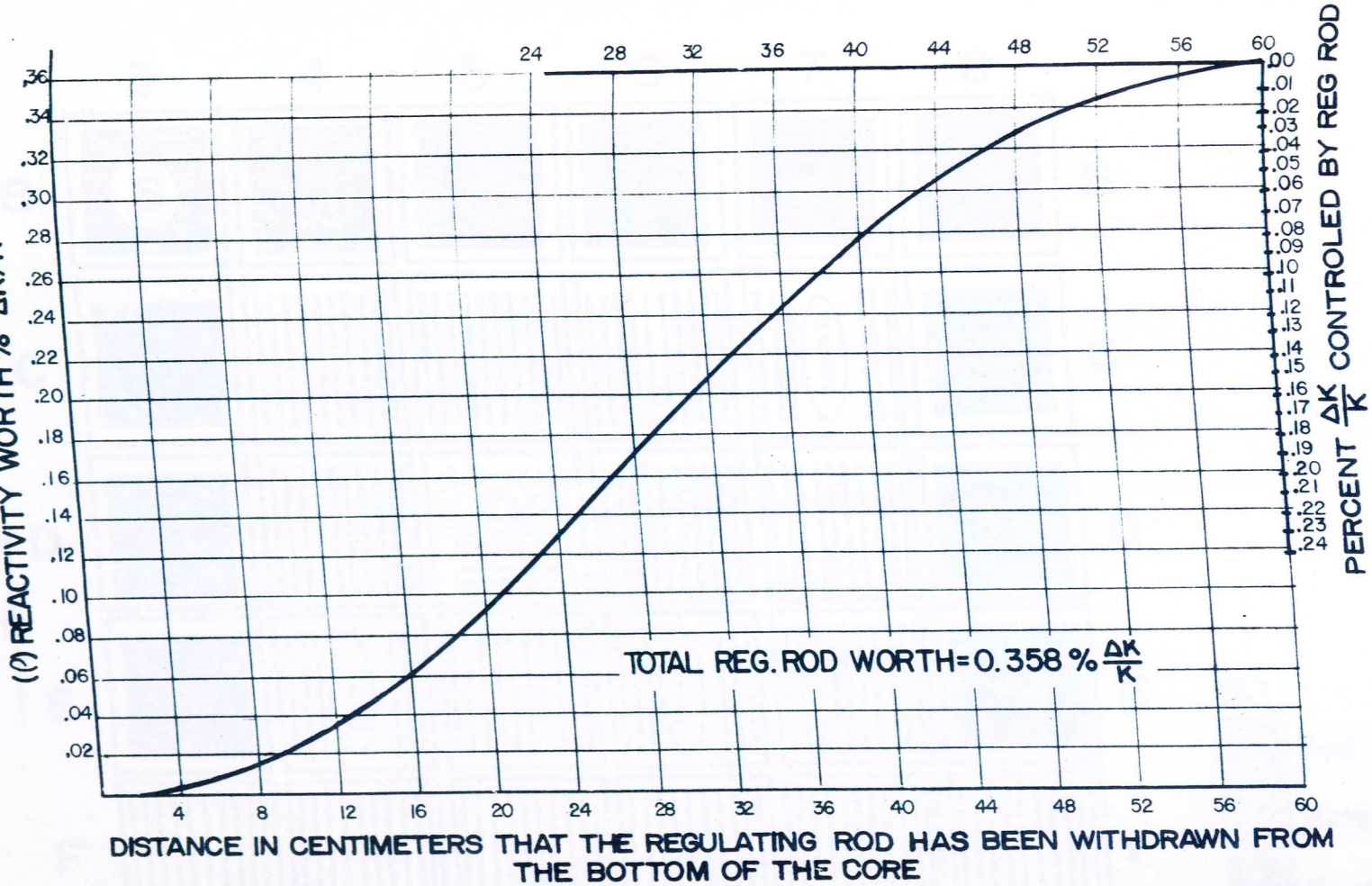

FIGURE 23 CALIBRATION OF THE U. OF MARYLAND PTR REGULATING ROD IN % $\frac{\Delta K}{K}$ VS. DISTANCE IN CM.

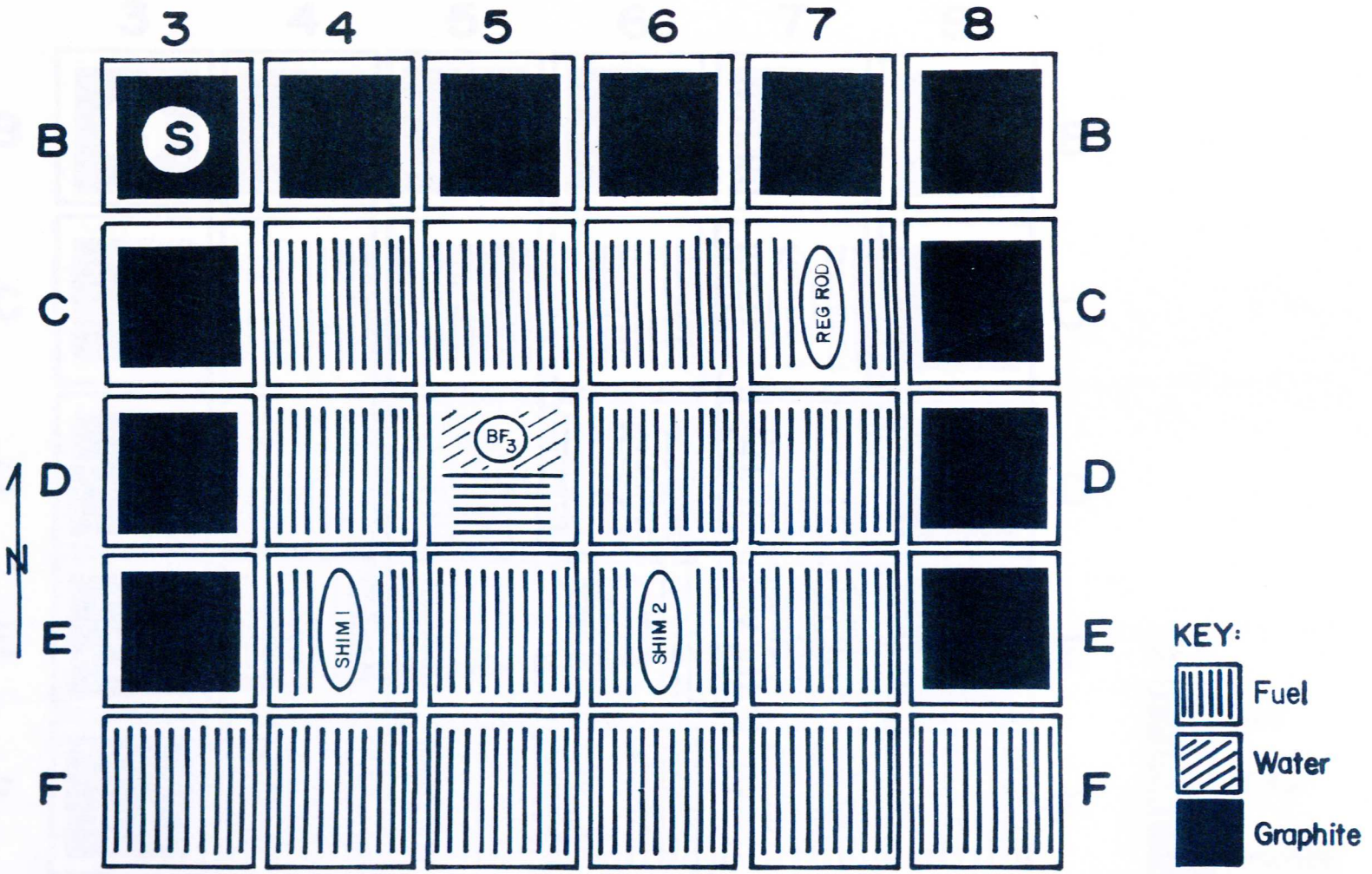

FIGURE 24 UMR FUEL ARRANGEMENT FOR UNLOADING STEP# 1 AND LOADING STEP# 13

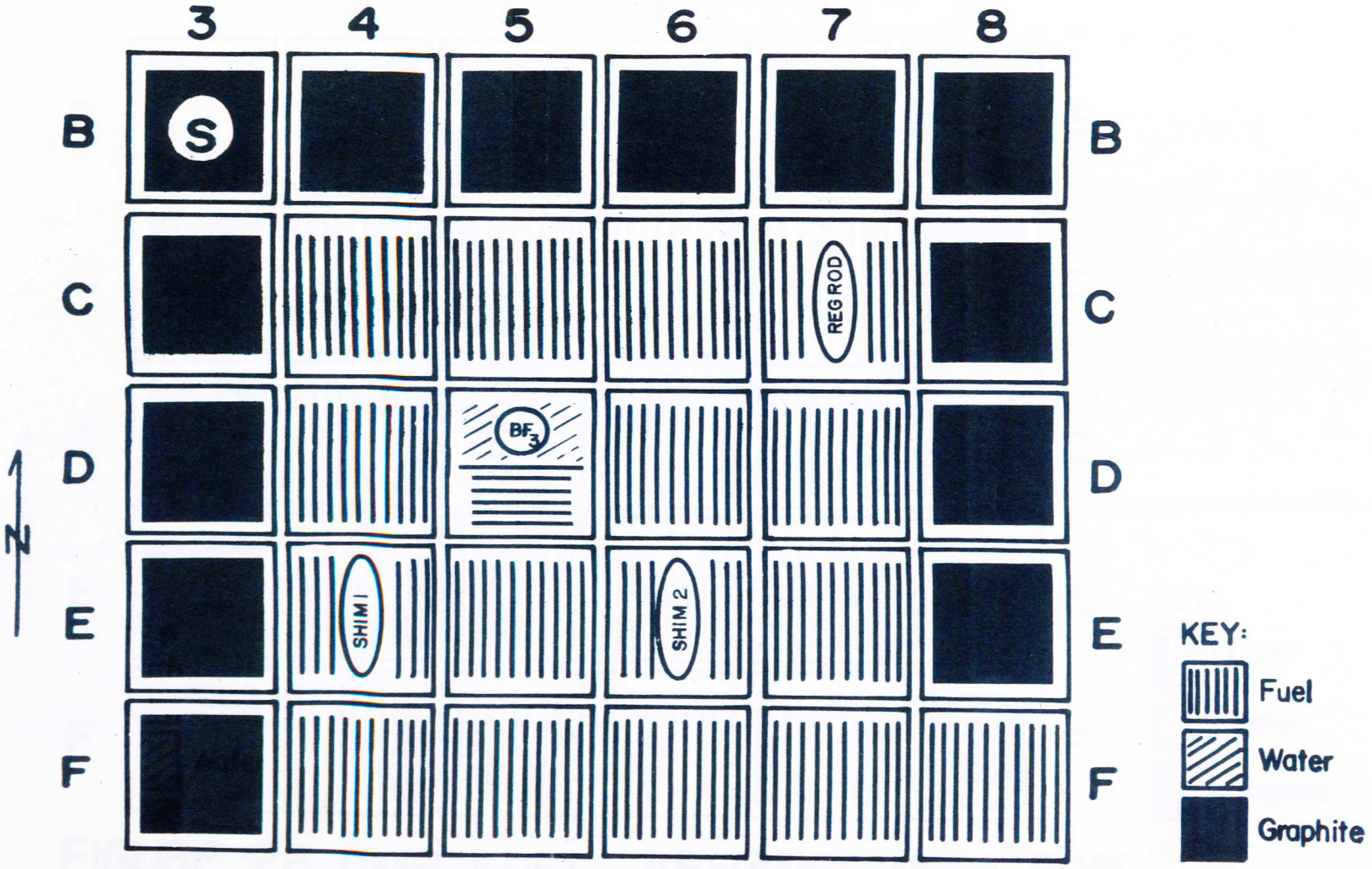

FIGURE 25 UMR FUEL ARRANGEMENT FOR UNLOADING STEP# 2 AND LOADING STEP# 12

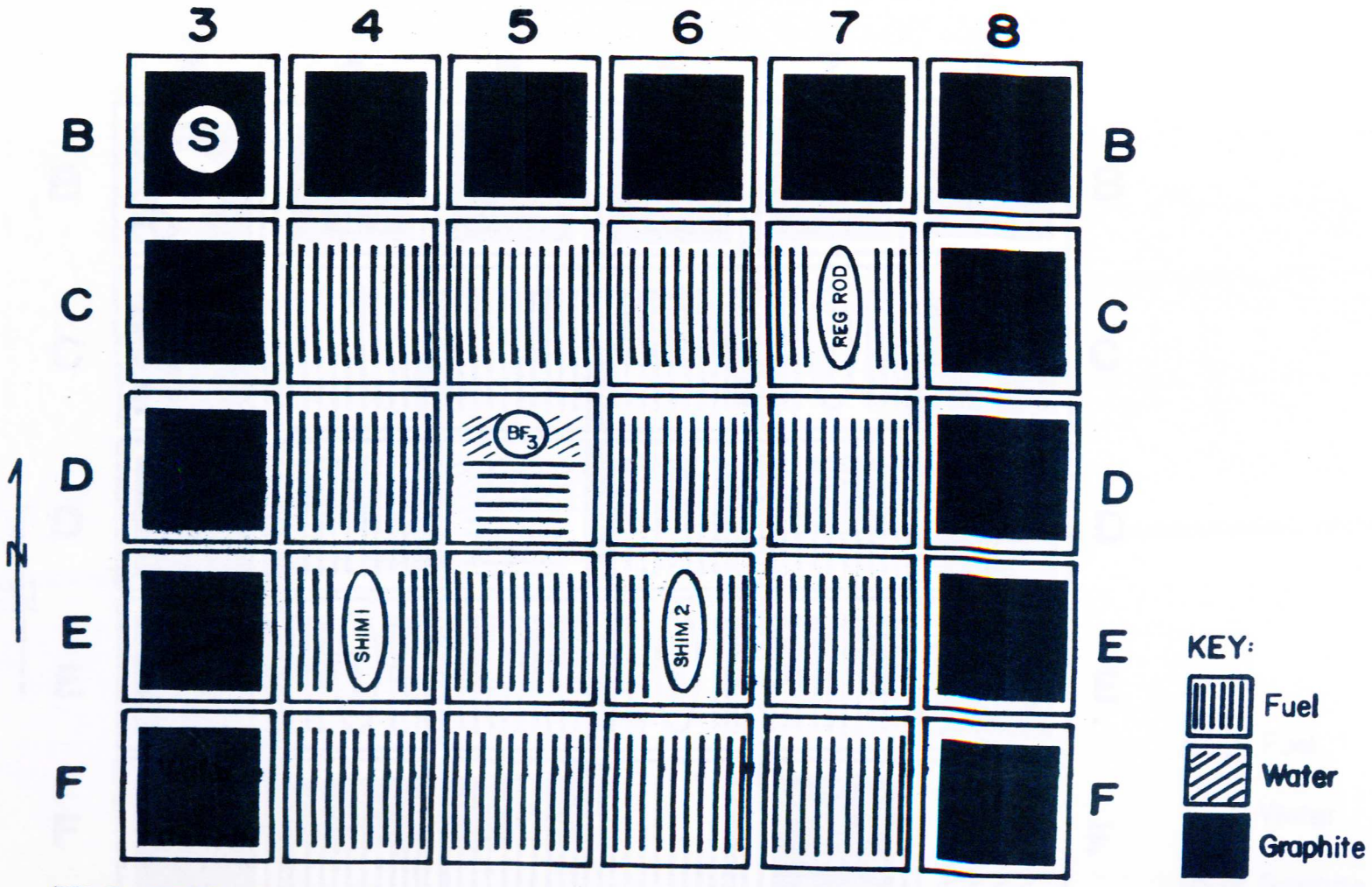

FIGURE 26 UMR FUEL ARRANGEMENT FOR UNLOADING STEP# 3 AND LOADING STEP# 11

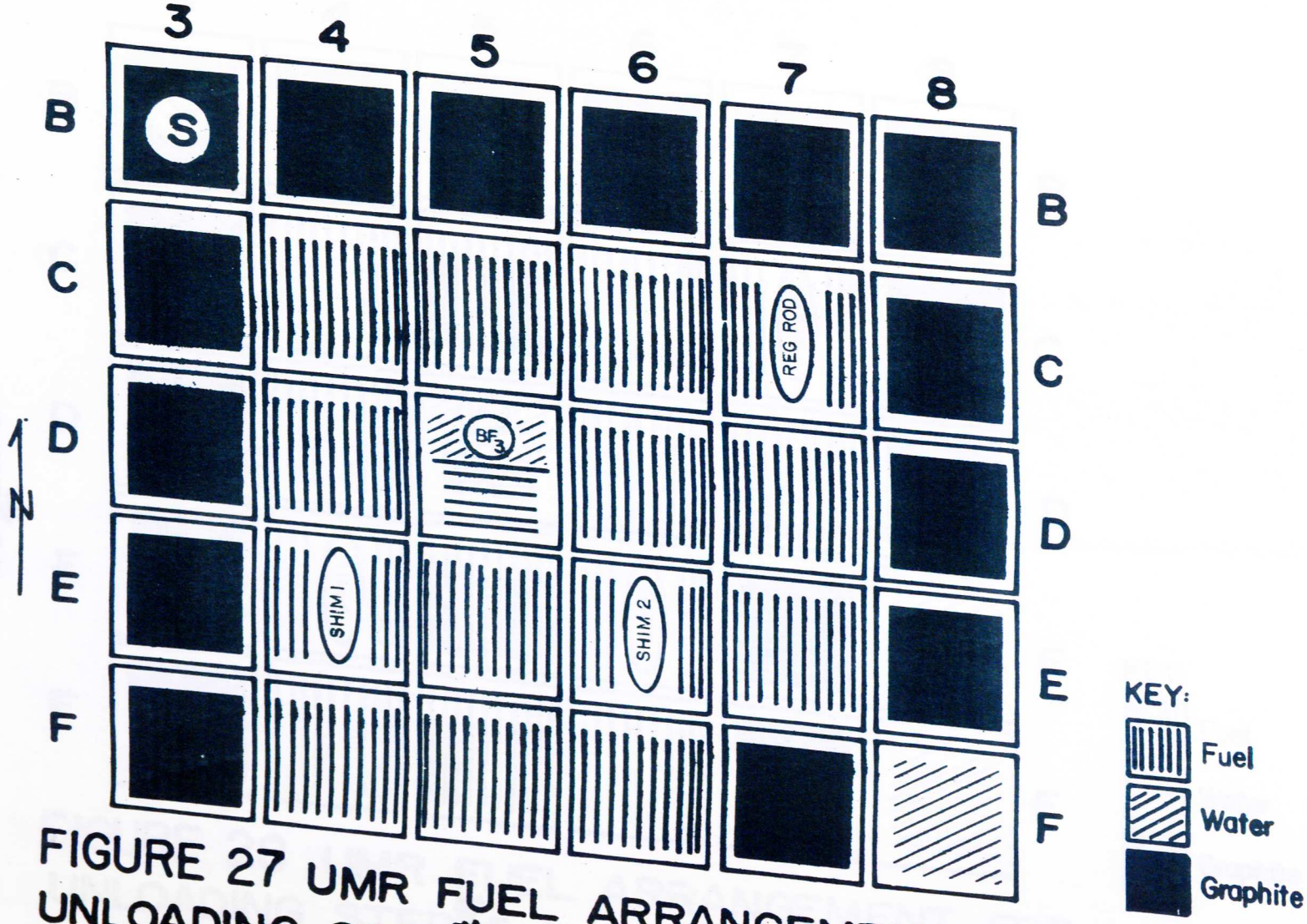

FIGURE 27 UMR FUEL ARRANGEMENT FOR UNLOADING STEP#4 AND LOADING STEP#10

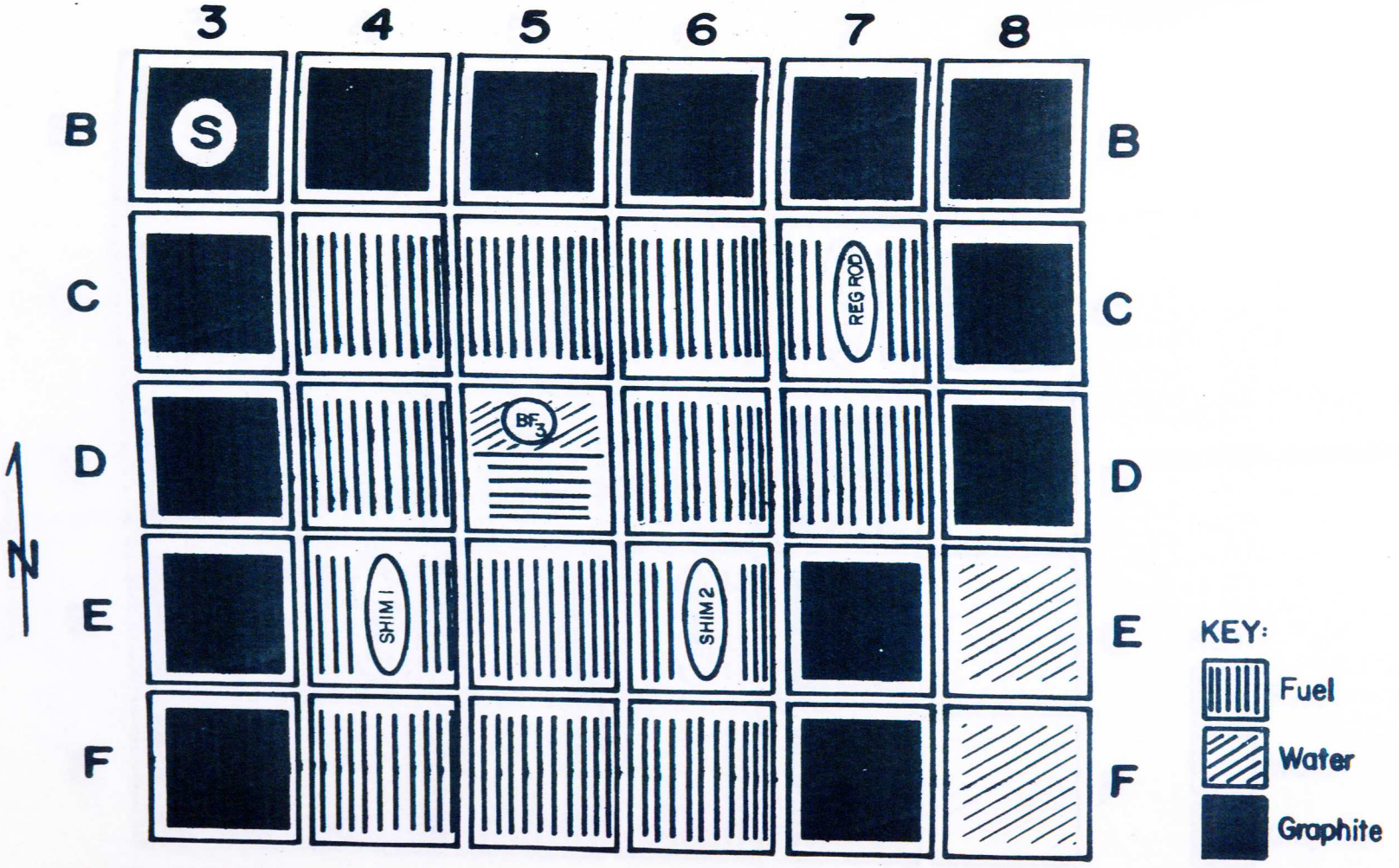

FIGURE 28 UMR FUEL ARRANGEMENT FOR UNLOADING STEP# 5 AND LOADING STEP# 9

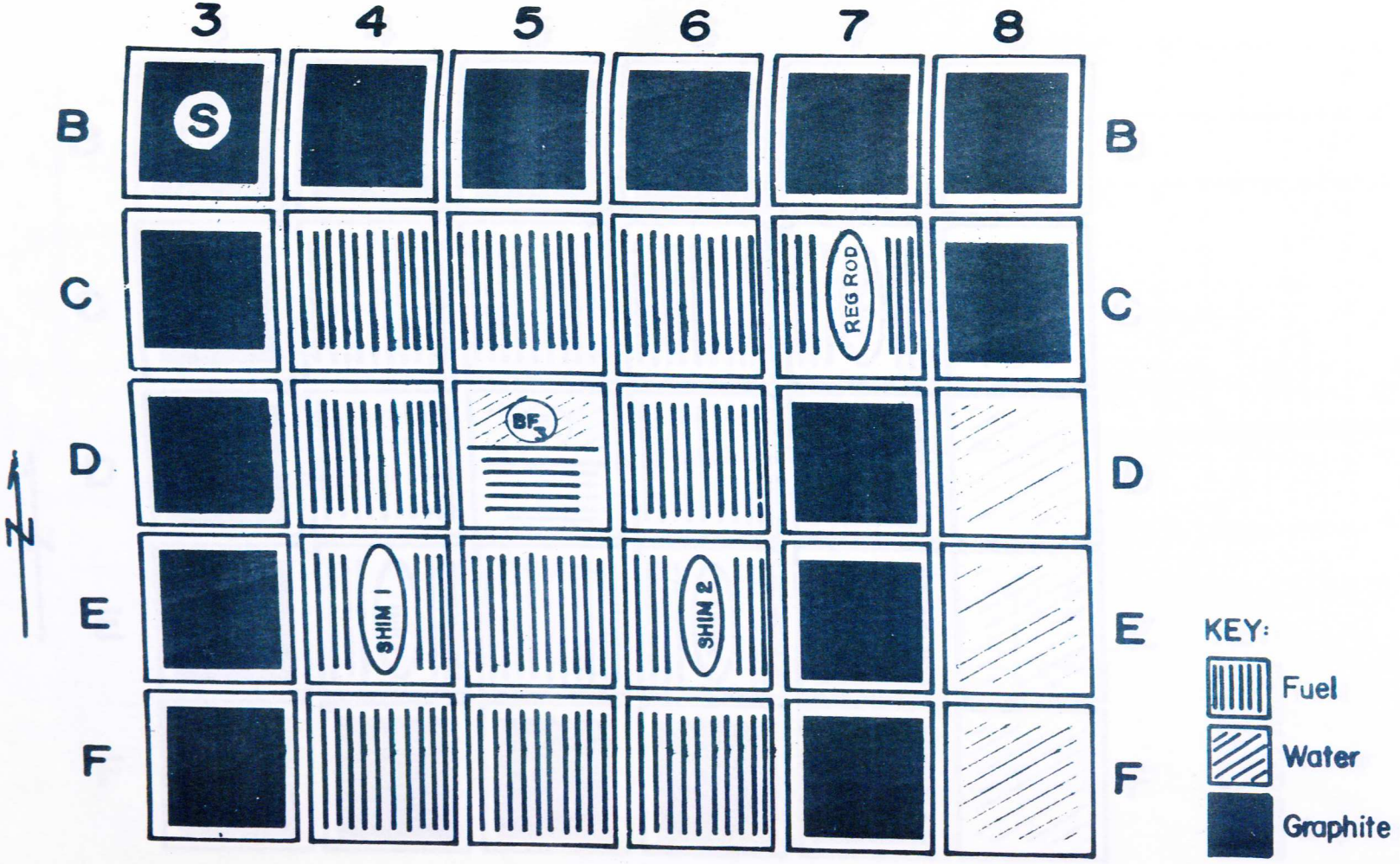

FIGURE 29 UMR FUEL ARRANGEMENT FOR UNLOADING STEP# 6 AND LOADING STEP# 8

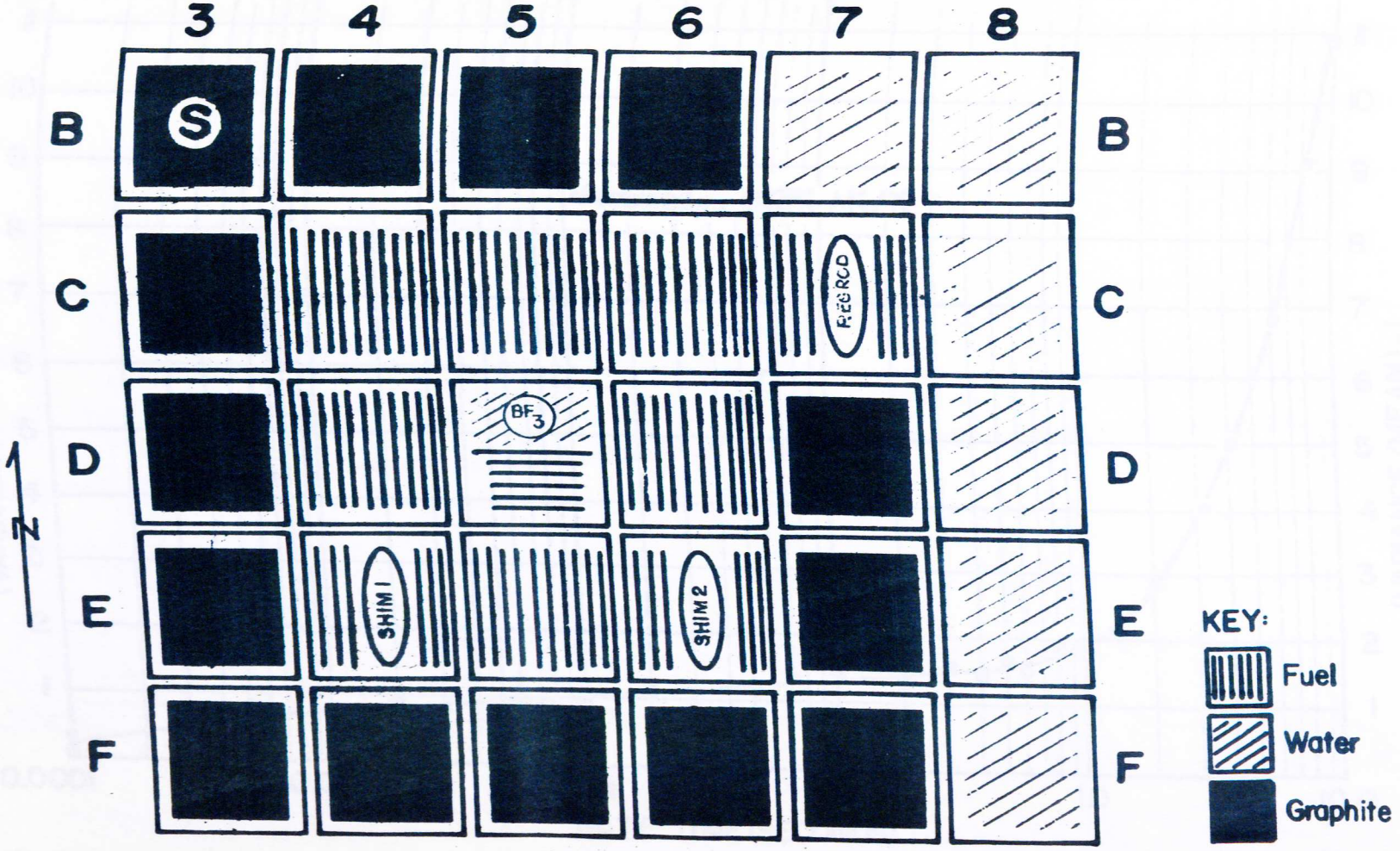

FIGURE 30 UMR FUEL ARRANGEMENT FOR UNLOADING STEP#7

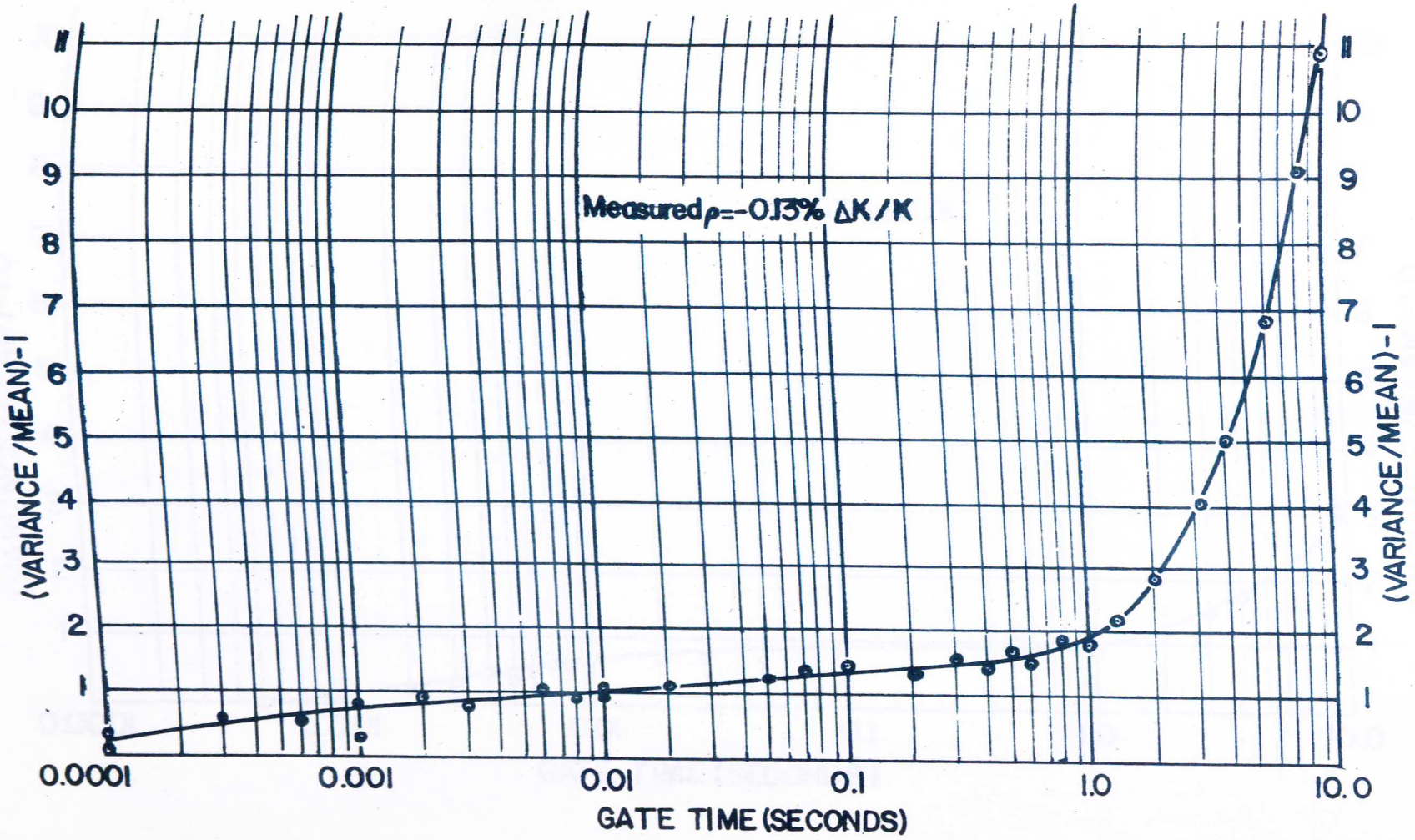

FIGURE 31 VARIANCE-TO-MEAN VERSUS GATE TIME FOR UMR FULL CORE WITH ALL RODS AT 45CM.

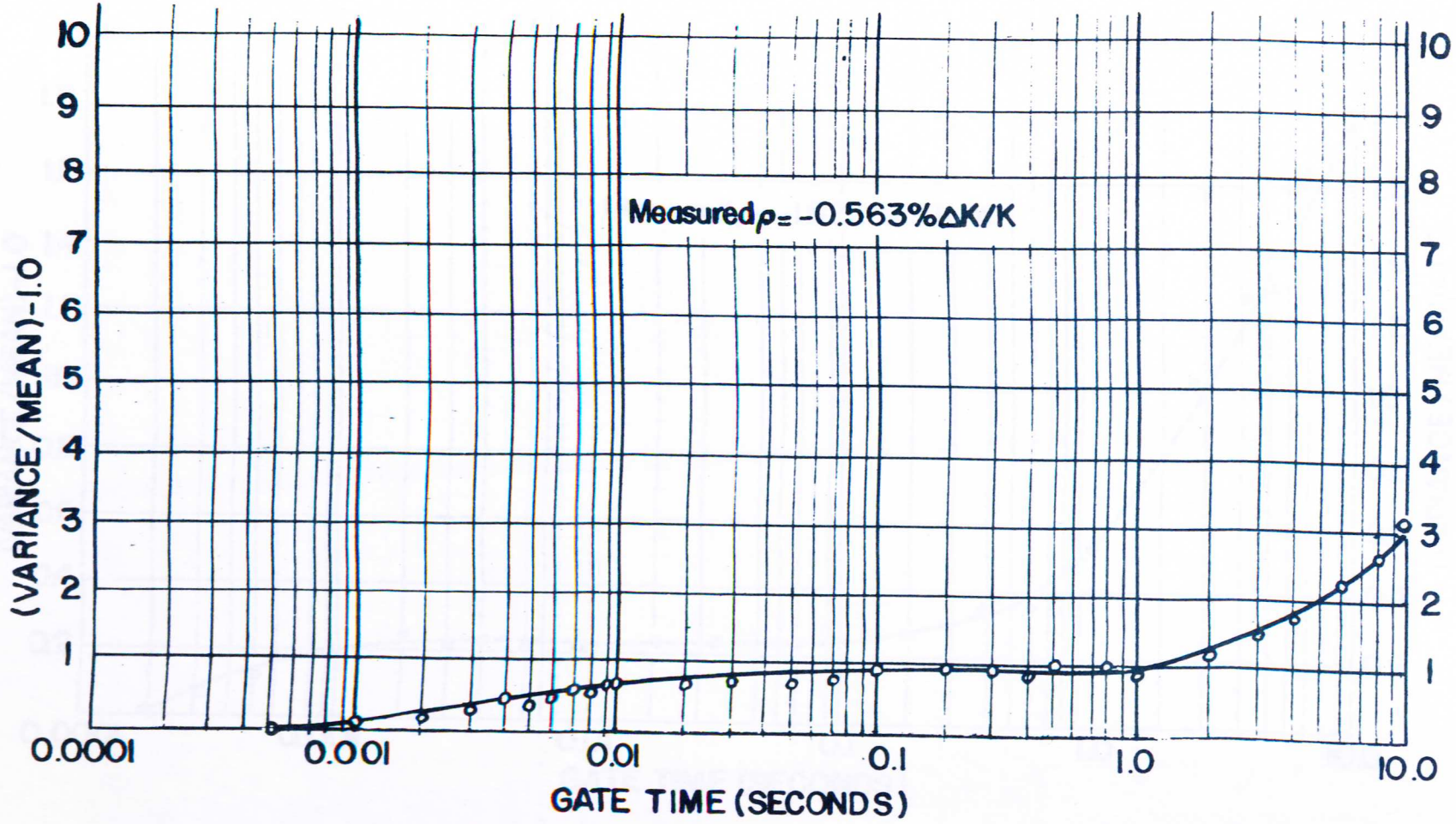

FIGURE 32 VARIANCE-TO-MEAN VERSUS GATE TIME FOR UMR FULL CORE WITH ALL RODS AT 42 CM.

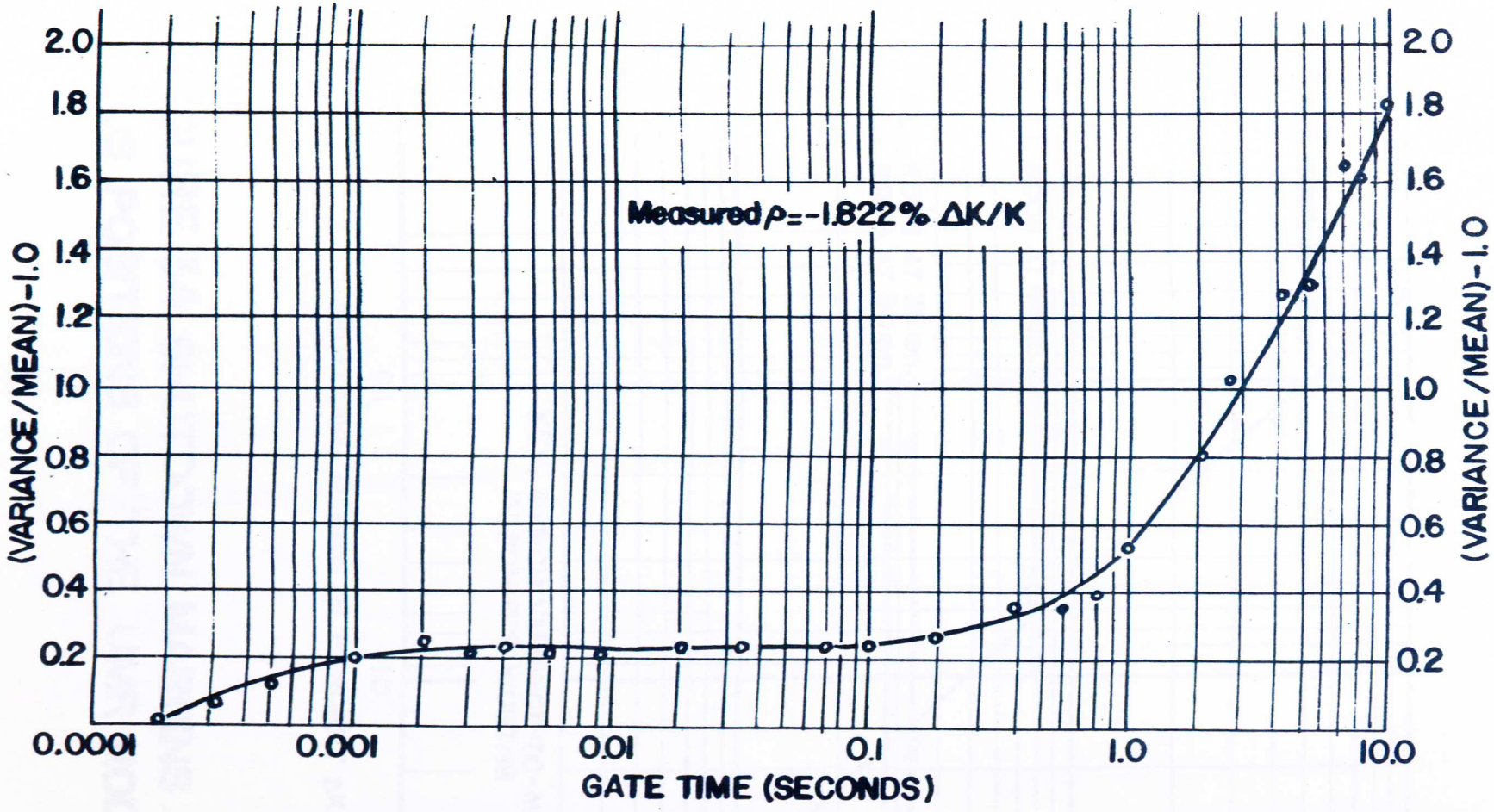

FIGURE 33 VARIANCE-TO-MEAN VERSUS GATE TIME FOR UMR FULL CORE WITH ALL RODS AT 35CM.

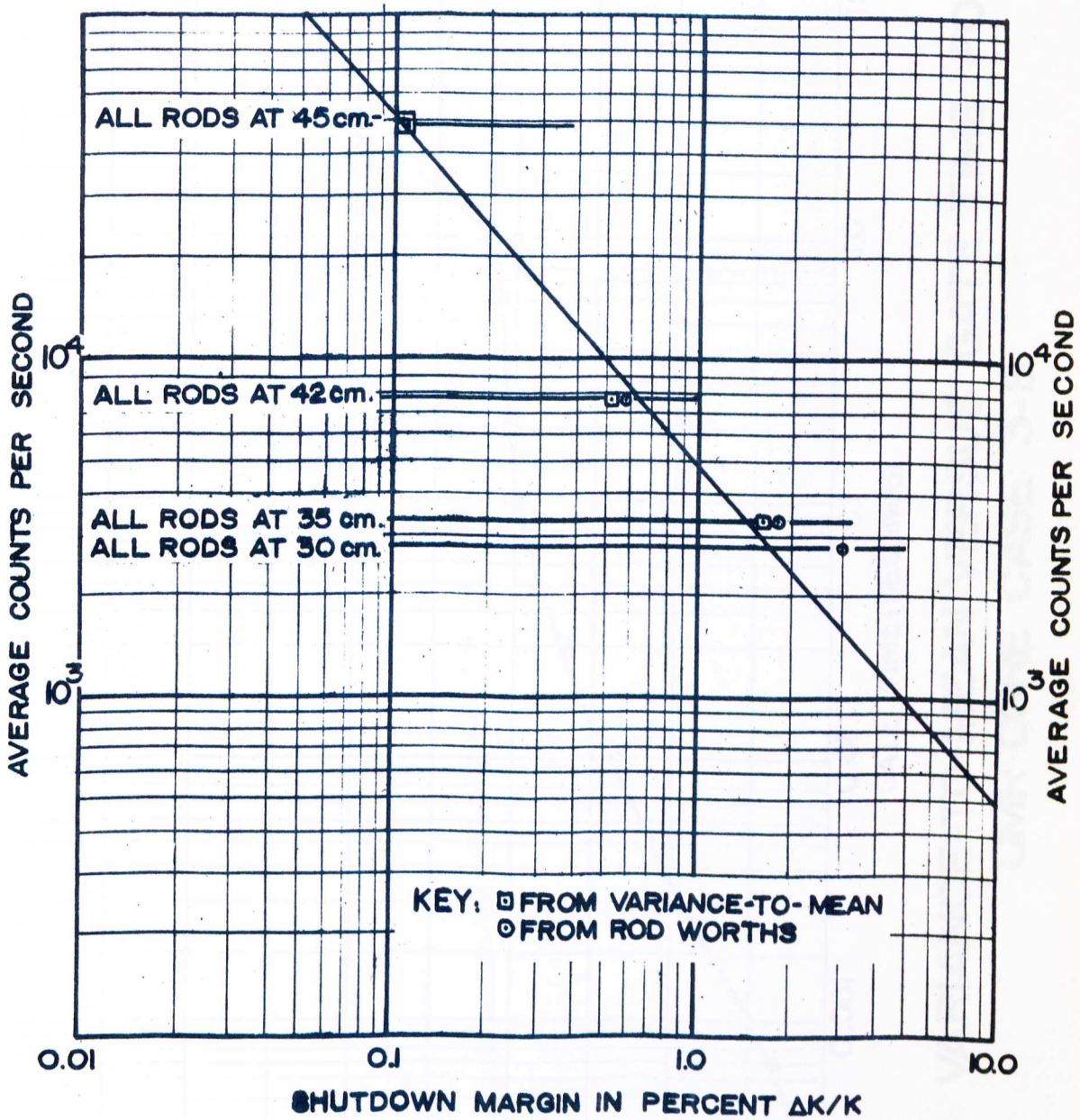

FIGURE 34 SHUTDOWN MARGINS FOR VARIOUS POSITIONS OF THE UMR ROD BANK

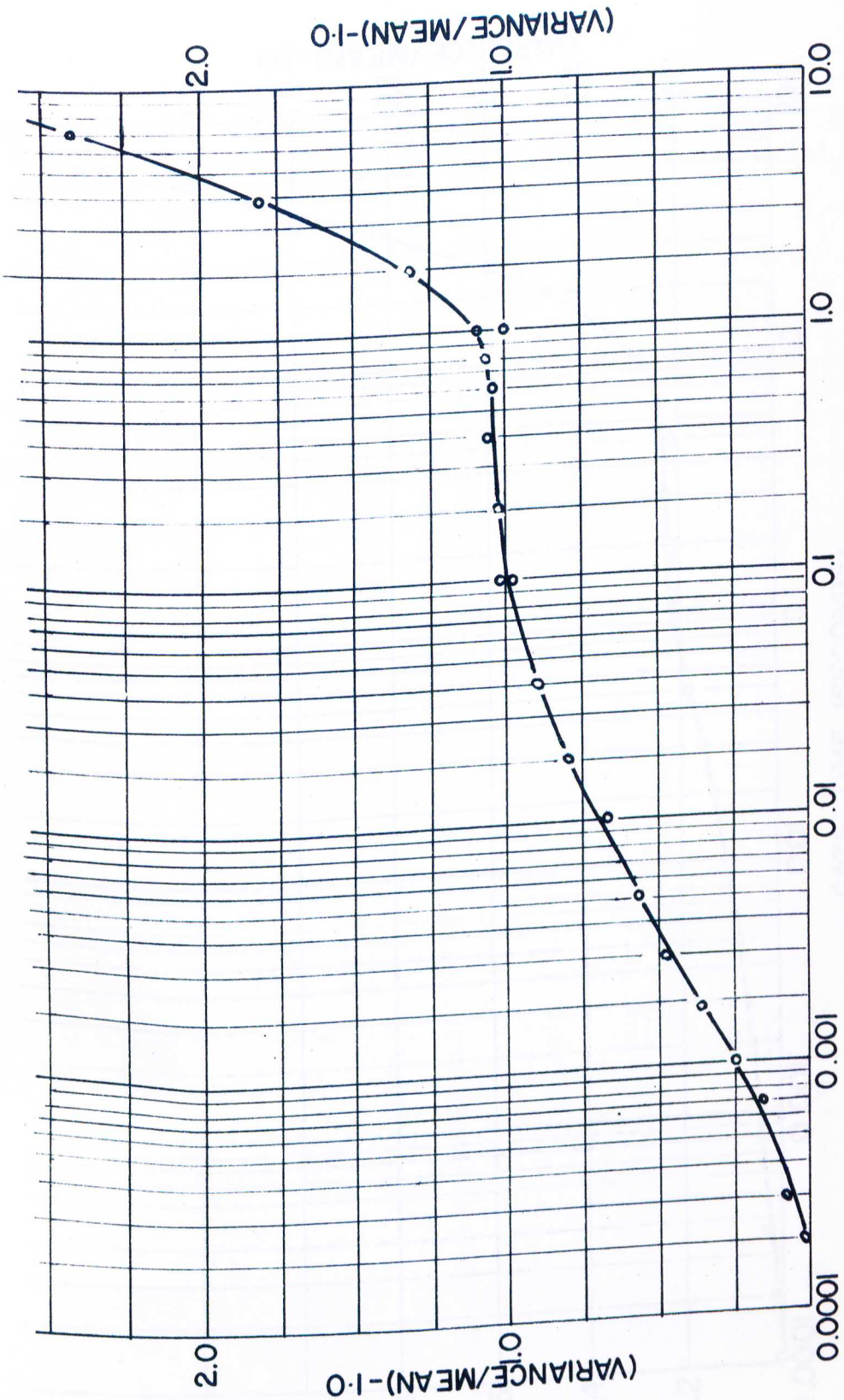

FIGURE 35 VARIANCE-TO-MEAN VERSUS GATE TIME FOR UMR CORE CASE 3-B

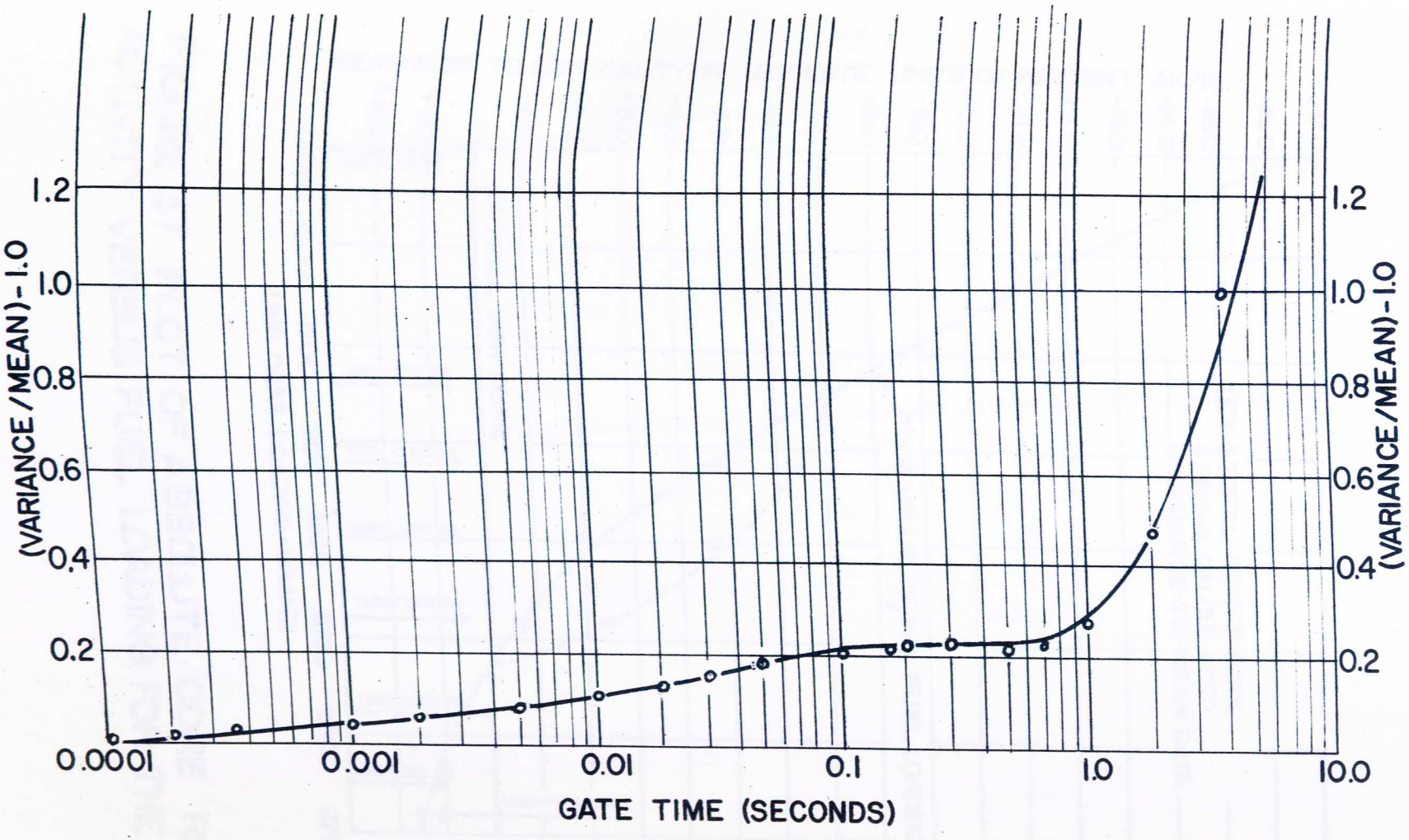

FIGURE 36 VARIANCE-TO-MEAN VERSUS GATE TIME FOR UMR CORE CASE 4-B

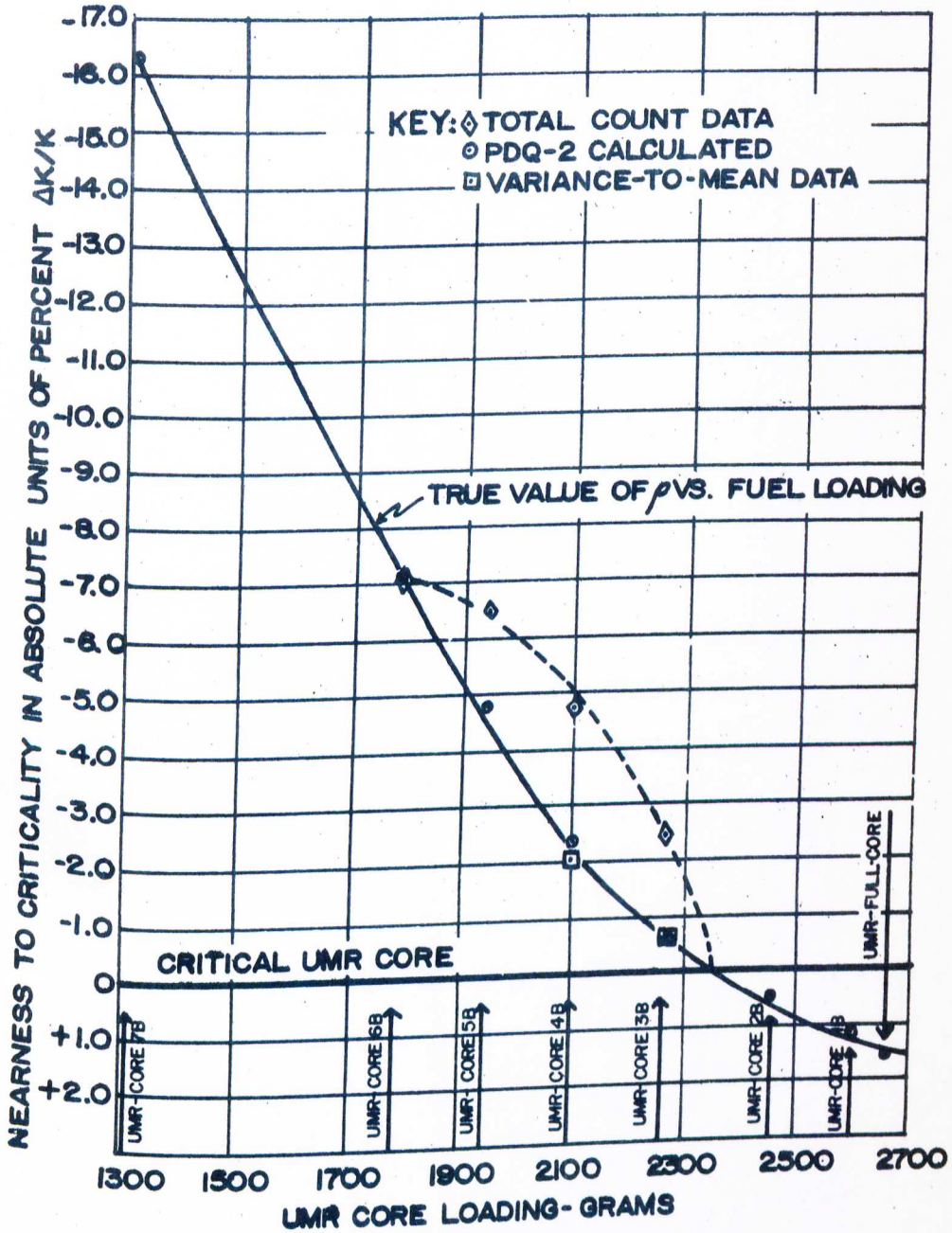

FIGURE 37 PLOT OF ABSOLUTE CORE REACTIVITY VERSUS FUEL LOADING FOR THE UMR